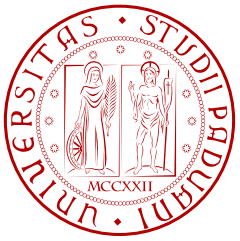

DIPARTIMENTO
DI INGEGNERIA
DELL'INFORMAZIONE

UNIVERSITÀ DEGLI STUDI DI PADOVA

Dipartimento di
Ingegneria dell'Informazione

Corso di laurea magistrale in *Ingegneria delle Telecomunicazioni*

Thesis on

MIMO Array Gain Techniques for Communications over mm-wave Channels

Supervisor:
prof. Nevio Benvenuto*

Author:
Nicola Belli

Co-supervisor:
dr. Federico Boccardi†

* Department of Information Engineering, University of Padova, Italy

† Bell Laboratories, Alcatel-Lucent

July 8, 2013 - A.A. 2012/2013

To Giulia,
when I think of you
it all makes sense.

Table of contents

Notation

Symbol	Description
$\mathbf{a}$	Column vector $\mathbf{a}$ (boldface lower-case letter)
$\mathbf{A}$	Matrix $\mathbf{A}$ (boldface capital letter)
$\mathrm{row}_i(\mathbf{A})$	The row i of matrix $\mathbf{A}$
$\mathrm{col}_j(\mathbf{A})$	The column j of matrix $\mathbf{A}$
$[\mathbf{A}]_{i,j}$	The entry on row i and column j of matrix $\mathbf{A}$
$\mathbf{A}^{\mathsf{T}}$	Transpose of $\mathbf{A}$
$\mathbf{A}^{\mathsf{H}}$	Conjugate transpose (Hermitian) of $\mathbf{A}$
$\mathbf{I}_n$	$n \times n$ identical matrix
$\mathrm{diag}(a_1, a_2, \ldots, a_n)$	$n \times n$ diagonal matrix with a_1, a_2, …, a_n on its main diagonal
$\mathrm{tr}(\mathbf{A})$	Trace of $\mathbf{A}$
$\mathrm{rank}(\mathbf{A})$	Rank of $\mathbf{A}$
$\mathbf{A} \succeq 0$	$\mathbf{A}$ is positive semi-definite
$\mathrm{abs}(\mathbf{A})$	Matrix constituted by amplitudes of entries of $\mathbf{A}$
$\angle(\mathbf{A})$	Matrix constituted by angle values of entries of $\mathbf{A}$
a^*	Conjugate of scalar a
$\angle(a)$	Angle value of scalar a
$\lvert a \rvert$	Amplitude of scalar a
$\lVert \mathbf{a} \rVert$	Two-norm of vector $\mathbf{a}$ (Euclidean norm)
$\lVert \mathbf{A} \rVert$	Two-norm of matrix $\mathbf{A}$ (Frobenius norm)
a_{M}	Maximum value taken by real scalar a
$\mathbb{E}[\cdot]$	Expected value
$\overline{x} = \mathbb{E}[x]$	Mean of random variable x
$\mathtt{M}_x = \mathbb{E}[\lvert x \rvert^2]$	Statistical power of random variable x
$\mathtt{Q}_x = \mathbb{E}[\lvert x \rvert^4]$	Moment of the 4^{th} order of random variable x
$\sigma_x^2 = \mathbb{E}[\lvert x - \overline{x} \rvert^2]$	Variance of random variable x
$F_x(\cdot)$	Cumulative distribution function CDF of random variable x
$f_x(\cdot)$	Probability density function PDF of random variable x
$\Pr(E)$	Probability value of event E
$\Re\{\cdot\}$	Real part
$\Im\{\cdot\}$	Imaginary part

List of acronyms

MMW	mm-wave
Tx	transmitter
Rx	receiver
UHF	ultra high frequencies
ULA	uniform linear array
UPA	uniform planar array
PDF	probability density function
LOS	line of sight
SNR	signal to noise ratio
RF	radio frequency
ADC	analog to digital converter
DAC	digital to analog converter
SISO	single input single output
AWGN	additive white Gaussian noise
i.i.d.	independent identically distributed
MRB	maximum ratio beamforming
SVD	singular value decomposition
CDF	cumulative distribution function
MIMO	multiple input multiple output
MISO	multiple input single output
SIMO	single input multiple output
I-MRB	iterative maximum ratio beamforming

I-RWB	iterative real weights beamforming
I-EGB	iterative equal gain beamforming
ADB	analog-digital beamforming
BB	base-band
CQ-KC	coarse quantization of received signal assuming a known channel
CQ-EC	coarse quantization of received signal assuming an estimated channel
MLS	maximum length sequence
CSI	channel state information
MMSE	minimum mean square error
SQR	signal to quantization noise ratio
MLS	maximum length sequence
D-PSK	differential phase shift keying
PSK	phase shift keying

Introduction

There are about 250 GHz of available bandwidth between 3 and 300 GHz (also referred as mm-wave (MMW) band) [1], which have the potential to unleash very high data-rates even with low spectral efficiencies. Such a 'spectrum El Dorado' in the last years led to a 'MMW rush', in which researchers with different backgrounds studied different aspects related to transmissions at high-frequencies, ranging from channel modeling, antenna and hardware design, beamforming solutions and system-related aspects (see e.g. references [2–7]).
From an industrial perspective, while MMW frequencies have been already standardized for niche applications (e.g. in 802.11ad or 802.153c) or used for test-bed prototypes, a mass commercial application of MMW in 5G wireless networks requires major technologies advances, from both a component and an architectural perspective. Component-wise, novel and cost-effective solutions for beamforming, waveform and antenna design and hardware implementations are needed [4–7]. Architecture-wise, MMWs require a redefinition of the functionalities in the network, for example via a separation between control and data channels and a tight integration and a fast handover with lower carriers [2]. From a deployment perspective, further studies on channel propagation and modeling at high frequencies are another important step for a throughout understanding of MMW communications [3].
In this thesis we focus on one of the problems mentioned above, i.e. the need of designing cost-effective beamforming solutions at MMW frequencies, to provide the link-budget required for a reliable communication. As a matter of fact, and as emphasized in [7], when assuming a single omnidirectional antenna, the path-loss increases with the frequency, e.g. an additional 20dB loss is expected for a system operating at 60 GHz compared to 6 GHz. On the other hand, by using a fixed directive antenna of a given aperture size, the antenna directivity increases with the square of the frequency. While fixed antennas are effective solutions for MMW *backhaul* applications, for *access* applications, flexible solutions based on beamforming via antenna arrays are essential to allow multi access. Moreover, while in traditional cellular frequencies, beamforming-related processing is performed at the baseband, at the MMW frequencies this design philosophy crashes against the high cost and high-energy consumption of radio frequency (RF) hardware [4]. Therefore, different solutions have been proposed based on either analog or hybrid digital-analog implementations. A good analysis of different analog implementations is carried out in [5]. While analog solutions (e.g. based on analog phase shifters) are competitive in terms of cost, they impose a constant modulo constraint on the beamforming weights. Therefore, in [4], a hybrid analog-digital solution is proposed, where the

antenna array is driven by a limited number of RF chains and multi-antenna processing is implemented via a layered baseband/analog solution.

Chapter 1

A channel model for mm-wave

While signals at lower frequencies can penetrate more easily through buildings, mm-wave signals do not penetrate most solid materials very well. Significant causes of attenuation at high frequency are foliage losses, raindrops and oxygen band absorption, which can be a limiting impairment for propagation in some cases. On the other hand for the same antenna aperture areas, shorter wavelengths (higher frequencies) should not have any inherent disadvantage compared to longer wavelengths (lower frequencies) in terms of free space loss. More antennas can be packed into the same area if the wave length is small, allowing beamforming with high gains.
We start from an expression of a static narrow-band mm-wave channel impulse response. Furthermore multiple input multiple output (MIMO) models will be considered.

1.1 Channel impulse response

The equivalent complex low-pass impulse response of a mm-wave MIMO channel with narrow-band impulses is a matrix $\mathbb{C}^{N\times M}$, where M and N are the number of antennas at transmitter (Tx) and receiver (Rx) sides respectively

$$\widehat{\mathbf{H}} = \sqrt{G}\begin{bmatrix} h_{11} & \cdots & h_{1M} \\ \vdots & \ddots & \vdots \\ h_{N1} & \cdots & h_{NM} \end{bmatrix} = \sqrt{G}\mathbf{H}, \tag{1.1}$$

G is the average path gain of the channel. While G is a deterministic factor, entries of $\mathbf{H}$ are, in general, complex random variables. Matrix $\mathbf{H}$ should satisfies the average constraint on its squared Frobenius norm

$$\mathbb{E}\left[\|\mathbf{H}\|^2\right] = MN. \tag{1.2}$$

1.1.1 Power attenuation characterization

A general expression for G is provided by

$$G = \left(\frac{\lambda}{4\pi d}\right)^n \Lambda_t\left(\phi_t,\, \vartheta_t\right) \Lambda_r\left(\phi_r,\, \vartheta_r\right) G^{(o)} G^{(r)} G^{(f)}, \tag{1.3}$$

where:

- $\lambda = c/f_c$ is the wave length at carrier frequency f_c;
- d is the distance between transmitter and receiver;
- n is the path-loss exponent factor;
- Λ_t is the Tx directional antenna gain, function of azimuth ϕ_t and elevation ϑ_t of the transmitted ray;
- Λ_r is the Rx directional antenna gain, function of azimuth ϕ_r and elevation ϑ_r of the received ray;
- $G^{(o)}$ is the average attenuation due to oxygen absorption;
- $G^{(r)}$ is the average attenuation due to rain;
- $G^{(f)}$ is the average attenuation due to foliage.

In this case antenna contributions Λ_t and Λ_r are considered constant for each ray angle of arrival and departure, therefore they are included in the global gain G-factor. The given attenuation model is valid for values of d which are in the far-field, or Fraunhofer region, of the transmitting antenna. This is defined as the region beyond the far-field distance, which is related to the largest linear dimension of the transmitter antenna aperture and the carrier wavelength, i.e. if [8, pp. 72]:

$$d \gg D_{\text{ant}}, \qquad d \gg \lambda \qquad \text{and} \qquad d \gg \frac{2D_{\text{ant}}^2}{\lambda} \tag{1.4}$$

where D_{ant} is the largest physical linear dimension of the antenna.

Free space path loss

The first gain term in (1.3) is the attenuation due to the free space propagation. The exponent factor n in free space is 2, but it is known that a two-ray model (represented in Figure 1.1) leads, under commonly satisfied conditions, to a fourth power law. One of these conditions is that the path length difference between the direct and reflected rays is less than $\lambda/2$, which defines the break-point distance $d_0 = 4h_t h_r/\lambda$ as a function of antennas height, beyond which the fourth power law can be used.
For the frequency range from 60 to 66 GHz and the receive and transmit antenna heights, $h_r = 1.8$ m and $h_t \in [5; 50]$ m, respectively, we get $d_0 \in [7.2; 79.21]$ km, which is far beyond the expected range of the transmission at mm-wave frequency. This means that the fourth power law is not expected at mm-wave therefore we set $n = 2$, which is confirmed by measurements [9, pp. 77].

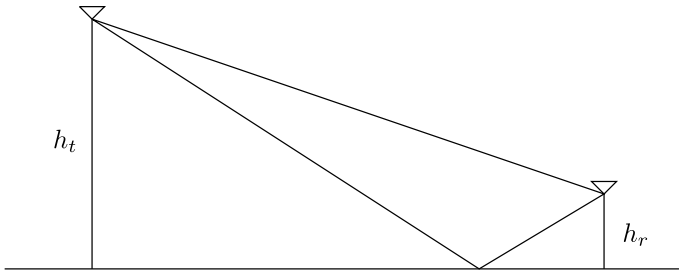

Figure 1.1: Two rays model used for the derivation of the fourth law attenuation expression.

Antennas gain

Due to high free space losses and other attenuations factors, that will be analyzed later, the usage of directional antenna is near mandatory for a successful communication. An advantage of using directive antennas is the limitation of multipath phenomena due to the antenna pattern gain.
As an example, a rectangular horn antenna of dimensions a and b has a radiation pattern [3, pp. 318] given by

$$\Lambda(\phi,\, \vartheta) = \left| \frac{\sin\left[\pi(a/\lambda)\sin(\phi)\right]\sin\left[\pi(b/\lambda)\sin(\vartheta)\right]}{\pi^2(ab/\lambda^2)\sin(\phi)\sin(\vartheta)} \right|^2 . \tag{1.5}$$

In Figure 1.2 the radiation patterns, expressed by (1.5), of two horn antennas with different dimensions are plotted in the azimuth plane. The main lobe is narrower if the antenna dimensions are bigger.
Another simple radiation pattern is:

$$\Lambda(\phi,\, \vartheta) = \begin{cases} \Lambda_0, & \phi \in [\phi_{\min};\, \phi_{\max}]\,, \quad \vartheta \in [\vartheta_{\min};\, \vartheta_{\max}] \\ 0, & \text{otherwise} \end{cases} \tag{1.6}$$

where Λ_0 is a constant gain over the sector defined by $\phi \in [\phi_{\min};\, \phi_{\max}]$ and $\vartheta \in [\vartheta_{\min};\, \vartheta_{\max}]$.
In the case of a ray-tracing approach, angle values are defined and constant. In other situations ϕ_t, ϕ_r, ϑ_t and ϑ_r are all considered uniformly distributed in their sectors as

$$\phi_t,\, \phi_r \sim \mathcal{U}\left[\phi_{\min};\, \phi_{\max}\right], \qquad \vartheta_t,\, \vartheta_r \sim \mathcal{U}\left[\vartheta_{\min};\, \vartheta_{\max}\right]. \tag{1.7}$$

Oxygen band absorption

Around 60 GHz there is a peak of attenuation due to oxygen resonance in atmosphere. The term $G^{(o)}$ is negligible in the ultra high frequencies (UHF) band, but cannot be neglected at higher frequencies. In [9, pp. 78] a model for the attenuation

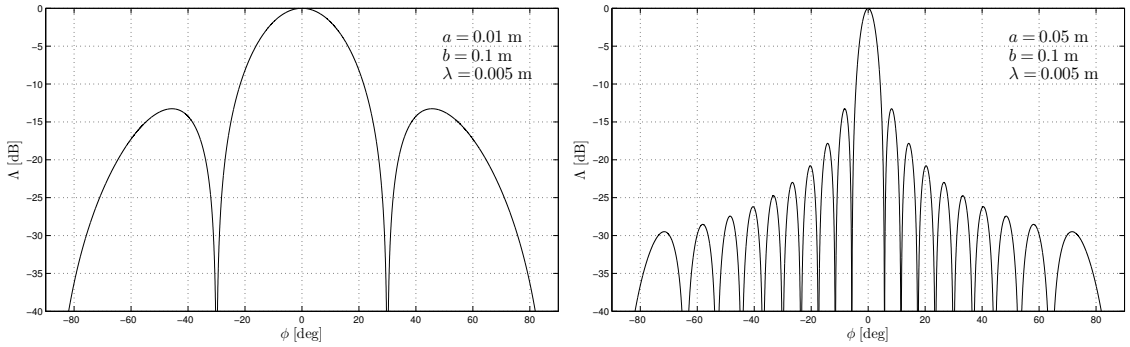

Figure 1.2: Normalized radiation patterns in azimuth plane for different rectangular horn antenna parameters.

due to oxygen absorption has been developed

$$G^{(o)}_{[\mathrm{dB/km}]}(f_{c\,[\mathrm{GHz}]}) = \begin{cases} 0.104(f_c - 60)^{3.26} - 15.10 & 60 \leq f_c \leq 63 \\ 5.33(f_c - 63)^{1.27} - 11.35 - (f_c - 63)^{2.25} & 63 < f_c \leq 66 \end{cases} \tag{1.8}$$

where f_c is the carrier frequency.
There are other attenuation phenomena due to water vapour or fog, but they can be neglected since their attenuation is in order of 0.1 dB/km [9, pp. 78].

Rain attenuation model

In mm-wave also rain has relevance in attenuating the transmitted signal. Depending on the rainfall rate R [mm/h] this model [9, pp. 78] yields:

$$G^{(r)}_{[\mathrm{dB/km}]}(f_{c\,[\mathrm{GHz}]},\, R_{[\mathrm{mm/h}]}) = -k(f_c)R^{a(f_c)}, \tag{1.9}$$

where

$$k(f_c) = 10^{1.203\log(f_c) - 2.290}, \qquad a(f_c) = 1.703 - 0.493\log(f_c). \tag{1.10}$$

Rain contribution to path gain plays an important role, and its attenuation can reach values larger than those for oxygen; for example $G^{(r)} = -18$ [dB/km] for R=50 mm/h.
Formulas show that oxygen and rain attenuations cannot be neglected if large distances (greater than 1 km) are to be considered, but for ranges less than 200 m they may not be so relevant.

Foliage attenuation

An attenuation formula due to foliage is given in [10]:

$$G^{(f)}(f_c,\, d_{\mathrm{fol}}) = \frac{5}{f_c^{0.3} d_{\mathrm{fol}}^{0.6}} \tag{1.11}$$

where d_{fol} is the depth of foliage area between transmitter and receiver.

Remarks on shadowing

Many studies on mm-wave indoor propagation (for example [11, pp. 9] and [12, pp. 2821]) add an additional random gain term to (1.3) due to shadowing. The gain is modelled as a log-normal random variable and it is justified by the exponential law attenuation when shadowing is due to blocking objects [13, pp. 44] present on the line of propagation.
However for an outdoor propagation environment no shadowing effects are contemplated. In fact, due to small penetration capabilities of mm-wave[1] through solid materials, the received power due to rays incurring in outdoor shadowing phenomena is negligible with respect to contribution by diffracted and reflected rays.

1.1.2 MIMO channel models

Two models are considered for $\mathbf{H}$:

- correlation based model;
- phase array model.

The first model starts from Tx and Rx correlation matrices, while the second is based on a geometrical approach that underline the signals phase differences in antenna arrays at Tx and Rx sides. The last model is characterized by limited spatial diversity and is suitable for arrays with a lot of antenna elements packed in a confined space.

Kronecker MIMO channel model

The Kronecker MIMO channel is probably the best-know correlation-based model. It's based on the assumption that the spatial correlation coefficients between Tx elements are independent of the specific Rx element. The following simple and generic definitions for the transmitter and receiver correlation matrices are given [14]:

$$\begin{aligned}
\mathbf{R}_{\mathrm{TX}} = \mathbb{E}\left[\mathbf{H}^{\mathsf{H}}\mathbf{H}\right] &= \begin{bmatrix} 1 & \mu & \mu^2 & \cdots & \mu^{M-1} \\ \mu & 1 & \mu & \ddots & \vdots \\ \mu^2 & \mu & 1 & \ddots & \mu^2 \\ \vdots & \ddots & \ddots & \ddots & \mu \\ \mu^{M-1} & \cdots & \mu^2 & \mu & 1 \end{bmatrix}_{M\times M} \\
\mathbf{R}_{\mathrm{RX}} = \mathbb{E}\left[\mathbf{H}\mathbf{H}^{\mathsf{H}}\right] &= \begin{bmatrix} 1 & \eta & \eta^2 & \cdots & \eta^{N-1} \\ \eta & 1 & \eta & \ddots & \vdots \\ \eta^2 & \eta & 1 & \ddots & \eta^2 \\ \vdots & \ddots & \ddots & \ddots & \eta \\ \eta^{N-1} & \cdots & \eta^2 & \eta & 1 \end{bmatrix}_{N\times N}
\end{aligned} \tag{1.12}$$

[1] Numerical values of specific attenuation are given in [1, pp. 103].

where $\mu \in [0; 1]$ and $\eta \in [0; 1]$ are the Tx and Rx correlation coefficients, respectively. Given the Tx and Rx correlations matrices, in [14], it has been shown that the channel $\mathbf{H} \in \mathbb{C}^{N \times M}$ can be expressed as

$$\mathbf{H} = \mathbf{R}_{\text{Rx}}^{1/2} \mathbf{H}_{\text{i.i.d.}} \mathbf{R}_{\text{Tx}}^{1/2} \tag{1.13}$$

where $\mathbf{H}_{\text{i.i.d.}} \in \mathbb{C}^{N \times M}$ is a matrix of i.i.d. circularly symmetric complex Gaussian random variables with zero mean and unit variance.
Two opposite and extreme cases are contemplated by the correlation based MIMO channel:

- if $\text{rank}\,(\mathbf{R}_{\text{Tx}}) = M$ ($\text{rank}\,(\mathbf{R}_{\text{Rx}}) = N$) the channel is said to be fully uncorrelated at Tx (Rx) side;
- if $\text{rank}\,(\mathbf{R}_{\text{Tx}}) = 1$ ($\text{rank}\,(\mathbf{R}_{\text{Rx}}) = 1$) the channel is said to be fully correlated at Tx (Rx) side.

Phase array MIMO channel model

This model is taken from [4, pp. 3783] and describes a channel matrix for an uniform linear array (ULA) for beamforming in azimuth plane and for a uniform planar array uniform planar array (UPA) which enables beamforming also in elevation.

Uniform linear array

Let us consider antenna elements to form an ULA on the azimuth plane with an inter-element spacing equal to D. For a uniform linear array with N elements, from Figure 1.3, let $\mathbf{a}$ be a vector of phasors

$$\mathbf{a}(\phi) = \frac{1}{\sqrt{N}} \begin{bmatrix} 1 & e^{j\zeta D \sin\phi} & \cdots & e^{j(N-1)\zeta D \sin\phi} \end{bmatrix}^{\mathsf{T}}, \tag{1.14}$$

where $\zeta = 2\pi/\lambda$ and ϕ represents the ray angle of arrival or the angle of departure in the azimuth plane. If

$$g_\ell \sim \mathcal{CN}(0,\, 1), \tag{1.15}$$

the narrow-band channel impulse response for a system with a ULA of M and N elements at Tx and Rx side, respectively, is a matrix $\mathbf{H}_{\text{ULA}} \in \mathbb{C}^{N \times M}$ defined as:

$$\mathbf{H}_{\text{ULA}} = \sqrt{\frac{MN}{L}} \sum_{\ell=1}^{L} g_\ell \mathbf{a}_r \left(\phi_\ell^{(r)}\right) \mathbf{a}_t^{\mathsf{H}} \left(\phi_\ell^{(t)}\right), \tag{1.16}$$

where L is the total number of rays and $\mathbf{a}_r(\cdot)$ and $\mathbf{a}_t(\cdot)$ are defined in (1.14). Note that the elements of $\mathbf{a}$ represent phase offsets due to distances between antenna elements. The relative phase difference for a ULA is a function only of the azimuth variable ϕ. Moreover, in (1.16), the average power gain factor $\sqrt{G}$ of (1.1) is dropped for simplicity.

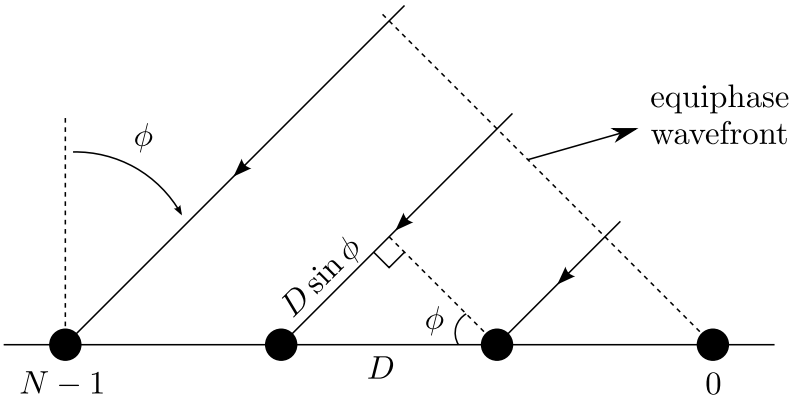

Figure 1.3: Relative path difference in an ULA.

Uniform planar array

We also consider an UPA constituted by $N = WH$ antenna elements, with W antennas, D spaced, on a dimension and H antennas with same D inter-element distance on the other dimension.
Let $\mathbf{b}$ is a vector of phasors defined as:

$$\mathbf{b}(\phi,\, \vartheta) = \frac{1}{\sqrt{N}} \left[1 \quad \cdots \quad e^{j\zeta D(w \sin\phi \sin\vartheta + h\cos\vartheta)} \quad \cdots \quad e^{j\zeta D[(W-1)\sin\phi\sin\vartheta + (H-1)\cos\vartheta]}\right]^{\mathsf{T}} \tag{1.17}$$

where $w = 0,\, 1,\, \ldots,\, W-1$ and $h = 0,\, 1,\, \ldots,\, H-1$, are indexes of antenna elements and $\zeta = 2\pi/\lambda$. The narrow-band channel impulse response for a system with a UPA of M and N elements at Tx and Rx side, respectively, as in (1.16), is a matrix $\mathbf{H}_{\text{UPA}} \in \mathbb{C}^{N\times M}$ expressed by

$$\mathbf{H}_{\text{UPA}} = \sqrt{\frac{MN}{L}} \sum_{\ell=1}^{L} g_\ell \mathbf{b}_r\left(\phi_\ell^{(r)},\, \vartheta_\ell^{(r)}\right) \mathbf{b}_t^{\mathsf{H}}\left(\phi_\ell^{(t)},\, \vartheta_\ell^{(t)}\right). \tag{1.18}$$

Two dimensions antennas array enable beamforming in elevation, indeed the channel impulse response is also function of elevation ϑ.

Matrix formulation

The expressions of MIMO channel impulse response given in (1.16) and (1.18) can be rewritten [15, pp. 27] into matrix synthetic and useful forms:

$$\mathbf{H}_{\text{ULA}} = \sqrt{\frac{MN}{L}} \left(\mathbf{A}_r \mathbf{H}_g \mathbf{A}_t^{\mathsf{H}}\right) \qquad \mathbf{H}_{\text{UPA}} = \sqrt{\frac{MN}{L}} \left(\mathbf{B}_r \mathbf{H}_g \mathbf{B}_t^{\mathsf{H}}\right) \tag{1.19}$$

where

$$\mathbf{A}_r = \left[\mathbf{a}_r\left(\phi_1^{(r)}\right) \quad \cdots \quad \mathbf{a}_r\left(\phi_L^{(r)}\right)\right] \qquad \mathbf{B}_r = \left[\mathbf{b}_r\left(\phi_1^{(r)},\, \vartheta_1^{(r)}\right) \quad \cdots \quad \mathbf{b}_r\left(\phi_L^{(r)},\, \vartheta_L^{(r)}\right)\right]$$
$$\mathbf{A}_t = \left[\mathbf{a}_t\left(\phi_1^{(t)}\right) \quad \cdots \quad \mathbf{a}_t\left(\phi_L^{(t)}\right)\right] \qquad \mathbf{B}_t = \left[\mathbf{b}_t\left(\phi_1^{(t)},\, \vartheta_1^{(t)}\right) \quad \cdots \quad \mathbf{b}_t\left(\phi_L^{(t)},\, \vartheta_L^{(t)}\right)\right]$$

(1.20)

and

$$\mathbf{H}_g = \mathrm{diag}\left(g_1, \ldots, g_L\right). \tag{1.21}$$

where the diag$(\cdot)$ operator denotes a matrix with only the main diagonal different from zero composed by the list arguments in given order.

Statistical remarks on ULA channel

In this section the mean and statistical power of the generic entry on row p and column q of the ULA matrix channel $\mathbf{H}_{\mathrm{ULA}}$ are evaluated. The generic $N \times M$ ULA channel matrix with L rays, given in (1.19), is expanded in (1.22), emphasizing the column $q \in [1;\, M]$ and the row $p \in [1;\, N]$. Considering (1.15), the mean of $\left[\mathbf{H}_{\mathrm{ULA}}\right]_{p,q}$ is equal to zero

$$\begin{aligned}
\mathbb{E}\left[\left[\mathbf{H}_{\mathrm{ULA}}\right]_{p,q}\right] &= \frac{1}{\sqrt{L}}\mathbb{E}\left[\sum_{\ell=1}^{L} g_\ell e^{j\zeta D(p-1)\sin\phi_\ell^{(r)}} e^{-j\zeta D(q-1)\sin\phi_\ell^{(t)}}\right] \\
&= \frac{1}{\sqrt{L}}\sum_{\ell=1}^{L} \underbrace{\mathbb{E}\left[g_\ell\right]}_{=0} \mathbb{E}\left[e^{j\zeta D(p-1)\sin\phi_\ell^{(r)}} e^{-j\zeta D(q-1)\sin\phi_\ell^{(t)}}\right] \\
&= 0.
\end{aligned} \tag{1.23}$$

and the statistical power is equal to

$$\begin{aligned}
\mathbb{E}\left[\left|\left[\mathbf{H}_{\mathrm{ULA}}\right]_{p,q}\right|^2\right] &= \frac{1}{L}\mathbb{E}\left[\sum_{\ell=1}^{L}\sum_{o=1}^{L} g_\ell g_o^* e^{j\zeta D(p-1)\sin\phi_\ell^{(r)}} e^{-j\zeta D(q-1)\sin\phi_\ell^{(t)}}\right. \\
&\qquad \left. e^{-j\zeta D(p-1)\sin\phi_o^{(r)}} e^{j\zeta D(q-1)\sin\phi_o^{(t)}}\right] \\
&= \frac{1}{L}\sum_{\ell=1}^{L} \mathbb{E}\left[|g_\ell|^2\right] \mathbb{E}\left[\left|e^{j\zeta D(p-1)\sin\phi_\ell^{(r)}} e^{-j\zeta D(q-1)\sin\phi_\ell^{(t)}}\right|^2\right] \\
&= 1.
\end{aligned} \tag{1.24}$$

The result in (1.24) is reached exploiting the independence between the gains g and the angle of rays ϕ, that leads to

$$\begin{cases}
\mathbb{E}\left[|g_\ell|^2\right] \mathbb{E}\left[\left|e^{j\zeta D(p-1)\sin\phi_\ell^{(r)}} e^{-j\zeta D(q-1)\sin\phi_\ell^{(t)}}\right|^2\right] = 1 & \text{if} \quad \ell = o \\
\underbrace{\mathbb{E}\left[g_\ell^*\right]}_{0}\underbrace{\mathbb{E}\left[g_o\right]}_{0} \mathbb{E}\left[\left|e^{j\zeta D(p-1)\sin\phi_\ell^{(r)}} e^{-j\zeta D(q-1)\sin\phi_o^{(t)}}\right|^2\right] = 0 & \text{if} \quad \ell \neq o.
\end{cases} \tag{1.25}$$

The statistical power value of each entry of $\mathbf{H}_{\mathrm{ULA}}$ in (1.24) assures that (1.2) is true for the ULA channel model.

$$\mathbf{H}_{\text{ULA}} = \frac{1}{\sqrt{L}} \begin{bmatrix} \sum_{\ell=1}^{L} g_\ell & \cdots & \sum_{\ell=1}^{L} g_\ell e^{-j\zeta D(q-1)\sin\phi_\ell^{(t)}} & \cdots & \sum_{\ell=1}^{L} g_\ell e^{-j\zeta D(M-1)\sin\phi_\ell^{(t)}} \\ \vdots & \ddots & \vdots & \ddots & \vdots \\ \sum_{\ell=1}^{L} g_\ell e^{j\zeta D(p-1)\sin\phi_\ell^{(r)}} & \cdots & \sum_{\ell=1}^{L} g_\ell e^{j\zeta D(p-1)\sin\phi_\ell^{(r)}} e^{-j\zeta D(q-1)\sin\phi_\ell^{(t)}} & \cdots & \sum_{\ell=1}^{L} g_\ell e^{j\zeta D(p-1)\sin\phi_\ell^{(r)}} e^{-j\zeta D(M-1)\sin\phi_\ell^{(t)}} \\ \vdots & \ddots & \vdots & \ddots & \vdots \\ \sum_{\ell=1}^{L} g_\ell e^{j\zeta D(N-1)\sin\phi_\ell^{(r)}} & \cdots & \sum_{\ell=1}^{L} g_\ell e^{j\zeta D(N-1)\sin\phi_\ell^{(r)}} e^{-j\zeta D(q-1)\sin\phi_\ell^{(t)}} & \cdots & \sum_{\ell=1}^{L} g_\ell e^{j\zeta D(N-1)\sin\phi_\ell^{(t)}} \end{bmatrix} \tag{1.22}$$

The correlation of ULA channel

In this section we provide an expression for the entries of the ULA channel Tx and Rx correlation matrices,

$$\mathbf{R}_{\mathrm{Tx}} = \mathbb{E}\left[\mathbf{H}_{\mathrm{ULA}}^{\mathsf{H}}\mathbf{H}_{\mathrm{ULA}}\right] \qquad \text{and} \qquad \mathbf{R}_{\mathrm{Rx}} = \mathbb{E}\left[\mathbf{H}_{\mathrm{ULA}}\mathbf{H}_{\mathrm{ULA}}^{\mathsf{H}}\right]. \tag{1.26}$$

According to matrix product, the expressions of the generic element on row p and column q are

$$[\mathbf{R}_{\mathrm{Tx}}]_{p,q} = \mathbb{E}\left[\mathrm{row}_p\left(\mathbf{H}_{\mathrm{ULA}}^{\mathsf{H}}\right)\mathrm{col}_q\left(\mathbf{H}_{\mathrm{ULA}}\right)\right] = \mathbb{E}\left[\left(\mathrm{col}_p\left(\mathbf{H}_{\mathrm{ULA}}\right)\right)^{\mathsf{H}}\mathrm{col}_q\left(\mathbf{H}_{\mathrm{ULA}}\right)\right] \tag{1.27}$$

and

$$[\mathbf{R}_{\mathrm{Rx}}]_{p,q} = \mathbb{E}\left[\mathrm{row}_p\left(\mathbf{H}_{\mathrm{ULA}}\right)\mathrm{col}_q\left(\mathbf{H}_{\mathrm{ULA}}^{\mathsf{H}}\right)\right] = \mathbb{E}\left[\mathrm{row}_p\left(\mathbf{H}_{\mathrm{ULA}}\right)\left(\mathrm{row}_q\left(\mathbf{H}_{\mathrm{ULA}}\right)\right)^{\mathsf{H}}\right]. \tag{1.28}$$

Starting from (1.27) we have

$$\begin{aligned}[\mathbf{R}_{\mathrm{Tx}}]_{p,q} =& \frac{1}{L}\mathbb{E}\left[\sum_{i=1}^{N}\sum_{\ell=1}^{L}\sum_{o=1}^{L} g_\ell^* g_o e^{j\zeta D(p-1)\sin\phi_\ell^{(t)}} e^{-j\zeta D(q-1)\sin\phi_o^{(t)}}\right] \\ =& \frac{N}{L}\sum_{\ell=1}^{L}\sum_{o=1}^{L}\mathbb{E}\left[g_\ell^* g_o e^{j\zeta D(p-1)\sin\phi_\ell^{(t)}} e^{-j\zeta D(q-1)\sin\phi_o^{(t)}}\right],\end{aligned} \tag{1.29}$$

as the terms in the summation are independent of the row index $i = 1, \ldots, N$. Exploiting the independence between the gains g and the angle of rays ϕ, the expectations in (1.29) are equal to

$$\begin{cases}\mathbb{E}\left[|g_\ell|^2\right]\mathbb{E}\left[e^{j\zeta D(p-q)\sin\phi_\ell^{(t)}}\right] & \text{if} \quad \ell = o \\ \underbrace{\mathbb{E}\left[g_\ell^*\right]}_{0}\underbrace{\mathbb{E}\left[g_o\right]}_{0}\mathbb{E}\left[e^{jkD(p-1)\sin\phi_\ell^{(t)}} e^{-j\zeta D(q-1)\sin\phi_o^{(t)}}\right] = 0 & \text{if} \quad \ell \neq o,\end{cases} \tag{1.30}$$

therefore (1.29) can be rewritten more compactly

$$[\mathbf{R}_{\mathrm{Tx}}]_{p,q} = \frac{N}{L}\sum_{\ell=1}^{L}\underbrace{\mathbb{E}\left[|g_\ell|^2\right]}_{=1}\mathbb{E}\left[e^{j\zeta D(p-q)\sin\phi_\ell^{(t)}}\right] = N\mathbb{E}\left[e^{j\zeta D(p-q)\sin\phi^{(t)}}\right], \tag{1.31}$$

where from (1.7) $\phi_\ell^{(t)} \sim \mathcal{U}\left[\phi_{\min};\, \phi_{\max}\right]$ for each $\ell = 1, \ldots, L$, hence, for simplicity, the subscript ℓ is dropped.
Similarly, the generic entry on row p and column q of the correlation matrix $\mathbf{R}_{\mathrm{Rx}}$ is equal to

$$[\mathbf{R}_{\mathrm{Rx}}]_{p,q} = M\mathbb{E}\left[e^{j\zeta D(p-q)\sin\phi^{(r)}}\right]. \tag{1.32}$$

From (1.7) $\phi^{(t)}$ and $\phi^{(r)}$ are both distributed as a random variable denoted by ϕ, uniform in $[\phi_{\min};\, \phi_{\max}]$, characterized by a probability density function (PDF) equal to

$$f_\phi(a) = \begin{cases}\frac{1}{\phi_{\max}-\phi_{\min}}, & a \in [\phi_{\min};\, \phi_{\max}] \\ 0, & \text{otherwise.}\end{cases} \tag{1.33}$$

Applying the expectation law of a function of a random variable, we are able to provide a closed form expression for the generic entry on row p and column q of the Tx correlation matrix

$$[\mathbf{R}_{\mathrm{Tx}}]_{p,q} = \frac{N}{\phi_{\max} - \phi_{\min}} \int_{\phi_{\min}}^{\phi_{\max}} e^{j\zeta D(p-q)\sin a} da \tag{1.34}$$

and of the Rx correlation matrix

$$[\mathbf{R}_{\mathrm{Rx}}]_{p,q} = \frac{M}{\phi_{\max} - \phi_{\min}} \int_{\phi_{\min}}^{\phi_{\max}} e^{j\zeta D(p-q)\sin a} da. \tag{1.35}$$

We note that the amplitudes of the correlation matrix entries are independent of the number of rays L for the ULA channel model.

Numerical examples of ULA correlation

A couple of numerical examples for the amplitude of (1.34) with $\phi_{\min} = -60°$, $\phi_{\max} = 60°$, wavelength $\lambda = 0.005$ m, $M = 6$, $L = 20$, are given with an antenna separation $D = \lambda/5$

$$\mathrm{abs}\left(\frac{1}{N}\mathbf{R}_{\mathrm{TX}}\right) = \begin{bmatrix} 1 & 0.78 & 0.28 & 0.16 & 0.30 & 0.13 \\ 0.78 & 1 & 0.78 & 0.28 & 0.16 & 0.30 \\ 0.28 & 0.78 & 1 & 0.78 & 0.28 & 0.16 \\ 0.16 & 0.28 & 0.78 & 1 & 0.78 & 0.28 \\ 0.30 & 0.16 & 0.28 & 0.78 & 1 & 0.78 \\ 0.13 & 0.30 & 0.16 & 0.28 & 0.78 & 1 \end{bmatrix} \tag{1.36}$$

and $D = 2\lambda$

$$\mathrm{abs}\left(\frac{1}{N}\mathbf{R}_{\mathrm{TX}}\right) = \begin{bmatrix} 1 & 0.12 & 0.01 & 0.06 & 0.02 & 0.04 \\ 0.12 & 1 & 0.12 & 0.01 & 0.06 & 0.02 \\ 0.01 & 0.12 & 1 & 0.12 & 0.01 & 0.06 \\ 0.06 & 0.01 & 0.12 & 1 & 0.12 & 0.01 \\ 0.02 & 0.06 & 0.01 & 0.12 & 1 & 0.12 \\ 0.04 & 0.02 & 0.06 & 0.01 & 0.12 & 1 \end{bmatrix}, \tag{1.37}$$

We observe that by increasing D leads to a decreasing correlation between elements. Moreover, for $D = \lambda/5$ the correlation between adjacent element can be quite high.

1.1.3 Remarks on the number of rays

Both ULA and UPA channels given by (1.19) need a value for L. How great is the number of rays due to reflections or difraction phenomena in a mm-wave scenario? Experiments [3, pp.314] at 38 GHz show that, in absence of rain and with a clear line of sight, no multipath reception could happen. This may be expected, since the specular reflected wave is reduced due the the rough surface scattering, moreover reflected waves with large angle of arrival are rejected by directional antenna radiation patterns. At higher frequencies, (more than 60GHz) these considerations are

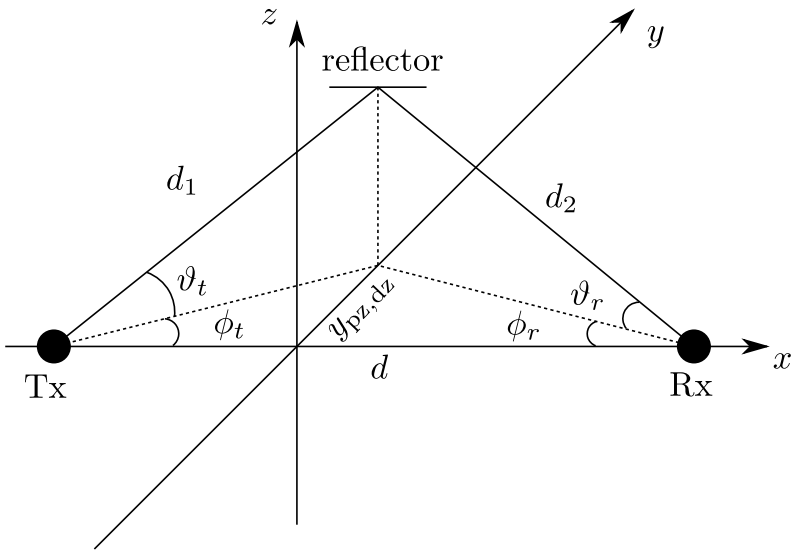

Figure 1.4: Geometrical reflection model.

much appreciated because scattering due to irregular surface is greater and antenna radiation patterns narrower. However multipath may be observed during rain and also in clear weather conditions, if the path is obstructed by foliage, or there are reflecting objects near the direction of propagation.
At this point a ray-tracing simulation for a given propagation environment may be a solution, but we are interested in a general approach, oriented to an estimate of L.
In [3, pp. 316], a simple geometrically based mm-wave channel model is developed, and it is summarized in the next sections.

Multipath considerations for mm-waves

The reflection coefficient, defined as the power percentage conserved after a ray undergoes a reflection, is dependent on polarization of the electro-magnetic field, angle of incidence, dielectric properties of the scatter and its surface roughness. In [16] some expressions are given.
When highly directional antennas are used, strong multipath components are caused only by scatters close to the line of sight (LOS) path, therefore the angle between the incident wave and reflecting surface is very small, hence effects of the surface roughness are negligible and the reflection coefficient has an amplitude close to unit value. For a worst case scenario each scatter in next considerations is assumed to be a perfect reflector. The simple reflection model in Figure 1.4 is considered and the definitions of "relative received power" and "excess delay time" are given for a scatter present in a point of coordinates x, y and z.

Relative received power

The relative received power of the ℓ-th ray, ΔP_ℓ, is defined as the ratio between the power of the LOS ray weighted by the radiation pattern of Rx and Tx antennas and

the power of the ℓ-th ray. If d represents the LOS length between antennas and if the distance covered by the ℓ-th ray from transmitter to receiver is $d_1 + d_2$, as in Figure 1.4, it is

$$\Delta P_\ell(x,\, y,\, z) = \Lambda_t\left(\phi_t,\, \vartheta_t\right) \Lambda_r\left(\phi_r,\, \vartheta_r\right) \left(\frac{d}{d_1 + d_2}\right)^2, \tag{1.38}$$

where the angles are defined in Figure 1.4.

Excess delay time

The *excess delay* time is defined as the delay between time of arrival of ℓ-th ray and LOS

$$\tau_\ell(x,\, y,\, z) = \frac{(d_1 + d_2 - d)}{c}. \tag{1.39}$$

Indeed it is path length difference between the two path divided by the propagation speed, in this case the speed of light c.

Relative power zone and excess delay zone

By equating (1.38) and (1.39) to a couple of constant desired values, a space surface can be drawn in an appropriate space system. For example, a surface generated by (1.38) with $[\Delta P_\ell]_{\mathrm{dB}} = 10$ represent the points loci where, if an ideal reflector is present, a reflected ray, 10 dB less powerful than the direct one, is generated. Moreover a reflector on the surface generated by (1.39) with $\tau = 3$ ns may generate a ray delayed 3 ns respect to the direct one. The surfaces are called relative power zone and excess delay zone respectively. A couple of illustrative example in azimuth plane are provided in [3, pp. 319].

A simple estimate of L

By overlaying the plots onto a site map and identifying potential scatters, the delay and power of possible multipath components can be estimated. On the other hand, by fixing the maximum ΔP_ℓ and τ_ℓ for the considered system, estimation of the number of significant rays L can be given by considering, as an example, only first order reflections.
We are interested on the maximum dimension of the space volume, inside which, objects can act as potential reflectors. We denote with y_{pz} and y_{dz} the radii of a couple of imaginary cylinders between Tx and Rx on which surfaces, potential scatters, could generate reflected rays described by a relative power and excess delay, defined in (1.38) and (1.39), respect to the direct ray. In Tables 1.1 and 1.2 are given example values for the transversal dimension of relative power zone, y_{pz} and of excess delay time zone, y_{dz}, showed together, for simplicity, in Figure 1.4. These values are taken from the configuration, presented in [3, pp. 319], of a system with a rectangular horn antenna as the transmitter and a circular parabolic antenna as the receiver. Given d and the maximum ΔP_ℓ (for example equal to

Table 1.1: Relative power zone radii, y_{pz}.

y_{pz} [m]		ΔP [dB]				
		5	10	20	30	35
d [km]	0.5	7	10	19	35	46
	1	14.5	19.5	38.5	70	92
	2	29	39	77	140	185
	5	72	96	192	352	461

Table 1.2: Excess delay zone radii, y_{dz}.

y_{dz} [m]		τ [ns]				
		10	20	30	40	50
d [km]	0.5	27.4	38.8	47.6	55.1	61.7
	1	38.8	54.9	67.2	77.7	86.9
	2	54.8	77.5	95.0	19.7	122.7
	3	67.1	94.9	116.3	134.3	150.2
	4	77.5	109.6	134.2	155.0	173.4
	5	86.6	122.5	150.1	173.3	193.8

the sensitivity of the receiver), an estimation of L can be provided with a few steps procedure:

1. find out y_{pz} from Table 1.1;
2. enumerate the number L' of possible scatters inside a cylinder with a radius equal to y_{pz}, with the help of a site map;
3. for each reflector evaluate the reflected ray excess delay τ_ℓ from Table 1.2, and compare it with the symbol period;
4. the number L of rays is comparable to the number[2] of reflectors L' and the delay of each ray can be estimated by using Table 1.2.

[2] L may be equal to reflectors number only if rays generated by first order reflections are considered, otherwise L my be greater than the number of scatters if second or third order reflections are taken into account.

Chapter 2

Optimal and sub-optimal beamforming

At the beginning of this chapter we introduce the general framework for the performance analysis, in terms of signal to noise ratio (SNR), of a mm-wave MIMO system.
Next we discuss, from a theoretical point of view, the state of art and various sub-optimal array gain techniques for conventional MIMO systems. These approaches require all antenna signals to be independently analog acquired and jointly processed at base band in the digital domain. This aspect could be a problem in the physical implementation of low cost wireless terminals, where hardware complexity should be limited.
Finally we investigate methods present in the technical literature that shift part of the spatial signal processing from base-band to the analog RF front-end in order to reduce the number of analog to digital converters. This perspective of reducing the hardware complexity should be very interesting for mm-wave systems.

2.1 SNR definitions

We introduce various definitions of SNR that are used later to evaluate and compare the performance of the systems considered. We start by defining the average SNR, with respect to noise and channel gain, of a simple single input single output (SISO) system denoted here additive white Gaussian noise (AWGN) channel. Next, we extend the definition of SNR for a MIMO system.

2.1.1 AWGN channel

System model

Figure 2.1 shows the base-band equivalent of a flat-fading AWGN channel system, while Table 2.1 gives the description of the signals. The noise n is Gaussian distributed with zero mean and variance σ_n^2,

$$n \sim \mathcal{CN}(0,\ \sigma_n^2). \tag{2.1}$$

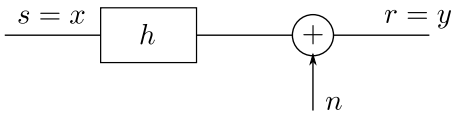

Figure 2.1: AWGN system.

Table 2.1: Signals associated to the AWGN system.

$x \in \mathbb{C}$	information symbol
$s \in \mathbb{C}$	transmitted signal
$h \in \mathbb{C}$	channel gain
$n \in \mathbb{C}$	additive noise
$r \in \mathbb{C}$	received signal
$y \in \mathbb{C}$	received symbol at decision point

In the system considered

$$s = x \qquad \text{and} \qquad r = y \tag{2.2}$$

because there is no presence of precoding or combining that could invalidates (2.2).

SNR expression

The received signal, considering (2.2), is equal to

$$y = r = hs + n = hx + n. \tag{2.3}$$

We denote with

$$\mathtt{M}_h = \mathbb{E}\left[|h|^2\right] \qquad \text{and} \qquad \mathtt{M}_x = \mathbb{E}\left[|x|^2\right] \tag{2.4}$$

the statistical power of the channel gain h and the information symbol x respectively. The expression of the average SNR at receiver, called Γ_{AWGN}, is given by

$$\Gamma_{\text{AWGN}} = \frac{\mathbb{E}_{h,x}\left[|hx|^2\right]}{\mathbb{E}_n\left[|n|^2\right]} = \frac{\mathbb{E}_h\left[|h|^2\right]\mathbb{E}_x\left[|x|^2\right]}{\sigma_n^2} = \frac{\mathtt{M}_h\mathtt{M}_x}{\sigma_n^2}. \tag{2.5}$$

Setting the statistical power of the input sample and of the channel to one

$$\mathtt{M}_x = \mathtt{M}_h = 1, \tag{2.6}$$

yields

$$\Gamma_{\text{AWGN}} = \frac{1}{\sigma_n^2}. \tag{2.7}$$

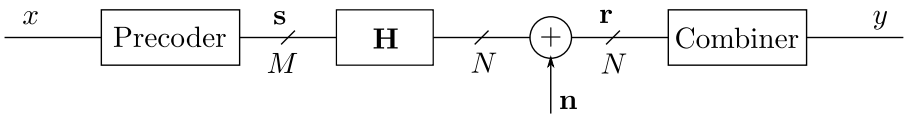

Figure 2.2: MIMO system.

Table 2.2: Signals associated to the MIMO system.

$M \in \mathbb{N}$	number of transmitted antennas
$N \in \mathbb{N}$	number of receive antennas
$x \in \mathbb{C}$	information symbol
$\mathbf{s} \in \mathbb{C}^M$	transmitted signal vector
$\mathbf{H} \in \mathbb{C}^{N \times M}$	matrix of channel gains
$\mathbf{n} \in \mathbb{C}^N$	additive noise vector
$\mathbf{r} \in \mathbb{C}^N$	received signal vector
$y \in \mathbb{C}$	received symbol at decision point

2.1.2 MIMO channel

We consider now a generic MIMO configuration with M antennas at the transmitter and N antennas at the receiver, characterized by a single input stream and a single output stream[1]. We provide a SNR definition associated to a specific channel realization and averaged with respect to the noise contribution. Moreover, we define a functional that measures the improvement, in terms of SNR, of the MIMO system respect to the AWGN case.

System model

Figure 2.2 shows the system considered and the *precoder* and *combiner* elements represent the most general form of processing that we prevision. Table 2.2 gives the description of the used symbols. The received vector noise $\mathbf{n}$ is modelled as a complex circular independent identically distributed (i.i.d.) Gaussian noise vector,

$$\mathbf{n} \sim \mathcal{N}\left(0,\, \sigma_n^2 \mathbf{I}_N\right), \tag{2.8}$$

where σ_n^2 is the variance of the generic entry of $\mathbf{n}$, which is distributed as (2.1).

SNR expression

At the decision point, for a given channel realization $\mathbf{H}$, after the combining operation of received signals, we consider the SNR, expressed by Γ, as the ratio between the statistical power of useful part of the signal over the statistical power of the

[1]The multiple antennas architectures considered throughout all this work are aimed at increasing the SNR, exploiting Tx and Rx diversity. In this scenario we are talking about *array gain*, see [17, p. 7]. In other words, we are interested on exploiting the array gain rather than the multiplexing gain of a multi antenna system.

noise component. Next we normalize Γ to the channel noise and define the metric

$$\gamma = \frac{\Gamma}{\Gamma_{\text{AWGN}}}. \tag{2.9}$$

Moreover we will characterize the system performance on average with respect to the channel and define

$$\overline{\Gamma} = \mathbb{E}_{\mathbf{H}}\left[\Gamma\right], \qquad \overline{\gamma} = \mathbb{E}_{\mathbf{H}}\left[\gamma\right] = \frac{\overline{\Gamma}}{\Gamma_{\text{AWGN}}}, \tag{2.10}$$

where $\mathbb{E}_{\mathbf{H}}\left[\cdot\right]$ denotes that the expectation is taken with the respect to the channel $\mathbf{H}$.

2.2 Optimal beamforming (state of art)

We seek now to design the optimal *precoder* and *combiner* of Figure 2.2 in order to maximize γ in (2.9). We will see that the optimal solution is represented, both at Tx and Rx side, by the maximum ratio beamforming (MRB).

2.2.1 Framing of the problem

The *precoder* and *combiner* in Figure 2.2 are substituted by two vectors of weights called *beamformers*. Let

$$\mathbf{f} = \begin{bmatrix} f_1 & \cdots & f_M \end{bmatrix}^{\mathsf{T}} \in \mathbb{C}^{M\times 1} \tag{2.11}$$

and

$$\mathbf{u} = \begin{bmatrix} u_1 & \cdots & u_N \end{bmatrix}^{\mathsf{T}} \in \mathbb{C}^{N\times 1} \tag{2.12}$$

be the transmit and receive beamformers. The input stream modulates the Tx antennas array by the weights of $\mathbf{f}$, while the received vector signal is recombined to an output single stream by weight vector $\mathbf{u}$ from the array of antennas at receiver. Figure 2.3 represents the described system. The transmitted vector signal $\mathbf{s}$ is represented by the entries

$$\mathbf{s} = \begin{bmatrix} s_1 & \cdots & s_M \end{bmatrix}^{\mathsf{T}} \in \mathbb{C}^{M\times 1}, \tag{2.13}$$

and its expression is

$$\mathbf{s} = \mathbf{f}x. \tag{2.14}$$

We note that if the transmitted signal $\mathbf{s}$ is subject to an average power constraint P it implies that also the power of the beamformer $\mathbf{f}$ is constrained and it must be,

$$\mathbb{E}_x\left[\|\mathbf{s}\|^2\right] = \|\mathbf{f}\|^2 \mathtt{M}_x \leq P \qquad \Longrightarrow \qquad \|\mathbf{f}\|^2 \leq \frac{P}{\mathtt{M}_x}. \tag{2.15}$$

The received signal $\mathbf{r}$ is denoted by the vector

$$\mathbf{r} = \begin{bmatrix} r_1 & \cdots & r_N \end{bmatrix}^{\mathsf{T}} \in \mathbb{C}^{N\times 1} \tag{2.16}$$

and it is equal to

$$\mathbf{r} = \mathbf{H}\mathbf{f}x + \mathbf{n}. \tag{2.17}$$

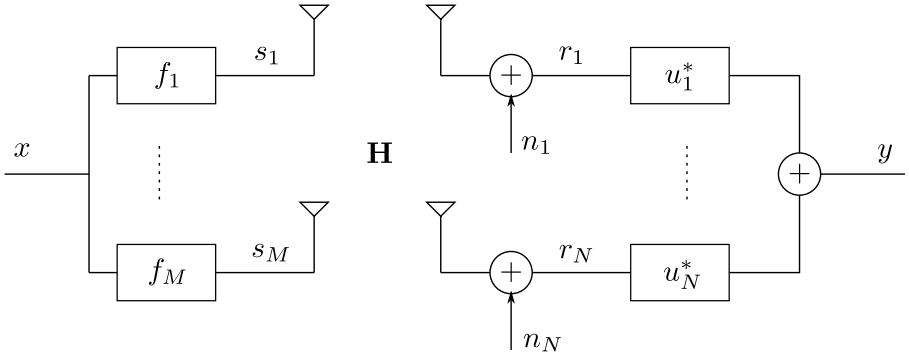

Figure 2.3: System model of optimal beamformer.

SNR expression

The reconstructed signal y is equal to

$$y = \mathbf{u}^{\mathsf{H}}\mathbf{r} = \mathbf{u}^{\mathsf{H}}\mathbf{H}\mathbf{f}x + \mathbf{u}^{\mathsf{H}}\mathbf{n}, \tag{2.18}$$

where $\mathbf{n}$ is defined in (2.8).
Without loss of generality, let is consider x with unitary average power ($\mathtt{M}_x = 1$) and a transmission power constraint $P = 1$. Hence from (2.15) it must be $\|\mathbf{f}\|^2 = 1$. Moreover we assume a unit statistical power for each entry of the channel matrix $\mathbf{H}$, as from (2.6)

$$\mathbb{E}\left[\left|[\mathbf{H}]_{p,q}\right|^2\right] = 1, \qquad p = 1, \ldots, N, \qquad q = 1, \ldots, M. \tag{2.19}$$

If also the power of the combiner is equal to one[2] ($\|\mathbf{u}\|^2 = 1$) we can provide the expression of Γ for the system if Figure 2.3

$$\Gamma = \frac{\mathbb{E}_x\left[\left|\mathbf{u}^{\mathsf{H}}\mathbf{H}\mathbf{f}x\right|^2\right]}{\mathbb{E}_n\left[\left|\mathbf{u}^{\mathsf{H}}\mathbf{n}\right|^2\right]} = \frac{\left|\mathbf{u}^{\mathsf{H}}\mathbf{H}\mathbf{f}\right|^2}{\sigma_n^2}, \tag{2.20}$$

[2]A power constraint on the combiner $\mathbf{u}$ has no effect on system performance; however, for simplicity, from now on we consider $\|\mathbf{u}\|^2 = 1$ unless otherwise specified.

which is dependent on the channel realization $\mathbf{H}$ and, therefore, random distributed. It can be worth to state that

$$\begin{aligned}
\mathbb{E}_n\left[\left|\mathbf{u}^{\mathsf{H}}\mathbf{n}\right|^2\right] &= \mathbb{E}\left[\left|\sum_{i=1}^{N} u_i^* n_i\right|^2\right] \\
&= \mathbb{E}_n\left[\sum_{i=1}^{N}\sum_{o=1}^{N} u_i^* n_i u_o n_o^*\right] \\
&\overset{(1)}{=} \sum_{i=1}^{N} \mathbb{E}\left[|u_i^* n_i|^2\right] \\
&= \sigma_n^2 \sum_{i=1}^{N} |u_i^*|^2 \\
&= \sigma_n^2 \left\|\mathbf{u}\right\|^2 \\
&= \sigma_n^2,
\end{aligned} \tag{2.21}$$

the equality (1) comes from the zero mean and statistical independence of the entry of $\mathbf{n}$.
In turn, from (2.20), (2.9) becomes

$$\gamma = \left|\mathbf{u}^{\mathsf{H}}\mathbf{H}\mathbf{f}\right|^2. \tag{2.22}$$

This means that for the system in Figure 2.3 γ is independent of the power of noise σ_n^2.
We note that for a SISO configuration with $M = N = 1$, it is $\mathbf{H} = h$, $\mathbf{f} = \mathbf{u} = 1$. Indeed all beamformers approach have identical performance and, from (2.22), $\gamma = |h|^2$. As $|h|$ is Rayleigh distributed and has a unit statistical power, $\mathbb{E}\left[|h|^2\right] = 1$. Instead $\gamma = |h|^2$ is exponential distributed and its mean and variance are given by:

$$\overline{\gamma} = \mathbb{E}\left[\gamma\right] = \mathbb{E}\left[|h|^2\right] = 1 \qquad \sigma_\gamma^2 = \mathtt{M}_\gamma - \overline{\gamma}^2 = 1 \tag{2.23}$$

because the statistical power of an exponential random variable is equal to $\mathtt{M}_\gamma = 2\left(\mathbb{E}\left[|h|^2\right]^2\right) = 2$.

The optimization problem

We are focused now on finding weight vectors $\mathbf{f}$ and $\mathbf{u}$ that maximize the functional (2.22). The optimization problem can be outlined as

$$\begin{aligned}
\underset{\mathbf{f},\,\mathbf{u}}{\arg\max} \quad & \left|\mathbf{u}^{\mathsf{H}}\mathbf{H}\mathbf{f}\right|^2 \\
\text{subject to} \quad & \left\|\mathbf{f}\right\|^2 = 1 \\
& \left\|\mathbf{u}\right\|^2 = 1.
\end{aligned} \tag{2.24}$$

The constraints on the squared norm of the beamformers suggest that γ should be maximized by choosing the optimal $\mathbf{f}$ and $\mathbf{u}$ with no increase of the needed power.

2.2.2 Singular value decomposition approach (SVD-MRB)

The solution of problem (2.24) is well known in the literature [17, pg. 44] and implies the singular value decomposition (SVD) decomposition of channel matrix $\mathbf{H}$. In the next section we briefly summarize the procedure and outline the maximum value reached by γ for a given channel, next, some numerical values of $\overline{\gamma}$ will be given.

The SVD-MRB solution

The complex $N \times M$ channel matrix $\mathbf{H}$ with rank ρ has the following SVD decomposition [17]

$$\mathbf{H} = \mathbf{U}\boldsymbol{\Xi}\mathbf{F}^{\mathsf{H}} = \begin{bmatrix}\mathbf{u}_1 & \dots & \mathbf{u}_N\end{bmatrix} \begin{bmatrix}\xi_1 & \cdots & 0 \\ \vdots & \ddots & \vdots \\ 0 & \cdots & \xi_\rho \\ 0 & \cdots & 0 \\ \vdots & \ddots & \vdots \\ 0 & \dots & 0\end{bmatrix} \begin{bmatrix}\mathbf{f}_1^{\mathsf{H}} \\ \vdots \\ \mathbf{f}_M^{\mathsf{H}}\end{bmatrix}, \tag{2.25}$$

where

- the non-zero diagonal real values of $\boldsymbol{\Xi} \in \mathbb{R}^{N\times M}$ are called *singular values* of $\mathbf{H}$ and they satisfy

$$\xi_1 \geq \xi_2 \geq \cdots \geq \xi_\rho \geq 0, \tag{2.26}$$

- the column vectors of $\mathbf{U} \in \mathbb{C}^{N\times N}$, denoted by $\mathbf{u}_1, \dots, \mathbf{u}_N$ are the *left singular vectors*[3] of $\mathbf{H}$,

- the column vectors of $\mathbf{F} \in \mathbb{C}^{M\times M}$, denoted by $\mathbf{f}_1, \dots, \mathbf{f}_M$ are the *right singular vectors* of $\mathbf{H}$.

The complex matrices $\mathbf{U}$ and $\mathbf{F}$ are said to be *unitary*, which entails

$$\mathbf{U}^{\mathsf{H}}\mathbf{U} = \mathbf{U}\mathbf{U}^{\mathsf{H}} = \mathbf{I}_N, \qquad \mathbf{F}^{\mathsf{H}}\mathbf{F} = \mathbf{F}\mathbf{F}^{\mathsf{H}} = \mathbf{I}_M. \tag{2.27}$$

It can be shown that the optimal beamformers for the problem (2.24), denoted by $\mathbf{f}_{\mathrm{SVD-MRB}}$ and $\mathbf{u}_{\mathrm{SVD-MRB}}$ are equal to the right singular vector associated to the largest sigular value and to the left sigular vector associated to the largest singular value respectively. In symbols

$$\mathbf{f}_{\mathrm{SVD-MRB}} = \mathbf{f}_1 \quad \text{and} \quad \mathbf{u}_{\mathrm{SVD-MRB}} = \mathbf{u}_1. \tag{2.28}$$

[3]We recall that the left singular vectors of a $N \times M$ matrix $\mathbf{A}$ are the eigenvectors of the hermitian matrix $\mathbf{A}\mathbf{A}^{\mathsf{H}}$, while the right singular vectors of the same matrix are the eigenvectors of $\mathbf{A}^{\mathsf{H}}\mathbf{A}$. Both $\mathbf{A}\mathbf{A}^{\mathsf{H}}$ and $\mathbf{A}^{\mathsf{H}}\mathbf{A}$ have the same eigenvalues which are equal to the squared singular values.

We note that the constraints on the squared norms of beamformers are satisfied as from (2.27)

$$\|\mathbf{f}_1\|^2 = \mathrm{tr}\left(\mathbf{f}_1^{\mathsf{H}}\mathbf{f}_1\right) = 1 \quad \text{and} \quad \|\mathbf{u}_1\|^2 = \mathrm{tr}\left(\mathbf{u}_1^{\mathsf{H}}\mathbf{u}_1\right) = 1. \tag{2.29}$$

Applying (2.28), γ in (2.22) is equal to

$$\begin{aligned}
\gamma &= \left|\mathbf{u}_1^{\mathsf{H}}\mathbf{H}\mathbf{f}_1\right|^2 \\
&= \left|\mathbf{u}_1^{\mathsf{H}}\begin{bmatrix}\mathbf{u}_1 & \dots & \mathbf{u}_N\end{bmatrix}\begin{bmatrix}\xi_1 & \cdots & 0 \\ \vdots & \ddots & \vdots \\ 0 & \dots & \xi_\rho \\ 0 & \cdots & 0 \\ \vdots & \ddots & \vdots \\ 0 & \dots & 0\end{bmatrix}\begin{bmatrix}\mathbf{f}_1^{\mathsf{H}} \\ \vdots \\ \mathbf{f}_M^{\mathsf{H}}\end{bmatrix}\mathbf{f}_1\right|^2 \\
&= \left|\underbrace{\left(\mathbf{u}_1^{\mathsf{H}}\mathbf{u}_1\right)}_{1}\underbrace{\left(\mathbf{f}_1^{\mathsf{H}}\mathbf{f}_1\right)}_{1}\xi_1 + \cdots + \underbrace{\left(\mathbf{u}_1^{\mathsf{H}}\mathbf{u}_\rho\right)}_{0}\underbrace{\left(\mathbf{f}_1^{\mathsf{H}}\mathbf{f}_\rho\right)}_{0}\xi_\rho\right|^2 \\
&= \xi_1^2,
\end{aligned} \tag{2.30}$$

which is equal to the largest eigenvalue of the Hermitian matrices $\mathbf{H}^{\mathsf{H}}\mathbf{H}$ or $\mathbf{H}\mathbf{H}^{\mathsf{H}}$. From (2.10) the average performance with respect to the channel is measured by

$$\overline{\gamma} = \mathbb{E}_{\mathbf{H}}\left[\xi_1^2\right], \tag{2.31}$$

some numerical values are given.

Performance analysis

Let us consider a $L = 20$ rays environment and a carrier with a wave length $\lambda = 0.005$ m. Two ULA arrays at Tx and Rx sides, made of antenna elements separated by $D = \lambda/5$, characterizes the channel, which is modelled as a matrix $\mathbf{H}_{\mathrm{ULA}} \in \mathbb{C}^{N\times M}$ expressed by (1.19). The transmitter and receiver rays angles, ϕ_t and ϕ_r, are both uniform random variables in the sector $[-60°;\ 60°]$ on azimuth plane, as from (1.7). Figure 2.4 shows how $\overline{\gamma}$ for the optimal SVD-MRB approach increases with the number of Tx antennas and Rx antennas. Table 2.3 collects some standard deviation values of (2.30). Finally it is interesting to see the distribution of the random variable (2.30) around its mean value for different channel realizations. In this perspective we consider the cumulative distribution function (CDF) of $\gamma = \xi_1^2$ defined as

$$F_\gamma(a) = \Pr\left(\gamma \le a\right) \qquad a \in \mathbb{R}, \tag{2.32}$$

while its PDF

$$f_\gamma(a) = \frac{dF_\gamma(a)}{da}. \tag{2.33}$$

Figure 2.5, reports a simulation of $f_\gamma(a)$ over 5000 channel realizations. From Table 2.3 and Figure 2.5 we note that the standard deviation σ_γ is comparable with the mean and therefore very high, this is due to the statistical properties of the channel considered.

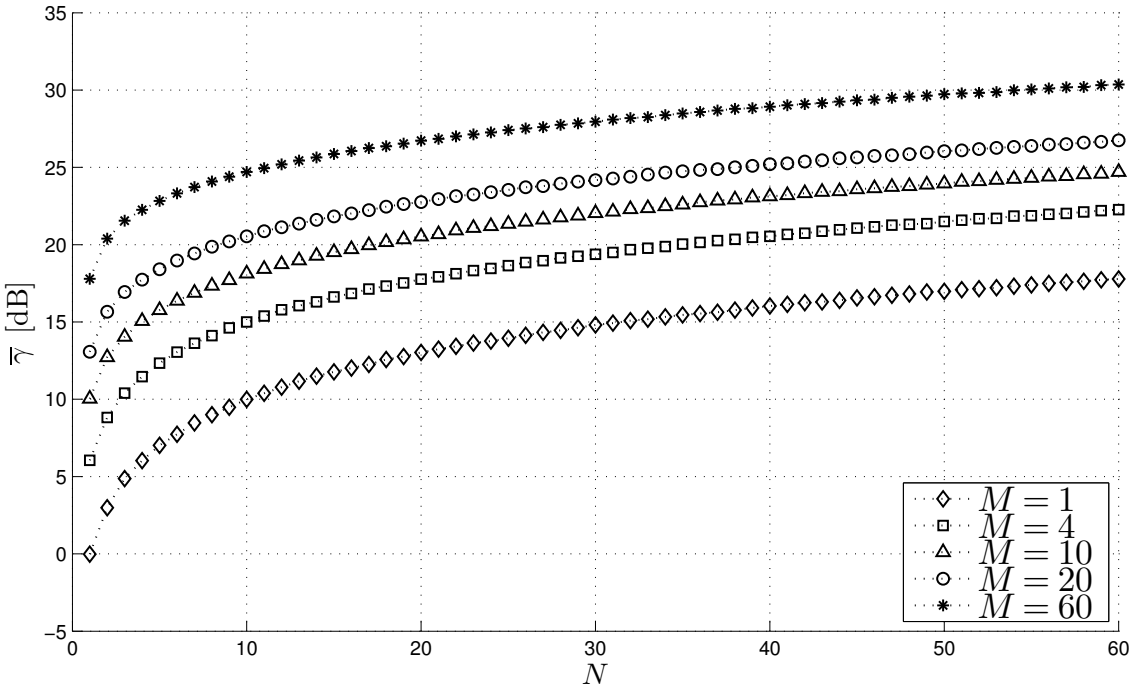

Figure 2.4: Simulated $\overline{\gamma}$ in (2.31) for various values of N and M, over 5000 channel realizations.

Table 2.3: Simulated values of the standard deviation, σ_γ, over 5000 channel realizations for SVD-MRB.

σ_γ [dB]		M				
		1	4	10	20	60
N	1	-0.01	4.65	7.24	9.34	12.64
	4	4.50	9.21	11.73	13.57	17.14
	10	7.17	11.59	13.90	15.97	19.60
	20	9.34	13.65	15.91	17.91	21.70
	60	12.65	17.22	19.60	21.63	25.39

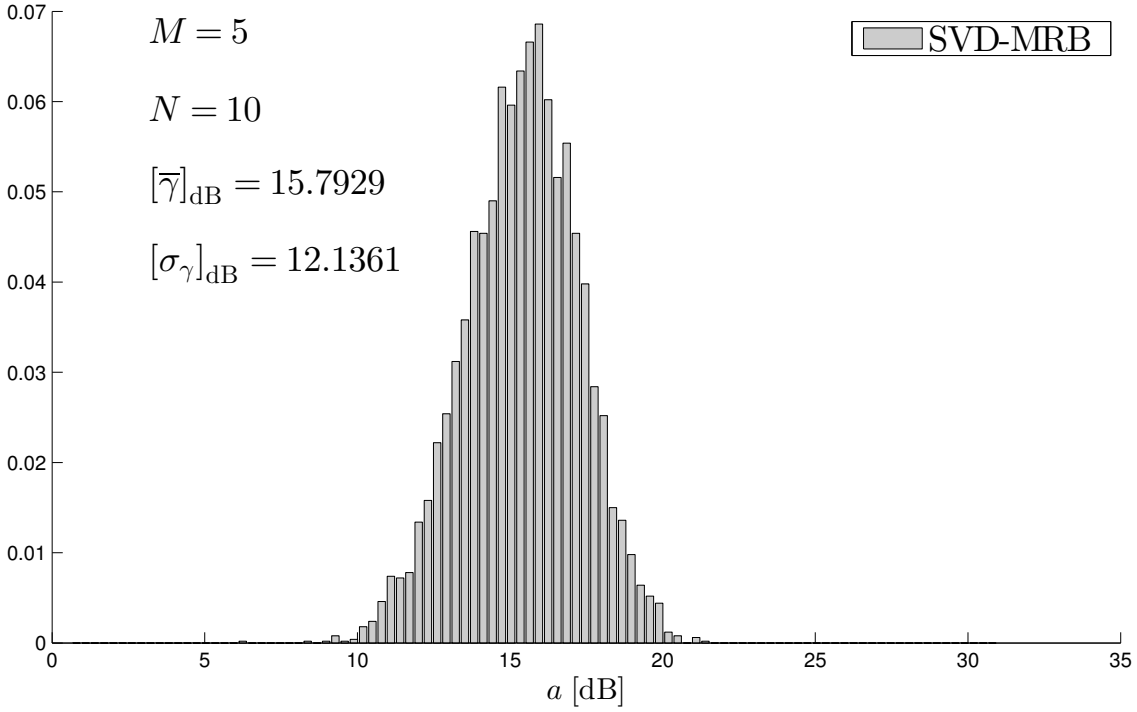

Figure 2.5: Simulated PDF of γ as from (2.30) for 5000 channel realizations.

Remarks on performance

As expected, from Figure 2.4, performance of the SVD-MRB improves with the number of Tx and Rx antennas. We note also that (2.30) is independent of the noise power σ_n^2, in other words the improvement of the SNR with respect to the AWGN case does not care about how high is the noise power. Of course this is an ideal solution: the perfect knowledge of the channel matrix is required at Rx and Tx side, moreover the procedure implies the SVD decomposition of $\mathbf{H}$ and this could be a challenging task from an implementation point of view. The result given by SVD-MRB, however, is important and represents an *upper-bound* for other approaches.

2.2.3 Iterative approach (I-MRB)

Applying the SVD decomposition of the channel matrix, the SVD-MRB provides a solution, in closed form, to the problem (2.24).
We investigate now an iterative approach to get the same solution [18].
For multiple input single output (MISO) ($N = 1$) or single input multiple output (SIMO) ($M = 1$) systems, the optimal solution to (2.24) is provided by simple expressions known in literature as *maximum ratio transmission* and *maximum ratio reception*. Part of the work in [18] exploits the simple MISO and SIMO solutions cyclically in a procedure that converges in few iterations ($3 \div 7$) to the SVD-MRB performance.
In next two sections this procedure is explained from a general point of view. This

will also represent a starting point for the resolution of (2.24) with more constraints on $\mathbf{f}$ and $\mathbf{u}$, which will be later considered for suboptimal beamforming solutions.

Splitting and reformulation of the problem

Assuming that optimal $\mathbf{f}_{\text{opt}}$ or, alternatively, $\mathbf{u}_{\text{opt}}$ is known, problem (2.24) can be splitted into an iterative SIMO and MISO optimization problem. Let us set

$$\mathbf{h}_{\text{SIMO}} = \mathbf{H}\mathbf{f}_{\text{opt}} \in \mathbb{C}^{N\times 1} \qquad \text{and} \qquad \mathbf{h}_{\text{MISO}} = \mathbf{u}_{\text{opt}}^{\mathsf{H}}\mathbf{H} \in \mathbb{C}^{1\times M}. \tag{2.34}$$

The SIMO and MISO optimization problems are, respectively, expressed by

$$\begin{array}{ll} \arg\max\limits_{\mathbf{u}} & \left|\mathbf{u}^{\mathsf{H}}\mathbf{h}_{\text{SIMO}}\right|^2 \\ \text{subject to} & \|\mathbf{u}\|^2 = 1 \end{array} \qquad \begin{array}{ll} \arg\max\limits_{\mathbf{f}} & |\mathbf{h}_{\text{MISO}}\mathbf{f}|^2 \\ \text{subject to} & \|\mathbf{f}\|^2 = 1. \end{array} \tag{2.35}$$

Let:

$$\begin{array}{lll} \mathbf{G}_{\text{SIMO}} = \mathbf{h}_{\text{SIMO}}\mathbf{h}_{\text{SIMO}}^{\mathsf{H}} & \in \mathbb{C}^{N\times N} & \mathbf{G}_{\text{MISO}} = \mathbf{h}_{\text{MISO}}^{\mathsf{H}}\mathbf{h}_{\text{MISO}} \quad \in \mathbb{C}^{M\times M} \\ \mathbf{R}_{\mathbf{u}} = \mathbf{u}\mathbf{u}^{\mathsf{H}} & \in \mathbb{C}^{N\times N} & \mathbf{R}_{\mathbf{f}} = \mathbf{f}\,\mathbf{f}^{\mathsf{H}} \quad\quad\quad \in \mathbb{C}^{M\times M}, \end{array} \tag{2.36}$$

both problems in (2.35) can be rewritten in an equivalent form

$$\begin{array}{lll} \arg\max\limits_{\mathbf{R}_{\mathbf{u}}} & \text{tr}\left(\mathbf{G}_{\text{SIMO}}\mathbf{R}_{\mathbf{u}}\right) & \\ \text{subject to} & \text{tr}\left(\mathbf{R}_{\mathbf{u}}\right) = 1 & \\ & \mathbf{R}_{\mathbf{u}} \succeq 0 & \\ & \text{rank}\left(\mathbf{R}_{\mathbf{u}}\right) = 1 & \end{array} \qquad \begin{array}{lll} \arg\max\limits_{\mathbf{R}_{\mathbf{f}}} & \text{tr}\left(\mathbf{R}_{\mathbf{f}}\mathbf{G}_{\text{MISO}}\right) & \\ \text{subject to} & \text{tr}\left(\mathbf{R}_{\mathbf{f}}\right) = 1 & \\ & \mathbf{R}_{\mathbf{f}} \succeq 0 & \\ & \text{rank}\left(\mathbf{R}_{\mathbf{f}}\right) = 1 & \end{array} \tag{2.37}$$

where $\succeq 0$ denotes that the matrix has to be positive semi-definite.
The split of MIMO optimization problem into SIMO or a MISO scenarios in (2.35) and the reformulation presented in (2.37) are not enough to carry out a simple solution. Indeed, the two optimization problems in (2.37) still remain non-convex. Note that the objective functions and power requirements are linear in $\mathbf{R}_{\mathbf{u}}$ and $\mathbf{R}_{\mathbf{f}}$, furthermore the positive semi-definite requirements are convex, however the rank-one constraints are non-convex.
The kind of problems in (2.37) can be relaxed to a convex optimization problems by omitting the rank-one constraint yielding to a semi-definite problem, which can be resolved by public domain algorithms. The solution of the relaxation may represents the optimum if it satisfies the rank-one constraint, otherwise a suboptimal solution can be found exploiting heuristics [18, pp. 5397].
Fortunately the semi-definite relaxation, in the particular case of SIMO or MISO, as the case in (2.37), leads to an optimal solution that can be given by a closed expression.

Cyclic optimization procedure

The original SNR maximization problem in (2.24) is based on the fundamental assumptions made in (2.34) that imply the knowledge, a priori, of the optimum

beamformer at transmitter and receiver for the SIMO or MISO problem, respectively. In order to bypass this issue, [18, pp. 5398] proposes a simple cyclic procedure that can be described in few steps.

step 0 Set $\mathbf{u}$ to an initial value, for example a vector where entries are all equals to $1/\sqrt{N}$);

step 1 obtain the transmitter beamformer $\mathbf{f}$ by solving the MISO problem in (2.37), setting $\mathbf{h}_{\text{MISO}} = \mathbf{u}^{\mathsf{H}}\mathbf{H}$, where $\mathbf{u}$ is fixed at its most recent value;

step 2 update the receiver beamformer $\mathbf{u}$ by solving the SIMO problem in (2.37), setting $\mathbf{h}_{\text{SIMO}} = \mathbf{H}\mathbf{f}$, where $\mathbf{f}$ was obtained in *step 1*;

step 3 iterate *step 1* and *step 2* until a given stop criterion is satisfied.

The procedure is simple and numerical simulations show that it converges in $3 \div 7$ iterations, depending on the values of M and N. Note that if the procedure is starts with the initialization of $\mathbf{f}$ instead of $\mathbf{u}$, the final result does not change.

The iterative maximum ratio beamforming (I-MRB) solution

The I-MRB approach represents the solution of problems (2.37) with only the rank-constraint relaxation, no other constraints are added, therefore, the considered optimization problems for SIMO and MISO are described by

$$\begin{array}{lll} \underset{\mathbf{R_u}}{\arg\max} & \text{tr}\left(\mathbf{G}_{\text{SIMO}}\mathbf{R}_{\mathbf{u}}\right) & \underset{\mathbf{R_f}}{\arg\max} \quad \text{tr}\left(\mathbf{R}_{\mathbf{f}}\mathbf{G}_{\text{MISO}}\right) \\ \text{subject to} & \text{tr}\left(\mathbf{R}_{\mathbf{u}}\right) = 1 & \text{subject to} \quad \text{tr}\left(\mathbf{R}_{\mathbf{f}}\right) = 1 \\ & \mathbf{R}_{\mathbf{u}} \succeq 0 & \mathbf{R}_{\mathbf{f}} \succeq 0 \end{array} \tag{2.38}$$

respectively. The optimal solutions $\mathbf{u}_{\text{I-MRB}}$ and $\mathbf{f}_{\text{I-MRB}}$ can be shown ([18, pp. 5396], [19, pp. 1459]) to be equal to

$$\mathbf{u}_{\text{I-MRB}} = \frac{\mathbf{h}_{\text{SIMO}}}{\|\mathbf{h}_{\text{SIMO}}\|} \qquad \text{and} \qquad \mathbf{f}_{\text{I-MRB}} = \frac{\mathbf{h}_{\text{MISO}}^{\mathsf{H}}}{\|\mathbf{h}_{\text{MISO}}\|}, \tag{2.39}$$

where $\mathbf{h}_{\text{SIMO}}$ and $\mathbf{h}_{\text{MISO}}$ are evaluated by the above cyclic optimization procedure. The beamformers in (2.39) are known as *maximum ratio combining* and *maximum ratio transmission*, respectively.
The corresponding SNR γ in (2.22) is given by

$$\gamma = \left|\mathbf{u}_{\text{I-MRB}}^{\mathsf{H}}\mathbf{H}\mathbf{f}_{\text{I-MRB}}\right|^2. \tag{2.40}$$

Figure 2.6 shows how the average functional (2.40), over 5000 channel realizations, converges to the SVD-MRB performance for a sample system configuration.

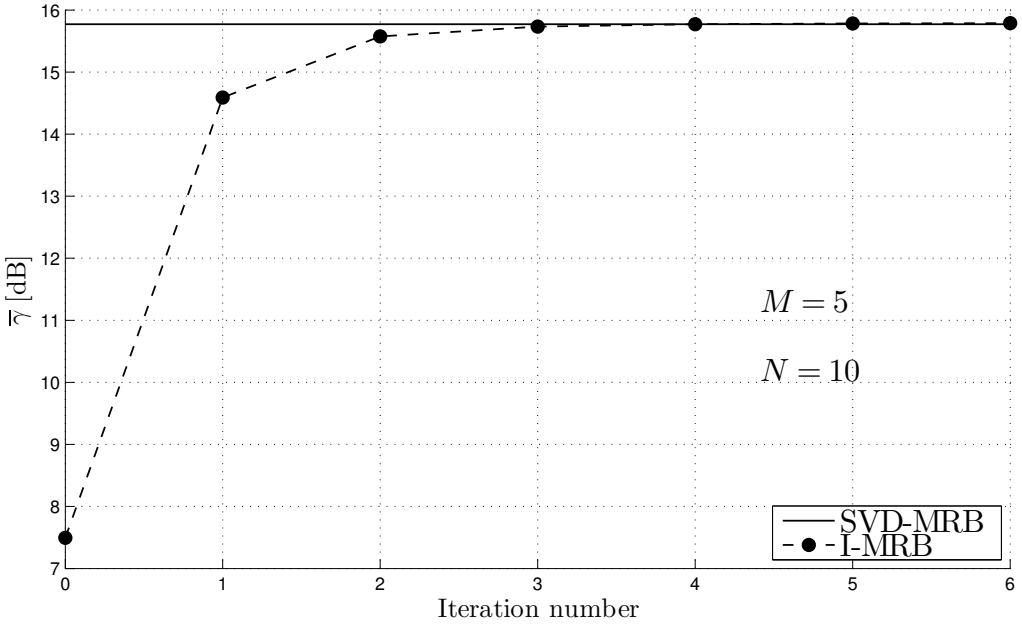

Figure 2.6: Convergence behaviour of the I-MRB approach.

Table 2.4: Simulated values of the standard deviation, σ_γ, on 5000 channel realizations for I-MRB with 6 iterations.

σ_γ [dB]		M				
		1	4	10	20	60
N	1	-0.01	4.65	7.24	9.34	12.64
	4	4.50	9.21	11.74	13.57	17.15
	10	7.17	11.59	13.91	15.99	19.65
	20	9.34	13.66	15.94	17.95	21.76
	60	12.65	17.24	19.65	21.68	25.48

Performance analysis

We report in this section the same performance evaluation for I-MRB that have been done previously for SVD-MRB. The propagation environment is also the same, as the channel model.
Figure 2.7 shows $\overline{\gamma}$ for the I-MRB approach versus the number of Tx and Rx antennas. Table 2.4 collects some standard deviation values and Figure 2.8, plots a simulated PDF over 5000 channel realization.

Remarks on performance

We note that the I-MRB (with 6 iterations) performance is equivalent[4] to that of SVD-MRB. The iterative procedure is simpler because it exploits closed form formulas of the MISO and SIMO beamformers.

[4]The average values of γ in Figures 2.4 and 2.7 are the same and also the standard deviations and the PDFs are comparable.

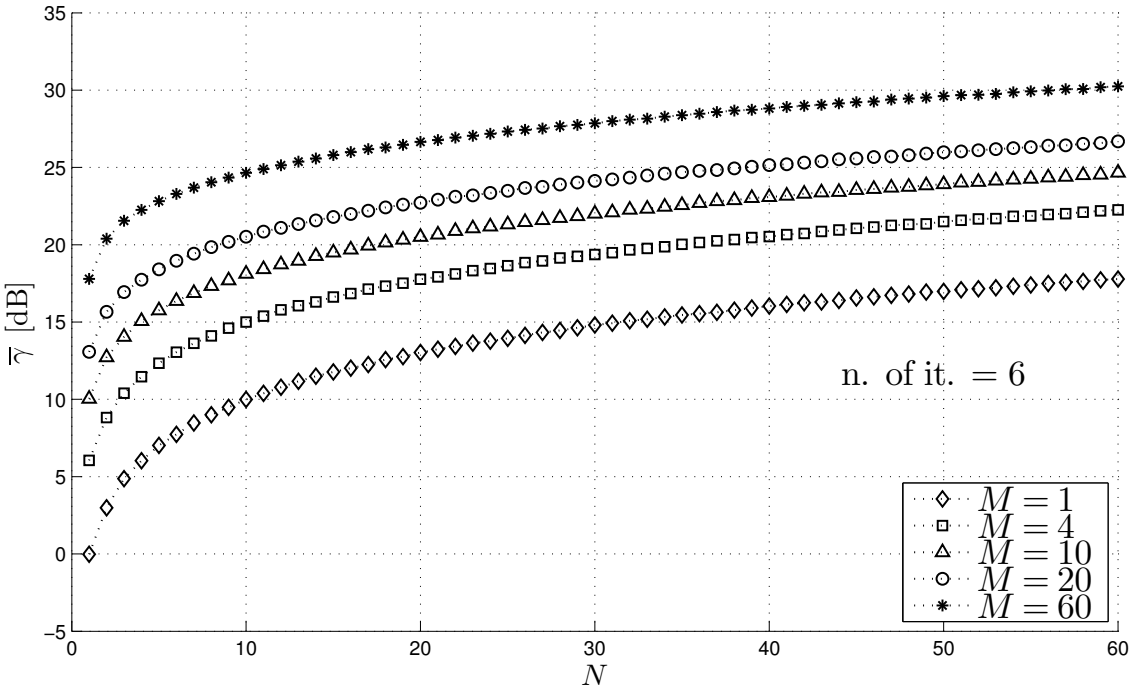

Figure 2.7: Simulated $\overline{\gamma}$ of I-MRB for various values of N and M, over 5000 channel realizations.

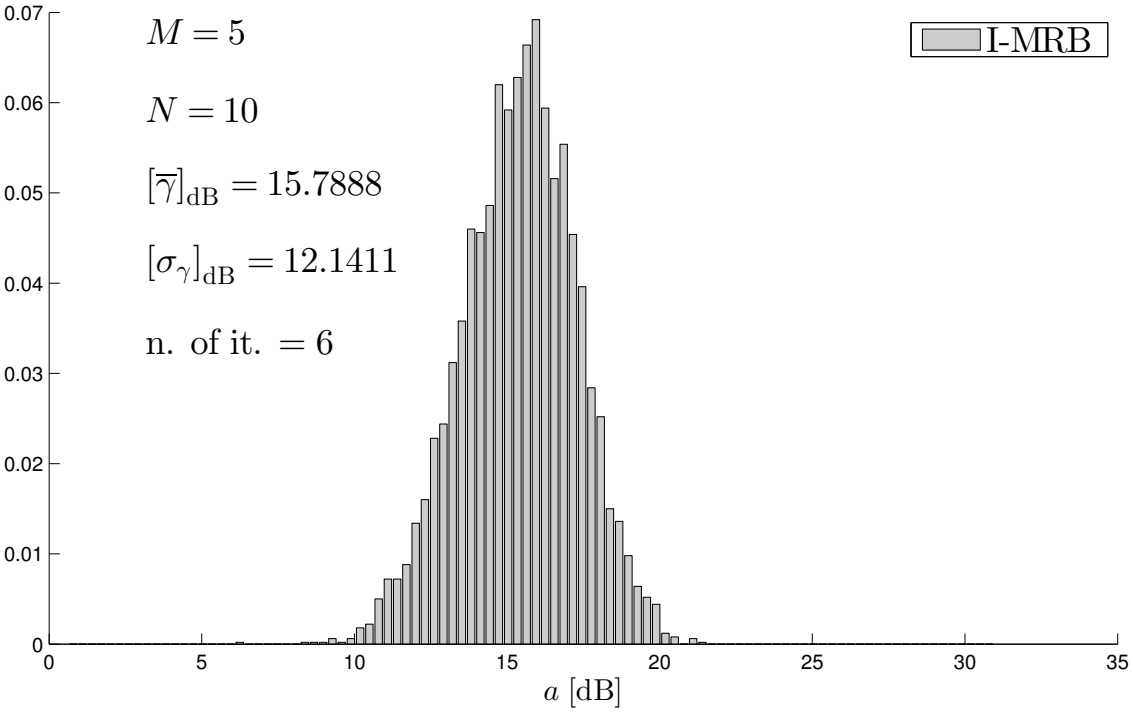

Figure 2.8: Simulated PDF of γ as from (2.40) for 5000 channel realizations.

However both optimal MRB approaches carry difficulties for a possible implementation in the analog domain: in fact a phase splitter has to separate the quadrature from in-phase component and two independent variable gain amplifiers should be applied at each branch before combining.

2.3 Suboptimal beamforming approaches

We have just said that the MRB represents an upper-bound to the MIMO array gain obtained by Tx and Rx beamformers. However, splitting the original problem into simpler SIMO and MISO problems (2.37) is useful to give an (iterative) solution for other suboptimal beamforming architectures.
In [5] various beamforming approaches are considered by adding increasing constraints, in problem (2.24) or equivalently in problems (2.37). Two of them are reported here:

- iterative real weights beamforming (I-RWB);
- iterative equal gain beamforming (I-EGB).

The former provides real beamformers, the latter implies beamformers with unitary amplitude. In particular, using an analog implementation, in the RF perspective, I-RWB solution simplifies hardware components, indeed the phase splitter is no more necessary and there is only one variable gain amplifier for each antenna. The I-EGB instead implies only a phase shifter for each antenna.

2.3.1 Iterative real weights beamforming I-RWB

This approach requires that beamformers are real valued. Two optimization problems are considered

$$\begin{array}{rl} \underset{\mathbf{R_u}}{\arg\max} & \mathrm{tr}\left(\mathbf{G}_{\mathrm{SIMO}}\mathbf{R_u}\right) \\ \text{subject to} & \mathrm{tr}\left(\mathbf{R_u}\right)=1 \\ & \mathbf{R_u}\succeq 0 \\ & \mathbf{u}\in\mathbb{R}^{N\times 1} \end{array} \qquad \begin{array}{rl} \underset{\mathbf{R_f}}{\arg\max} & \mathrm{tr}\left(\mathbf{R_f}\mathbf{G}_{\mathrm{MISO}}\right) \\ \text{subject to} & \mathrm{tr}\left(\mathbf{R_f}\right)=1 \\ & \mathbf{R_f}\succeq 0 \\ & \mathbf{f}\in\mathbb{R}^{M\times 1}. \end{array} \tag{2.41}$$

In this case the optimal solutions $\mathbf{u}_{\mathrm{I-RWB}}$ and $\mathbf{f}_{\mathrm{I-RWB}}$ are given in closed forms as the eigenvector corresponding to the largest eigenvalue of $\Re\{\mathbf{G}_{\mathrm{SIMO}}\}$ and $\Re\{\mathbf{G}_{\mathrm{MISO}}\}$, respectively [5, pp. 2376].

Table 2.5: Simulated values of the standard deviation, σ_γ, on 5000 channel realizations for I-RWB with 6 iterations.

σ_γ [dB]		M				
		1	4	10	20	60
	1	-0.01	4.24	6.35	8.03	10.89
	4	4.12	8.51	10.54	12.12	15.05
N	10	6.34	10.38	12.24	13.94	16.96
	20	8.07	12.15	13.85	15.54	18.66
	60	10.90	15.23	16.87	18.56	21.66

2.3.2 Iterative equal gain beamforming I-EGB

The I-EGB approach works only on the phase of beamformers, keeping the gain constant. The I-EGB optimization problems are expressed by

$$\begin{aligned} \arg\max_{\mathbf{R_u}} \quad & \mathrm{tr}\left(\mathbf{G}_{\mathrm{SIMO}}\mathbf{R_u}\right) \\ \text{subject to} \quad & \mathbf{R_u} \succeq 0 \\ & [\mathbf{R_u}]_{i,i} = \frac{1}{N},\ i = 1,\ \ldots,\ N \end{aligned} \qquad \begin{aligned} \arg\max_{\mathbf{R_f}} \quad & \mathrm{tr}\left(\mathbf{R_f}\mathbf{G}_{\mathrm{MISO}}\right) \\ \text{subject to} \quad & \mathbf{R_f} \succeq 0 \\ & [\mathbf{R_f}]_{i,i} = \frac{1}{M},\ i = 1,\ \ldots,\ M \end{aligned} \tag{2.42}$$

in this way, the amplitude of all beamformers entries are forced to be equal to $1/\sqrt{N}$ and $1/\sqrt{M}$ for $\mathbf{u}$ and $\mathbf{f}$, respectively. Note that the amplification constraint is implied in the equal gain constraint and, therefore, omitted.
The optimal solutions $\mathbf{u}_{\mathrm{I-EGB}}$ and $\mathbf{f}_{\mathrm{I-EGB}}$ to problems (2.42) have been shown [18, pp. 5397] to yield

$$\mathbf{u}_{\mathrm{I-EGB}} = \frac{1}{\sqrt{N}} e^{j\angle(\mathbf{h}_{\mathrm{SIMO}})+\varphi_R} \qquad \text{and} \qquad \mathbf{f}_{\mathrm{I-EGB}} = \frac{1}{\sqrt{M}} e^{j\angle\left(\mathbf{h}_{\mathrm{MISO}}^{\mathsf{H}}\right)+\varphi_T} \tag{2.43}$$

where $\angle(\cdot)$ represents the vector formed only by angles values of the operator argument entries. Moreover φ_R and φ_T are constant phase factor in $[0;\ 2\pi[$ and, for simplicity they are set to zero: $\varphi_R = \varphi_T = 0$.

2.3.3 Performance analysis

With the same channel model of Section 2.2.2 in Figure 2.9 we show $\overline{\gamma}$ for I-RWB and I-EGB beamformers. For a comparison, performance of I-MRB is also reported. Tables 2.5 and 2.6 collect some standard deviation values for I-RWB and I-EGB, respectively.

Remarks on performance

As expected, I-RWB and I-EGB are characterized by lower performance with respect to the optimal SVD-MRB because more constraints on beamformers. On the

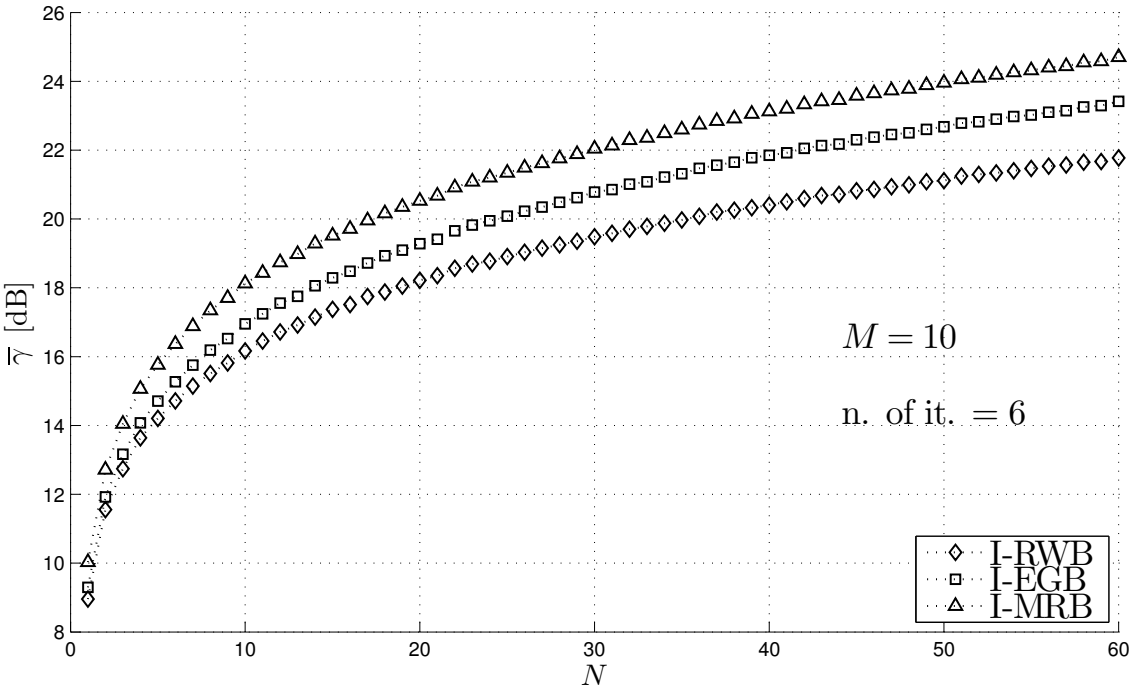

Figure 2.9: Simulated $\overline{\gamma}$ comparison for $M = 10$ versus N, over 5000 channel realizations.

Table 2.6: Simulated values of the standard deviation, σ_γ, on 5000 channel realizations for I-EGB with 6 iterations.

σ_γ [dB]		M				
		1	4	10	20	60
N	1	-0.01	4.33	6.65	8.60	11.80
	4	4.16	8.70	11.04	12.77	16.28
	10	6.56	10.91	13.14	15.23	18.89
	20	8.62	12.90	15.15	17.13	21.05
	60	11.80	16.40	18.87	21.00	24.94

other hand, this suboptimal approaches implies simpler hardware implementation if they are performed in analog domain. Moreover the design procedures have a low complexity, especially for the I-EGB, similar to that of I-MRB.

2.4 Analog-digital beamforming (ADB)

Until now, only weight vector beamformers have been considered. In a mm-wave scenario, working in the RF domain could be more convenient, but, often, we lose the digital base-band flexibility.
It is known from SVD-MRB approach that the best transmit beamformer is the dominant right singular vector of $\mathbf{H}$ and the best receive beamformer is the dominant left singular vector of $\mathbf{H}$. We investigate now a analog-digital beamforming (ADB) layered architecture[5] [4] that takes advantages from the I-EGB (which is simpler to construct in the analog domain) combined to a reduced number, with respect to the antenna elements, of RF chains. However, this configurations needs a base-band (BB) precoder and combiner in order to achieve MRB performance.

2.4.1 Framing of the problem

As in the previous sections, we consider a transmitter and a receiver with M and N, antennas, respectively. However, in this section, the transmitter is equipped with M_{RF} RF chains with $M_{\mathrm{RF}} < M$. Analogously the receiver has N_{RF} RF chains with $N_{\mathrm{RF}} < N$. The transmitter is assumed to apply an $M_{\mathrm{RF}} \times 1$ complex valued base-band precoder, called $\mathbf{f}_{\mathrm{BB}}$, followed by a RF precoder $\mathbf{F}_{\mathrm{RF}} \in \mathbb{C}^{M \times M_{\mathrm{RF}}}$. Similarly, the receiver is constituted by a RF combiner $\mathbf{U}_{\mathrm{RF}} \in \mathbb{C}^{N \times N_{\mathrm{RF}}}$ and a base-band combiner $\mathbf{u}_{\mathrm{BB}} \in \mathbb{C}^{N_{\mathrm{RF}} \times 1}$. The received signal is written as

$$y = \mathbf{u}_{\mathrm{BB}}^{\mathsf{H}} \mathbf{U}_{\mathrm{RF}}^{\mathsf{H}} \mathbf{H} \mathbf{F}_{\mathrm{RF}} \mathbf{f}_{\mathrm{BB}} x + \mathbf{u}_{\mathrm{BB}}^{\mathsf{H}} \mathbf{U}_{\mathrm{RF}}^{\mathsf{H}} \mathbf{n}, \tag{2.44}$$

$\mathbf{n}$ is defined in (2.8). The described system is illustrated in Figure 2.10, the digital BB part is located before the digital to analog converter (DAC) at Tx and after the analog to digital converter (ADC) at Rx. Moreover

$$\mathbf{f}_{\mathrm{BB}} = \begin{bmatrix} f_{\mathrm{BB},1} & f_{\mathrm{BB},2} & \cdots & f_{\mathrm{BB},M_{\mathrm{RF}}} \end{bmatrix}^{\mathsf{T}} \in \mathbb{C}^{M_{\mathrm{RF}} \times 1} \tag{2.45}$$

and

$$\mathbf{u}_{\mathrm{BB}} = \begin{bmatrix} u_{\mathrm{BB},1} & u_{\mathrm{BB},2} & \cdots & u_{\mathrm{BB},N_{\mathrm{RF}}} \end{bmatrix}^{\mathsf{T}} \in \mathbb{C}^{N_{\mathrm{RF}} \times 1}. \tag{2.46}$$

We seek to design the precoder and combiner to maximize the performance in term of γ, defined in (2.9), which, in this case, can be written as

$$\gamma = \left| \mathbf{u}_{\mathrm{BB}}^{\mathsf{H}} \mathbf{U}_{\mathrm{RF}}^{\mathsf{H}} \mathbf{H} \mathbf{F}_{\mathrm{RF}} \mathbf{f}_{\mathrm{BB}} \right|^2. \tag{2.47}$$

[5]The main difference between our analysis and [4] is that we send only one data stream as we do not exploit spatial multiplexing. Moreover, the system performance here are evaluated in terms of SNR improvement respect to a single antenna architecture, differently, in [4], a capacity maximization has been considered.

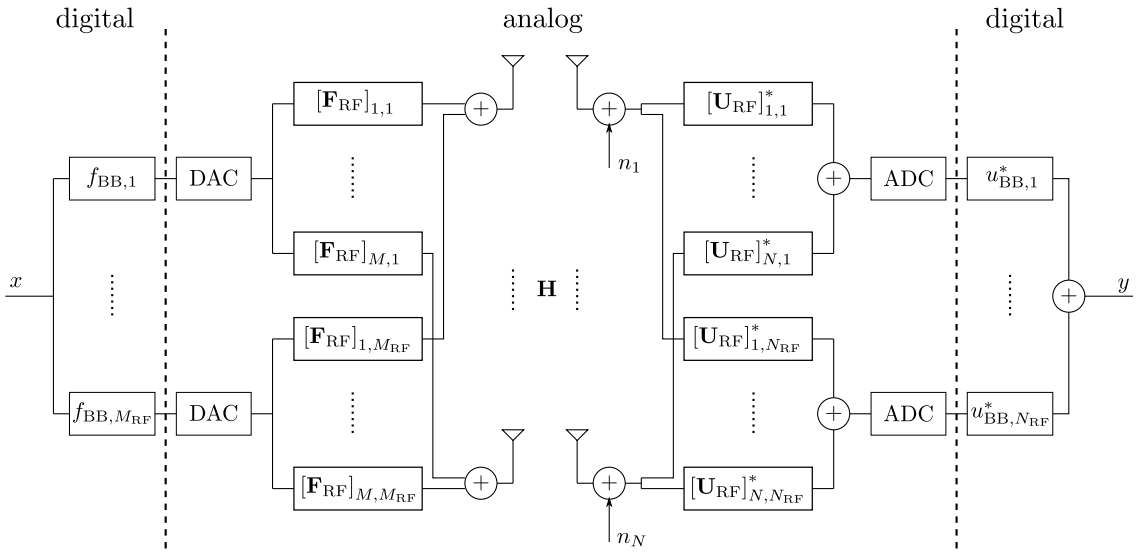

Figure 2.10: ADB architecture: BB equivalent model.

Optimization problem

From (2.47) the maximization problem is

$$\begin{aligned} \underset{\mathbf{F}_{\mathrm{RF}},\mathbf{f}_{\mathrm{BB}},\mathbf{U}_{\mathrm{RF}},\mathbf{u}_{\mathrm{BB}}}{\arg\max} \quad & \left|\mathbf{u}_{\mathrm{BB}}^{\mathsf{H}}\mathbf{U}_{\mathrm{RF}}^{\mathsf{H}}\mathbf{H}\mathbf{F}_{\mathrm{RF}}\mathbf{f}_{\mathrm{BB}}\right|^2 \\ \text{subject to} \quad & \left|[\mathbf{F}_{\mathrm{RF}}]_{i,j}\right| = 1, \quad i = 1\ldots, M, \quad j = 1\ldots, M_{\mathrm{RF}} \\ & \left|[\mathbf{U}_{\mathrm{RF}}]_{i,j}\right| = 1, \quad i = 1\ldots, N, \quad j = 1\ldots, N_{\mathrm{RF}} \\ & \|\mathbf{F}_{\mathrm{RF}}\mathbf{f}_{\mathrm{BB}}\|^2 = 1 \\ & \left\|\mathbf{u}_{\mathrm{BB}}^{\mathsf{H}}\mathbf{U}_{\mathrm{RF}}^{\mathsf{H}}\right\|^2 = 1, \end{aligned} \tag{2.48}$$

where the constraints underline that the RF part of beamformer must apply changes only on signals phases, and, as usual, beamformers do not amplify powers.

2.4.2 The precoder and combiner design

No general solutions are known for the optimization problem (2.48). The optimization procedure is splitted between Rx and Tx side and a solution for an approximation of the original problem is proposed in the next section.

Joint analog-digital precoder

The receiver operations are abstracted[6] and the focus is set on the precoder design. From (2.39), the optimal MIMO transmit precoder is the $M \times 1$ dominant right singular vector of $\mathbf{H}$ denoted by $\mathbf{f}_{\mathrm{opt}}$. The key intuition presented in [4] is to exploit the structure of the ULA MIMO channel and the knowledge of the optimal precoder.

[6] Abstracting the receiver operations assumes that optimal combining is performed at Rx side.

In practice $\mathbf{f}_{\text{opt}}$ is approximated by a linear combination of M_{RF} columns of matrix $\mathbf{A}_t$, given in (1.20), weighted by $\mathbf{f}_{\text{BB}}$ entries:

$$\mathbf{f}_{\text{opt}} \simeq \mathbf{F}_{\text{RF}}\mathbf{f}_{\text{BB}} = f_{\text{BB},1}\left[\text{col}_1\left(\mathbf{F}_{\text{RF}}\right)\right] + \cdots + f_{\text{BB},M_{\text{RF}}}\left[\text{col}_{M_{\text{RF}}}\left(\mathbf{F}_{\text{RF}}\right)\right], \tag{2.49}$$

where the columns of $\mathbf{F}_{\text{RF}}$, indicated with $\text{col}_j\left(\mathbf{F}_{\text{RF}}\right)$, $j = 1, \ldots, M_{\text{RF}}$, are chosen between the best columns of $\mathbf{A}_t$. This solution ensures compliance with the unitary amplitude constraints on entries of $\mathbf{F}_{\text{RF}}$.
The optimization problem in (2.48) is rewritten, from the precoder point of view, as the best layered precoder $\mathbf{F}_{\text{RF}}\mathbf{f}_{\text{BB}}$ that minimize the "distance" from the optimum precoder $\mathbf{f}_{\text{opt}}$

$$\begin{aligned} \underset{\mathbf{F}_{\text{RF}},\,\mathbf{f}_{\text{BB}}}{\arg\min} \quad & \left\|\mathbf{f}_{\text{opt}} - \mathbf{F}_{\text{RF}}\mathbf{f}_{\text{BB}}\right\| \\ \text{subject to} \quad & \text{col}_j\left(\mathbf{F}_{\text{RF}}\right) \in \left\{\mathbf{a}_t\left(\phi_\ell^{(t)}\right),\ 1 \le \ell \le L\right\}, \quad j = 1, \ldots, M_{\text{RF}} \\ & \left\|\mathbf{F}_{\text{RF}}\mathbf{f}_{\text{BB}}\right\|^2 = 1. \end{aligned} \tag{2.50}$$

Now the precoding problem consists of selecting the best M_{RF} columns of $\mathbf{A}_t$ and finding their optimal combination $\mathbf{f}_{\text{BB}}$.
To solve the problem (2.50), [4, pp. 3785] proposes a simple iterative algorithm displayed in Algorithm 1. The precoding procedure is based on the concept of basis

Algorithm 1 Precoder construction.

$\mathbf{F}_{\text{RF}} \leftarrow$ empty matrix
$\mathbf{f}_{\text{BB}} \leftarrow$ empty vector
$\mathbf{f}_{\text{res}} \leftarrow \mathbf{f}_{\text{opt}}$
for $i = 1$ **to** M_{RF} **do**
  $\boldsymbol{\Psi} \leftarrow \mathbf{A}_t^{\mathsf{H}}\mathbf{f}_{\text{res}}$
  $o \leftarrow \underset{\ell \in \{1, \ldots, L\}}{\arg\max} \left[\boldsymbol{\Psi}\boldsymbol{\Psi}^{\mathsf{H}}\right]_{\ell,\ell}$
  $\mathbf{F}_{\text{RF}} \leftarrow \left[\mathbf{F}_{\text{RF}} | \text{col}_o\left(\mathbf{A}_t\right)\right]$
  $\mathbf{f}_{\text{BB}} \leftarrow \left(\mathbf{F}_{\text{RF}}^{\mathsf{H}}\mathbf{F}_{\text{RF}}\right)^{-1}\mathbf{F}_{\text{RF}}^{\mathsf{H}}\mathbf{f}_{\text{opt}}$
  $\mathbf{f}_{\text{res}} \leftarrow \frac{\mathbf{f}_{\text{opt}} - \mathbf{F}_{\text{RF}}\mathbf{f}_{\text{BB}}}{\left\|\mathbf{f}_{\text{opt}} - \mathbf{F}_{\text{RF}}\mathbf{f}_{\text{BB}}\right\|}$
end for
$\mathbf{f}_{\text{BB}} \leftarrow \frac{\mathbf{f}_{\text{BB}}}{\left\|\mathbf{F}_{\text{RF}}\mathbf{f}_{\text{BB}}\right\|}$
return $\mathbf{F}_{\text{RF}}$, $\mathbf{f}_{\text{BB}}$

pursuit and least squares. Algorithm 1 is summarized by next steps:

- find the vector $\mathbf{a}_t\left(\phi_o^{(t)}\right)$, $1 \le o \le L$, between the columns of $\mathbf{A}_t$ along which the optimal precoder has the maximum projection;
- append the o^{th} column of $\mathbf{A}_t$, denoted by $\text{col}_o\left(\mathbf{A}_t\right)$, to the RF precoder $\mathbf{F}_{\text{RF}}$;
- evaluates the least squares solution to $\mathbf{f}_{\text{BB}}$;

- the contribution of selected vector is removed from $\mathbf{f}_{\text{opt}}$ and the procedure iterates finding the column along which the residual precoding vector $\mathbf{f}_{\text{res}}$ has the largest projection;
- the procedure ends when M_{RF} columns of $\mathbf{A}_t$ are selected, finally the transmit power is normalized.

Receiver operations

So far, the focus has been set on the transmitter, abstracting the receiver operations. In a similar way, abstracting the transmitter operations, the basis pursuit approach, displayed in Algorithm 1 for the precoder, can be adopted also for the combiner with the differences outlined in Algorithm 2. Separately designing the precoder and

Algorithm 2 Combiner construction.

$\mathbf{U}_{\text{RF}} \leftarrow$ empty matrix
$\mathbf{u}_{\text{BB}} \leftarrow$ empty vector
$\mathbf{u}_{\text{res}} \leftarrow \mathbf{u}_{\text{opt}}$
for $i = 1$ **to** N_{RF} **do**
  $\boldsymbol{\Psi} \leftarrow \mathbf{A}_r^{\mathsf{H}} \mathbf{u}_{\text{res}}$
  $o \leftarrow \underset{\ell \in \{1,\ldots,L\}}{\arg\max} \left[\boldsymbol{\Psi}\boldsymbol{\Psi}^{\mathsf{H}}\right]_{\ell,\ell}$
  $\mathbf{U}_{\text{RF}} \leftarrow \left[\mathbf{U}_{\text{RF}} | \text{col}_o\left(\mathbf{A}_r\right)\right]$
  $\mathbf{u}_{\text{BB}} \leftarrow \left(\mathbf{U}_{\text{RF}}^{\mathsf{H}} \mathbf{U}_{\text{RF}}\right)^{-1} \mathbf{U}_{\text{RF}}^{\mathsf{H}} \mathbf{u}_{\text{opt}}$
  $\mathbf{u}_{\text{res}} \leftarrow \frac{\mathbf{u}_{\text{opt}} - \mathbf{U}_{\text{RF}} \mathbf{u}_{\text{BB}}}{\|\mathbf{u}_{\text{opt}} - \mathbf{U}_{\text{RF}} \mathbf{u}_{\text{BB}}\|}$
end for
$\mathbf{u}_{\text{BB}} \leftarrow \frac{\mathbf{u}_{\text{BB}}}{\|\mathbf{U}_{\text{RF}} \mathbf{u}_{\text{BB}}\|}$
return $\mathbf{U}_{\text{RF}}$, $\mathbf{u}_{\text{BB}}$

combiner, however, may leads to a loss in received power if at Rx side the number of RF chains is lower than the number of RF chains at Tx side. In this case, a performance loss happens because beamforming degrees of freedom at receiver are limited and power can't be collected in a lot of directions. Conversely a flexible beamforming at receiver may be not useful if the Tx beamformer has few degrees of freedom. As a result, transmitter has to consider the constrains, in terms of number of RF chains, at receiver and vice versa.
In order to avoid the issue of mismatched precoder and combiner, [4] proposes to schedule Algorithms 1 and 2 in according to rules expressed in Algorithm 3.

2.4.3 Performances analysis

With the propagation environment and channel model described in the *performance analysis* in Section 2.2.2, a set of simulations is performed in order to evaluate the ADB performance. In Table 2.7 are reported values of $\overline{\gamma}$ for different values of M, N, M_{RF} and N_{RF}. Table 2.8, instead, shows standard deviations for the same configurations.

Algorithm 3 Precoder and combiner scheduler design.

if $M_{\mathrm{RF}} < N_{\mathrm{RF}}$ **then**
  $\mathbf{f}_{\mathrm{opt}} \leftarrow$ dominant right singular vector of $\mathbf{H}$
  Solve Algorithm 1 which returns $\mathbf{F}_{\mathrm{RF}}$ and $\mathbf{f}_{\mathrm{BB}}$
  $\mathbf{u}_{\mathrm{opt}} \leftarrow \mathbf{H}\mathbf{F}_{\mathrm{RF}}\mathbf{f}_{\mathrm{BB}}$
  Solve Algorithm 2 which returns $\mathbf{U}_{\mathrm{RF}}$ and $\mathbf{u}_{\mathrm{BB}}$
else
  $\mathbf{u}_{\mathrm{opt}} \leftarrow$ dominant left singular vector of $\mathbf{H}$
  Solve Algorithm 2 which returns $\mathbf{U}_{\mathrm{RF}}$ and $\mathbf{u}_{\mathrm{BB}}$
  $\mathbf{f}_{\mathrm{opt}} \leftarrow \mathbf{H}^{\mathsf{H}}\mathbf{U}_{\mathrm{RF}}\mathbf{u}_{\mathrm{BB}}$
  Solve Algorithm 1 which returns $\mathbf{F}_{\mathrm{RF}}$ and $\mathbf{f}_{\mathrm{BB}}$
end if

Table 2.7: Simulated $\overline{\gamma}$ on 5000 $\mathbf{H}_{\mathrm{ULA}}$ realizations for ADB.

$\overline{\gamma}$ [dB]		$(M,\ M_{\mathrm{RF}})$				
		(1, 1)	(4, 2)	(10, 5)	(20, 10)	(60, 15)
$(N,\ N_{\mathrm{RF}})$	(1, 1)	-0.02	5.78	9.96	12.99	17.76
	(4, 2)	5.85	11.27	14.91	17.70	22.18
	(10, 5)	10.03	14.93	18.10	20.57	24.69
	(20, 10)	13.04	17.67	20.56	22.78	26.70
	(60, 15)	17.78	22.18	24.66	26.69	30.31

Table 2.8: Simulated σ_γ on 5000 $\mathbf{H}_{\mathrm{ULA}}$ realizations for ADB.

σ_γ [dB]		$(M,\ M_{\mathrm{RF}})$				
		(1, 1)	(4, 2)	(10, 5)	(20, 10)	(60, 15)
$(N,\ N_{\mathrm{RF}})$	(1, 1)	-0.01	4.45	7.17	9.22	12.68
	(4, 2)	4.57	9.00	11.60	13.57	17.16
	(10, 5)	7.23	11.58	13.89	15.91	19.51
	(20, 10)	9.12	13.61	16.00	17.89	21.58
	(60, 15)	12.73	17.02	19.42	21.59	25.31

Remarks on performance

From Table 2.7 we note that ADB reaches the performance of optimum SVD-MRB of Figure 2.4 with the advantage of a reduced number of RF chains. We underline that, we have sought to move, as much as possible, the beamforming in the analog domain and reduce the number of analog to digital conversions. Indeed for mm-wave this is convenient in terms of hardware cost and power consumption.
However the ADB approach carries also some disadvantages. First of all the algorithm that compute the digital optimal weights, represented by the entries of $\mathbf{f}_{\mathrm{BB}}$ and of $\mathbf{u}_{\mathrm{BB}}$, needs further knowledge about the channel as matrices $\mathbf{A}_t$ and $\mathbf{A}_r$ defined in (1.20) which are factors of $\mathbf{H}_{\mathrm{ULA}}$. Moreover, the ADB procedure entails inversion of matrices which could be numerically ill conditioned in some cases.

Chapter 3

MRB with coarse quantization

In the previous chapters we have described the optimal and some sub-optimal beamforming architectures; in addition we gave performance evaluations with some comparisons between different systems. Each of these solution considers an array gain also at Tx side, which implies a perfect channel knowledge at transmitter. Moreover, with the exception of ADB, nothing has been said if the implementation of beamforming scheme is in the digital or analog domain.
In order to give a low-complexity approach, in this chapter we investigate a SIMO configuration where the array-gain is exploited only at Rx side and there is no need to transmit the channel state information (CSI) back at Tx. In particular the receiver performs a MRB in digital domain with the use of uniform ADCs with very few bits. Performance is carried out under the assumption of both perfect channel knowledge and with an estimate of it. We call these two approaches CQ-KC and CQ-EC, respectively. Moreover, for both solutions, antenna selection can be considered in order to reduce the number of RF chains. After an analytical evaluation that makes use of some assumptions, we also report a system simulation to validate the analytical results.

3.1 System model

In Figure 3.1 is reported the BB equivalent of the reference system architecture. A fully digital MRB needs $2N$ ADCs (one for in-phase and one for the quadrature component), in the scheme the ADC couple is represented by one block for each branch for simplicity.

3.1.1 Signals description

By introducing the channel vector

$$\mathbf{h} = \begin{bmatrix} h_1 & \cdots & h_p & \cdots & h_N \end{bmatrix}^{\mathsf{T}} \in \mathbb{C}^{N\times 1}, \tag{3.1}$$

from the received signal $\mathbf{r} \in \mathbb{C}^{N\times 1}$,

$$\mathbf{r} = \mathbf{h}x + \mathbf{n}, \tag{3.2}$$

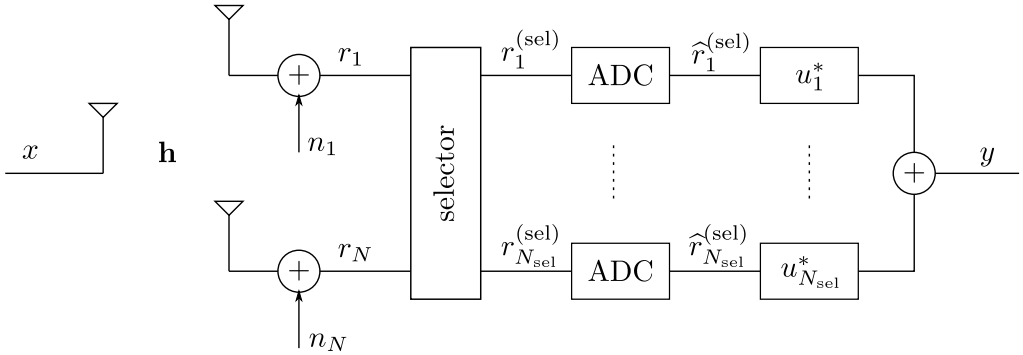

Figure 3.1: Receiver with antenna selections and ADCs.

where $\mathbf{n}$ is defined in (2.8), a selector chooses, in the analog domain, the N_{sel} ($N_{\mathrm{sel}} \leq N$) best branches

$$\mathbf{r}^{(\mathrm{sel})} = \begin{bmatrix} r_1^{(\mathrm{sel})} & \cdots & r_p^{(\mathrm{sel})} & \cdots & r_{N_{\mathrm{sel}}}^{(\mathrm{sel})} \end{bmatrix}^{\mathsf{T}} \in \mathbb{C}^{N_{\mathrm{sel}} \times 1}. \tag{3.3}$$

The vector

$$\mathbf{w} = \begin{bmatrix} w_1 & \cdots & w_p & \cdots & w_{N_{\mathrm{sel}}} \end{bmatrix}^{\mathsf{T}} \in \mathbb{C}^{N_{\mathrm{sel}} \times 1}, \tag{3.4}$$

gathers the quantization noise samples for each selected branch. The real and imaginary parts of w_p in (3.4) are assumed to be uncorrelated.
The quantized received vector is written as

$$\widehat{\mathbf{r}}^{(\mathrm{sel})} = \mathbf{r}^{(\mathrm{sel})} + \mathbf{w} = \mathbf{h}^{(\mathrm{sel})} x + \mathbf{n} + \mathbf{w}, \tag{3.5}$$

where $\mathbf{h}^{(\mathrm{sel})}$ represents the channel vector after the selector which gathers the chosen channel gains.
Finally, the N_{sel} components of $\widehat{\mathbf{r}}^{(\mathrm{sel})}$ are weighted by the combiner

$$\mathbf{u} = \begin{bmatrix} u_1 & \cdots & u_{N_{\mathrm{sel}}} \end{bmatrix}^{\mathsf{T}} \in \mathbb{C}^{N_{\mathrm{sel}} \times 1} \tag{3.6}$$

and the output sample y is obtained.
As the combining procedure is performed in digital domain there are more degrees of freedom, indeed MRB is considered.

3.1.2 The selector policy

In Figure 3.1 the selector block chooses N_{sel} antennas from the total set N of received signals. For each antenna branch the signal to noise ratio Θ_p is given by

$$\Theta_p = \frac{\mathbb{E}_x \left[|h_p x|^2 \right]}{\mathbb{E}_n \left[|n_p|^2 \right]} = \frac{|h_p|^2}{\sigma_n^2}, \qquad p = 1, \ldots, N. \tag{3.7}$$

The selection policy is based on the choice of the branches with the best N_{sel} values of Θ_p in (3.7).

3.1.3 ADC model

The in-phase and quadrature components of the received signal r_p, $p = 1, \ldots, N$, are digitally converted by two identical ADCs, which, for simplicity, in Figure 3.1 are represented by one block per Rx branch. Both converters are characterized by a mid-riser [20] uniform minimum mean square error (MMSE) quantizer with symmetrical saturation level $\tau_p^{(\mathrm{sat})}$ and $2^{\mathtt{b}}$ thresholds, where $\mathtt{b}$ denotes the number of bits.
Let us consider the p-th branch. If we define the quantization error as $w_p = \widehat{r}_p^{(\mathrm{sel})} - r_p^{(\mathrm{sel})}$ (and correspondingly $\mathbf{w} = \widehat{\mathbf{r}}^{(\mathrm{sel})} - \mathbf{r}^{(\mathrm{sel})}$), the p-th ADC is characterized by the signal to quantization noise ratio (SQR)

$$\Omega = \frac{\mathtt{M}_{r_p}}{\mathtt{M}_{w_p}} = \frac{|h_p|^2 + \sigma_n^2}{\mathtt{M}_{w_p}} \tag{3.8}$$

and by the parameter defined in [20]

$$\beta = \frac{\Delta_p}{\sqrt{\mathtt{M}_{r_p}/2}}, \tag{3.9}$$

where $\mathtt{M}_{r_p}$ and $\mathtt{M}_{w_p}$ represent the statistical power of $r_p^{(\mathrm{sel})}$ and w_p, respectively, while Δ_p is the quantizer step size.
The introduction of the additive quantization error w_p can be represented with the equivalent model of Figure 3.2.
In [20] the optimal β which maximize Ω is given by a joint minimization of the granular and saturation errors for a Gaussian distributed input. Values are reported in Tab. 3.1 for $\mathtt{b} = 1,\ 2,\ 3$.

Table 3.1: Optimal β and corresponding maximum Ω defined in (3.9) and (3.8), respectively, for a Gaussian input.

$\mathtt{b}$	β	$\max(\Omega)$ (in dB)
1	1.5956	4.40
2	0.9957	9.25
3	0.5860	14.27

3.1.4 Two useful definitions

For later use a couple of useful definitions are given,

$$\widetilde{\mathtt{M}}_h = \frac{1}{N_{\mathrm{sel}}} \sum_{p=1}^{N_{\mathrm{sel}}} \left| h_p^{(\mathrm{sel})} \right|^2 \tag{3.10}$$

and

$$\widetilde{\mathtt{Q}}_h = \frac{1}{N_{\mathrm{sel}}} \sum_{p=1}^{N_{\mathrm{sel}}} \left| h_p^{(\mathrm{sel})} \right|^4, \tag{3.11}$$

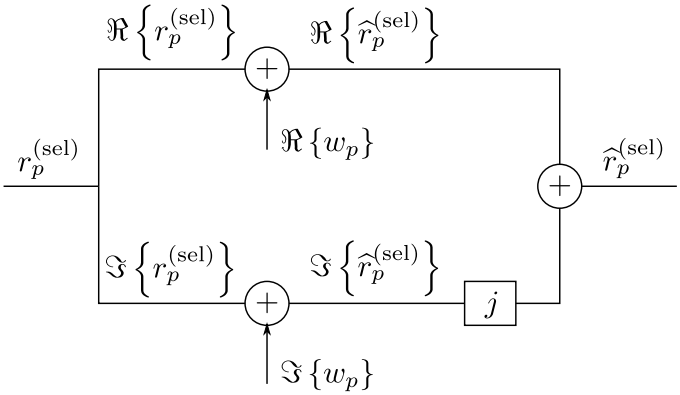

Figure 3.2: The equivalent model of the p^{th} ADC.

if the elements of $\mathbf{h}^{(\mathrm{sel})}$ are statistical independent of each others and N_{sel} becomes large, it holds

$$\widetilde{\mathtt{M}}_h \to \mathtt{M}_h = \mathbb{E}\left[\left|h_p^{(\mathrm{sel})}\right|^2\right] \quad \text{and} \quad \widetilde{\mathtt{Q}}_h \to \mathtt{Q}_h = \mathbb{E}\left[\left|h_p^{(\mathrm{sel})}\right|^4\right] \quad \text{for} \quad N_{\mathrm{sel}} \to \infty. \tag{3.12}$$

3.2 Analytical evaluation

In this section we give an analytical evaluation of the system for both CQ-KC and CQ-EC approaches. The received signal, quantization noise and channel estimation error are considered uncorrelated of each others and with these assumptions we provide the analytical expression, in closed form, for the SNR improvement γ.

3.2.1 Analytical CQ-KC

We begin from the case of a perfect channel knowledge at Rx side.
In this situation the combiner is set equal to MRB, expressed in (2.39),

$$\mathbf{u} = \frac{\mathbf{h}^{(\mathrm{sel})}}{\|\mathbf{h}^{(\mathrm{sel})}\|}. \tag{3.13}$$

SNR characterization

From (3.5), the received signal at the decision point is

$$y = \mathbf{u}^{\mathsf{H}}\widehat{\mathbf{r}}^{(\mathrm{sel})} = \mathbf{u}^{\mathsf{H}}\left(x\mathbf{h}^{(\mathrm{sel})} + \mathbf{n} + \mathbf{w}\right). \tag{3.14}$$

We consider, optimistically, that each ADC yields the maximum SQR as from Tab. 3.1. Next, we can use (3.8) to obtain

$$\mathtt{M}_{w_p} = \frac{\sigma_n^2 + |h_p|^2}{\Omega}. \tag{3.15}$$

If the entries of $\mathbf{n}$ and $\mathbf{w}$ are assumed statistically uncorrelated and $\mathbf{u}$ is equal to (3.13), the overall noise power component of y in (3.14) yields

$$\begin{aligned}\mathbb{E}_{\mathbf{n},\mathbf{w}}\left[\left|\mathbf{u}^{\mathsf{H}}(\mathbf{n}+\mathbf{w})\right|^2\right] &= \sum_{p=1}^{N_{\text{sel}}}\mathbb{E}_{\mathbf{n},\mathbf{w}}\left[\left|u_p^*\right|^2|n_p+w_p|^2\right] \\ &= \frac{1}{\|\mathbf{h}^{(\text{sel})}\|^2}\sum_{p=1}^{N_{\text{sel}}}\left|h_p^{(\text{sel})}\right|^2\left(\sigma_n^2+\mathtt{M}_{w_p}\right) \\ &= \sigma_n^2+\frac{\sigma_n^2}{\Omega}+\frac{1}{\Omega}\frac{\widetilde{\mathtt{Q}}_h}{\widetilde{\mathtt{M}}_h},\end{aligned} \tag{3.16}$$

using (3.15).
Under the same conditions the power of the useful component of y is

$$\mathbb{E}_x\left[\left|\mathbf{u}^{\mathsf{H}}x\mathbf{h}^{(\text{sel})}\right|^2\right] = \frac{1}{\|\mathbf{h}^{(\text{sel})}\|^2}\left|\sum_{p=1}^{N_{\text{sel}}}\left|h_p^{(\text{sel})}\right|^2\right|^2\mathbb{E}_x\left[|x|^2\right] = \left\|\mathbf{h}^{(\text{sel})}\right\|^2 = N_{\text{sel}}\widetilde{\mathtt{M}}_h. \tag{3.17}$$

Therefore, γ in (2.9) becomes

$$\gamma_{\text{CQKC}}^{(a)} = \frac{\widetilde{\mathtt{M}}_h}{\frac{1}{N_{\text{sel}}}\left(1+\frac{1}{\Omega}+\frac{1}{\Omega\sigma_n^2}\frac{\widetilde{\mathtt{Q}}_h}{\widetilde{\mathtt{M}}_h}\right)}. \tag{3.18}$$

Let us note that, if no quantization errors are present ($\Omega \to \infty$), (3.18) becomes equal to the SVD-MRB bound expressed in (2.30).

3.2.2 Analytical CQ-EC

Now at Rx side we know only an estimate of the channel. In other words $\mathbf{h}$ is affected by a random additive vector noise $\mathbf{z}$.
The combiner, is set to be as much as possible "close" to the MRB combiner in (3.13), i.e.

$$\mathbf{u} = \frac{\widehat{\mathbf{h}}^{(\text{sel})}}{\|\mathbf{h}^{(\text{sel})}\|} = \frac{\mathbf{h}^{(\text{sel})}+\mathbf{z}}{\|\mathbf{h}^{(\text{sel})}\|}, \tag{3.19}$$

where

$$\widehat{\mathbf{h}}^{(\text{sel})} = \left[\widehat{h}_1^{(\text{sel})} \quad \cdots \quad \widehat{h}_p^{(\text{sel})} \quad \cdots \quad \widehat{h}_{N_{\text{sel}}}^{(\text{sel})}\right]^{\mathsf{T}} \in \mathbb{C}^{N_{\text{sel}}\times 1}, \tag{3.20}$$

is the estimated channel and

$$\mathbf{z} = \left[z_1 \quad \cdots \quad z_p \quad \cdots \quad z_{N_{\text{sel}}}\right]^{\mathsf{T}} \in \mathbb{C}^{N_{\text{sel}}\times 1}, \tag{3.21}$$

represents channel estimation error vector.

Estimation procedure and estimation noise

In this section the channel estimation procedure is briefly described and a statistical model for the random estimation error is developed.
For the channel estimation we use a training maximum length sequence (MLS), with unit amplitude samples x_k, of length K. At the receiver, the MLS is correlated with the received signal

$$\widehat{r}_{p,k}^{(\mathrm{sel})} = x_{p,k}h_p + n_{p,k} + w_{p,k}. \tag{3.22}$$

If o denotes a lag time index, the correlation signal $\mathtt{r}_{x_p,\widehat{r}_p^{(\mathrm{sel})}}[o]$ between x and $\widehat{r}_p^{(\mathrm{sel})}$ is defined by

$$\mathtt{r}_{x,\widehat{r}_p^{(\mathrm{sel})}}[o] = \frac{1}{K}\sum_{k=0}^{K-1} x_k^* \widehat{r}_{p,k+o}^{(\mathrm{sel})} \tag{3.23}$$

if $\left|\mathtt{r}_{x,\widehat{r}_p^{(\mathrm{sel})}}[o]\right|$ assumes its maximum for $o = 0$ it is

$$\widehat{h}_p^{(\mathrm{sel})} = \mathtt{r}_{x,\widehat{r}_p^{(\mathrm{sel})}}[0] = \frac{1}{K}\sum_{k=0}^{K-1}\underbrace{|x_k|^2}_{1} h_p^{(\mathrm{sel})} + \underbrace{\frac{1}{K}\sum_{k=0}^{K-1} x_k^*\left(n_{p,k}+w_{p,k}\right)}_{z_p} = h_p^{(\mathrm{sel})} + z_p. \tag{3.24}$$

If K is large enough and if the random variables $x_k^*\left(n_{p,k}+w_{p,k}\right)$ are independent through time instants k the random variable z_p, thanks to the *central limit theorem*[1], can be approximated by a normal distribution

$$z_p \sim \mathcal{CN}\left(0,\ \frac{\sigma_n^2 + \mathtt{M}_{w_p}}{K}\right), \tag{3.25}$$

where the noise n_p and the quantization noise w_p are considered statistically independent. It is clear that a large K leads to a smaller variance for z_p, therefore to a better channel estimate.

SNR characterization

If $\mathbf{u}$ is equal to (3.19) the received signal becomes

$$\begin{aligned} y &= \mathbf{u}^{\mathsf{H}}\left(x\mathbf{h}^{(\mathrm{sel})} + \mathbf{n} + \mathbf{w}\right) \\ &= \frac{1}{\|\mathbf{h}^{(\mathrm{sel})}\|}\left(x\mathbf{h}^{(\mathrm{sel})\mathsf{H}}\mathbf{h}^{(\mathrm{sel})} + x\mathbf{z}^{\mathsf{H}}\mathbf{h}^{(\mathrm{sel})} + \mathbf{h}^{(\mathrm{sel})\mathsf{H}}\mathbf{n} + \mathbf{z}^{\mathsf{H}}\mathbf{n} + \mathbf{h}^{(\mathrm{sel})\mathsf{H}}\mathbf{w} + \mathbf{z}^{\mathsf{H}}\mathbf{w}\right), \end{aligned} \tag{3.26}$$

[1] If $X_1, X_2, \ldots$ is a sequence of i.i.d. random variables with mean $\overline{X}$ and variance $\sigma_X^2 < \infty$, as K approach infinity, the random variables $\frac{1}{K}\sum_{k=1}^{K} X_k - \overline{X}$ converge in distribution to a normal distribution $\mathcal{N}\left(0,\ \frac{\sigma_X^2}{K}\right)$.

which, under the assumption of uncorrelated noises, yields a SNR improvement γ given by

$$\gamma_{\mathrm{CQEC}}^{(a)} = \frac{\widetilde{\mathtt{M}}_h}{\frac{1}{K}\left\{\frac{1}{N} + \frac{\sigma_n^2}{\|\mathbf{h}\|^2} + \frac{1}{\Omega\|\mathbf{h}\|^2}\left[\left(3+\frac{2}{\Omega}\right)\widetilde{\mathtt{M}}_h\left(1+\frac{1}{\Omega}\right)\frac{\widetilde{\mathtt{Q}}_h}{\sigma_n^2} + \left(2+\frac{1}{\Omega}\right)\sigma_n^2\right]\right\} + \frac{1}{N}\left(1+\frac{1}{\Omega}+\frac{1}{\Omega\sigma_n^2}\frac{\widetilde{\mathtt{Q}}_h}{\widetilde{\mathtt{M}}_h}\right)}. \tag{3.27}$$

Note that if the estimation is perfect (K goes to ∞) (3.27) becomes equal to (3.18) as expected.

3.3 Simulative evaluation

Above assumptions of uncorrelation may not hold if thermal noise is low and channel gain is correlated across different antennas. To validate (3.18) and (3.27), values of γ are obtained by simulations of the quantization errors. For a given channel vector $\mathbf{h}$, the overall noise vector $\mathbf{v}$ is obtained as the difference between the quantized version of the received signal and the useful part, i.e.

$$\mathbf{v} = \widehat{\mathbf{r}}^{(\mathrm{sel})} - x\mathbf{h}^{(\mathrm{sel})} = \mathbf{n} + \mathbf{w}. \tag{3.28}$$

3.3.1 Simulative CQ-KC

We start from the case where the channel is perfectly known at the receiver side. Recalling the expression of y, given in (3.14), with a MRB combiner $\mathbf{u}$ equal to (3.13), the SNR Γ becomes

$$\Gamma = \frac{\mathbb{E}_x\left[\left|\mathbf{u}^{\mathsf{H}} x\mathbf{h}^{(\mathrm{sel})}\right|^2\right]}{\mathbb{E}_{\mathbf{n},\mathbf{w}}\left[\left|\mathbf{u}^{\mathsf{H}}\left(\mathbf{n}+\mathbf{w}\right)\right|^2\right]} = \frac{\left\|\mathbf{h}^{(\mathrm{sel})}\right\|^2 / N_{\mathrm{sel}}}{\frac{1}{N_{\mathrm{sel}}\left\|\mathbf{h}^{(\mathrm{sel})}\right\|^2}\mathbb{E}_{\mathbf{v}}\left[\left|\mathbf{h}^{(\mathrm{sel})\mathsf{H}}\mathbf{v}\right|^2\right]} \tag{3.29}$$

and γ

$$\gamma_{\mathrm{CQKC}}^{(s)} = \frac{\widetilde{\mathtt{M}}_h}{\frac{1}{\sigma_n^2 N_{\mathrm{sel}}\left\|\mathbf{h}^{(\mathrm{sel})}\right\|^2}\mathbb{E}_{\mathbf{v}}\left[\left|\mathbf{h}^{(\mathrm{sel})\mathsf{H}}\mathbf{v}\right|^2\right]}. \tag{3.30}$$

The expectation at the denominator of (3.30) is approximated over many realizations of $\mathbf{v}$, which is obtained by (3.28).

3.3.2 Simulative CQ-EC

Now we consider a channel estimate at the receiver by a training MLS x_k of length K.

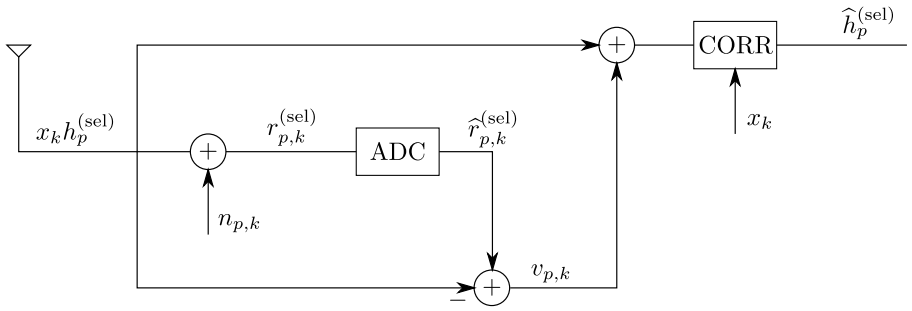

Figure 3.3: The p-th ADC scheme with correlator for channel estimation.

The simulation of the estimation procedure

From (3.28), at instant k

$$v_{p,k} = \widehat{r}_{p,k}^{(\mathrm{sel})} - x_k h_p^{(\mathrm{sel})} = x_k h_p^{(\mathrm{sel})} + n_{p,k} + w_{p,k} - x_k h_p^{(\mathrm{sel})} = n_{p,k} + w_{p,k}. \tag{3.31}$$

Recalling the expression of the p-th estimated channel gain $\widehat{h}_p^{(\mathrm{sel})}$, given in (3.24), we report the expression of the p-th estimation error z_p in relation to the overall noise $v_{p,k}$ defined in (3.31)

$$z_p = \widehat{h}_p^{(\mathrm{sel})} - h_p^{(\mathrm{sel})} = \frac{1}{K}\sum_{k=0}^{K-1} x_k^* \left(n_{p,k} + w_{p,k}\right) = \frac{1}{K}\sum_{k=0}^{K-1} x_k^* v_{p,k}. \tag{3.32}$$

The simulation of the estimation procedure is illustrated in Figure 3.3.
It is important to underline that, in this case, no assumptions on the statistical independence over time k for $x_k^* v_{p,k}$ is done, therefore the central limit theorem is not used to obtain the distribution of z_p.

SNR characterization

After the simulation of the channel estimation error vector $\mathbf{z}$, composed by the entries z_p given in (3.32), we are able to test the performance of the receiver with the approximated MRB combiner defined in (3.19). The expression of the output signal y, recalling (3.26) with the use of the equivalent noise vector $\mathbf{v}$, becomes equal to

$$\begin{aligned} y &= \mathbf{u}^{\mathsf{H}} \left(x\mathbf{h}^{(\mathrm{sel})} + \mathbf{v}\right) \\ &= \frac{1}{\|\mathbf{h}^{(\mathrm{sel})}\|} \left(x\mathbf{h}^{(\mathrm{sel})\mathsf{H}}\mathbf{h}^{(\mathrm{sel})} + x\mathbf{z}^{\mathsf{H}}\mathbf{h}^{(\mathrm{sel})} + \mathbf{h}^{(\mathrm{sel})\mathsf{H}}\mathbf{v} + \mathbf{z}^{\mathsf{H}}\mathbf{v}\right), \end{aligned} \tag{3.33}$$

that yields

$$\gamma_{\mathrm{CQEC}}^{(s)} = \frac{\widetilde{\mathtt{M}}_h}{\frac{1}{\sigma_n^2 N_{\mathrm{sel}} \left\|\mathbf{h}^{(\mathrm{sel})}\right\|^2} \mathbb{E}_{\mathbf{v},\mathbf{z}} \left[\left|x\mathbf{z}^{\mathsf{H}}\mathbf{h}^{(\mathrm{sel})} + \mathbf{h}^{(\mathrm{sel})\mathsf{H}}\mathbf{v} + \mathbf{z}^{\mathsf{H}}\mathbf{v}\right|^2\right]}, \tag{3.34}$$

where $\widetilde{\mathtt{M}}_h$ is defined in (3.10).

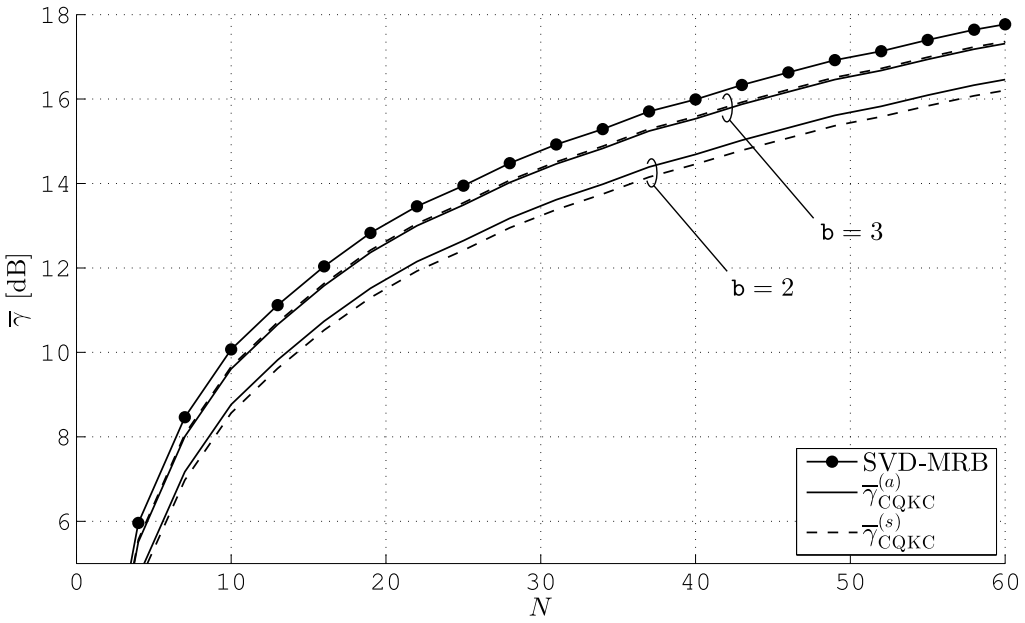

Figure 3.4: Analytical and simulative CQ-KC average γ curves vs. the number of antennas N. The values are averaged over 1000 noise realizations and 5000 channel realizations, $\Gamma_{\mathrm{AWGN}} = 0$ dB.

3.4 Performance evaluation

In this section we show some curves of the average SNR improvement γ versus the number of antennas. Performance evaluation is for the same channel settings and propagation characteristics of Section 2.2.2.

3.4.1 CQ-KC performance

Figures 3.4 and 3.6 show, for two values of Γ_{AWGN}, the average SNR improvement $\overline{\gamma}$ versus the number of receiver antennas N. Figures 3.5 and 3.7, on the other hand, show the same curves versus the number of selected antennas N_{sel} over the total array size of $N = 60$. The solid curves with full circles represent the SVD-MRB bound without quantization, or equivalently when $\mathbf{w} = \mathbf{0}$, the solid curves denote the analytical performance (3.18), while the dashed curves represent the simulated performance (3.30). For each Γ_{AWGN}, results, are reported for two different quantization granularity, $\mathtt{b} = 2$ and $\mathtt{b} = 3$.

Remarks on performance

In the high noise scenario ($\Gamma_{\mathrm{AWGN}} = 0$ dB) in Figures 3.4 and 3.5, the average SNR improvement $\overline{\gamma}$ is relevant and greater than the case when $\Gamma_{\mathrm{AWGN}} = 5$ dB, reported in Figures 3.6 and 3.7. From a general point of view, in the case of low noise, the quantization noise dominates over the thermal noise and only with a high number of bits we can reduce the SVD-MRB bound gap. We note also that the gap between analytical and simulated curves is remarkable only with few bits and

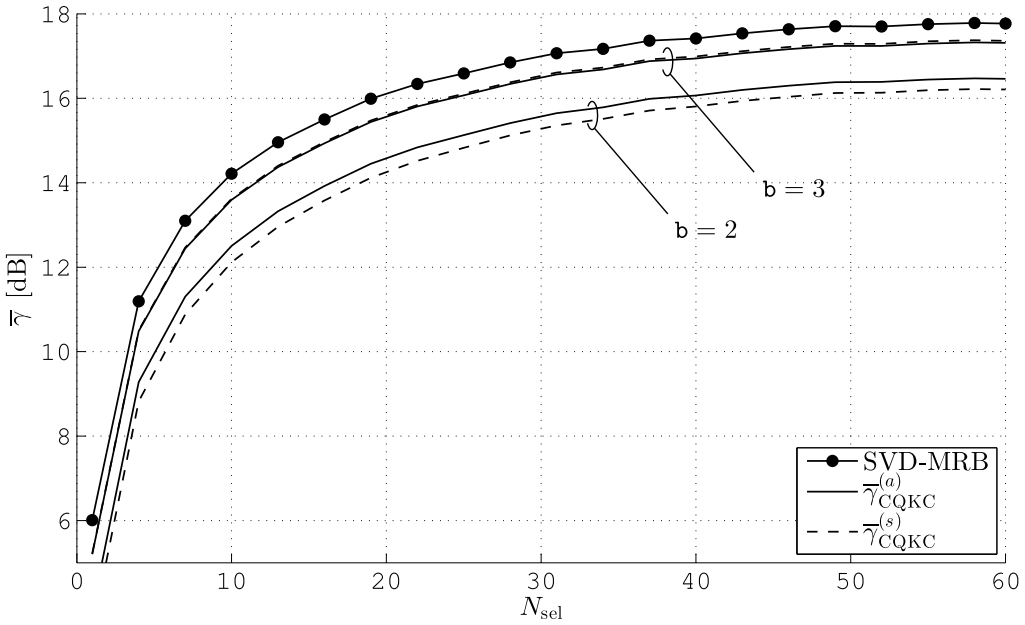

Figure 3.5: Analytical and simulative CQ-KC average γ curves vs. the number of selected antennas N_{sel} over $N = 60$ Rx antennas. The values are averaged over 1000 noise realizations and 5000 channel realizations, $\Gamma_{\text{AWGN}} = 0$ dB.

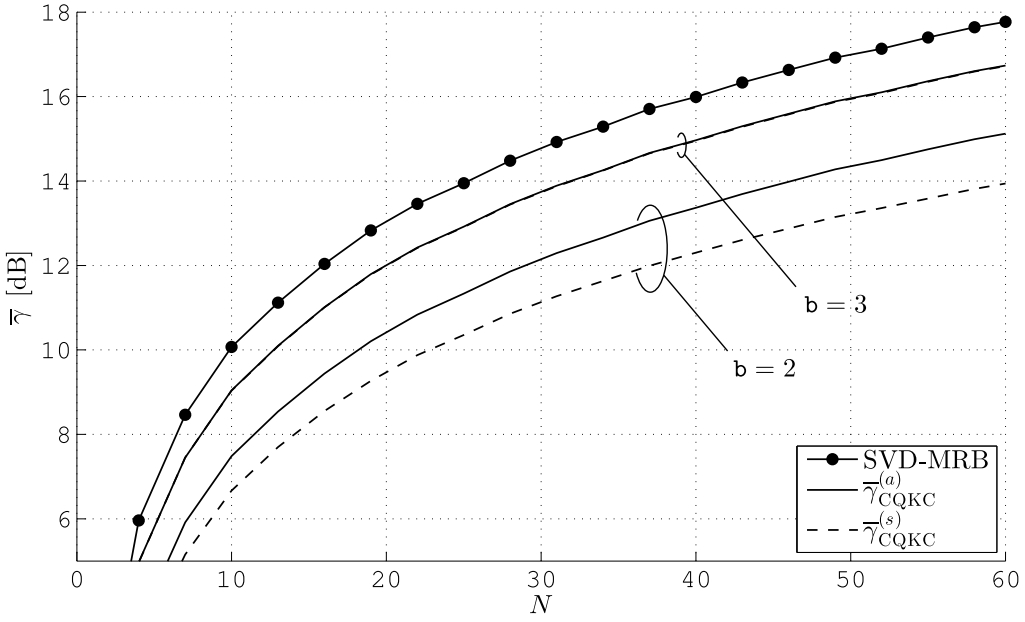

Figure 3.6: Analytical and simulative CQ-KC average γ curves vs. the number of antennas N. The values are averaged over 1000 noise realizations and 5000 channel realizations, $\Gamma_{\text{AWGN}} = 5$ dB.

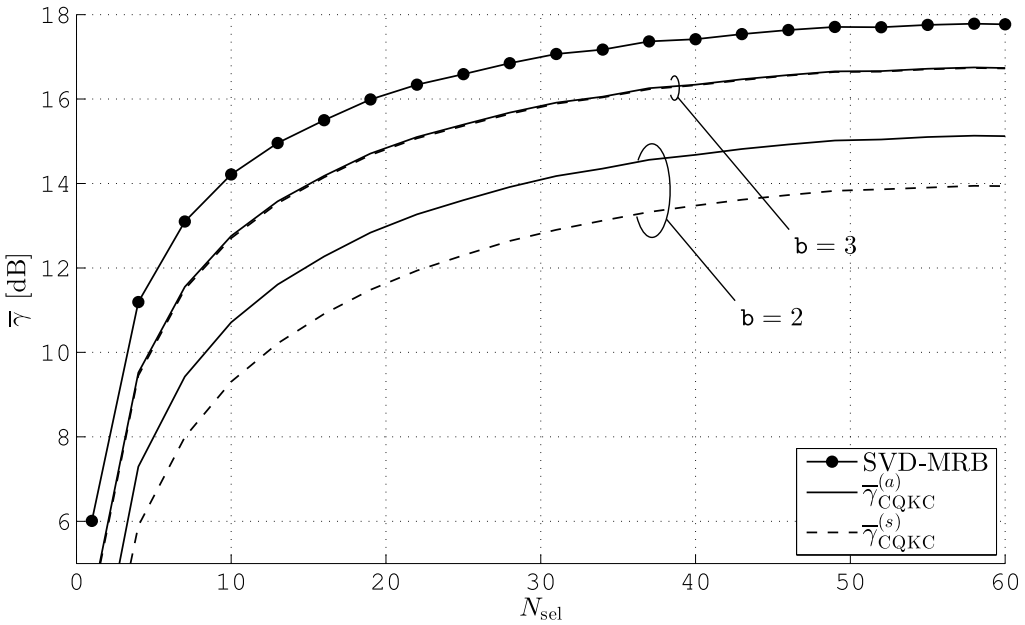

Figure 3.7: Analytical and simulative CQ-KC average γ curves vs. the number of selected antennas N_{sel} over $N = 60$ Rx antennas. The values are averaged over 1000 noise realizations and 5000 channel realizations, $\Gamma_{\text{AWGN}} = 5$ dB.

low noise, because, in this case, the assumption of Gaussian input is only partially true and values of β in Tab. 3.1 are not optimum. Indeed, just for $\mathtt{b} = 3$, the quantization noise is less relevant and the simulated and analytical curves are very close. Antenna selection leads to a remarkable improvement of $\overline{\gamma}$ with the few best antennas, while when N_{sel} approaches N the curves become flat.

3.4.2 CQ-EC performance

For the same propagation characteristic and identical Rx antenna array described for the performance of CQ-KC, Figures 3.8 and 3.10 show the analytical and simulated curves of $\overline{\gamma}$ versus N for CQ-EC, while Figuers 3.9 and 3.11 show the same curves versus the number of selected antennas N_{sel} over an array of $N = 60$ antennas.

Remarks on performance

The remarks on performance of CQ-EC are analogous to the remarks that have been made for CQ-KC. In addition, we note that the gap between the SVD-MRB bound and the curves obtained by coarse quantization with the channel estimate is bigger with respect to the performance obtained with the known channel: this gap can be lowered by using higher values of K.

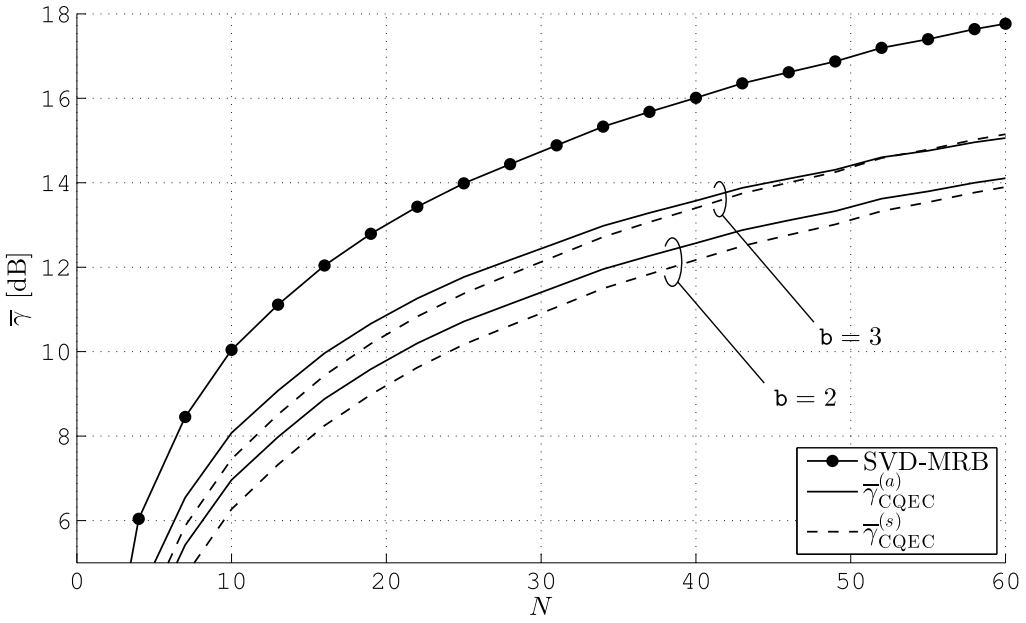

Figure 3.8: Analytical and simulative CQ-EC average γ curves vs. the number of antennas N. The values are averaged over 1000 noise realizations and 5000 channel realizations, $\Gamma_{\mathrm{AWGN}} = 0$ dB, $K = 3$.

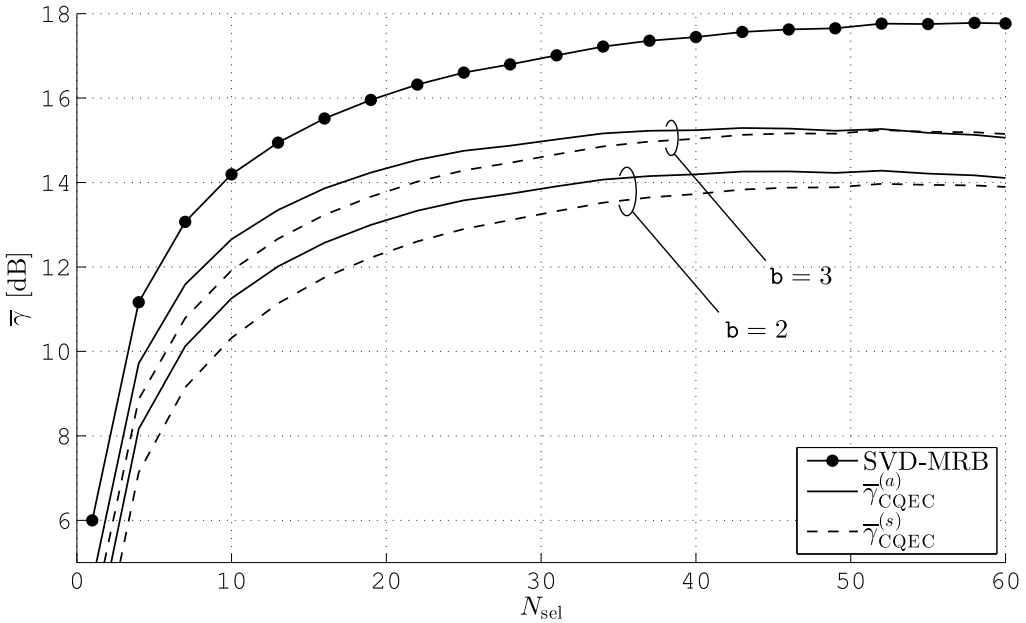

Figure 3.9: Analytical and simulative CQ-EC average γ curves vs. the number of selected antennas N_{sel} over $N = 60$ Rx antennas. The values are averaged over 1000 noise realizations and 5000 channel realizations, $\Gamma_{\mathrm{AWGN}} = 0$ dB, $K = 3$.

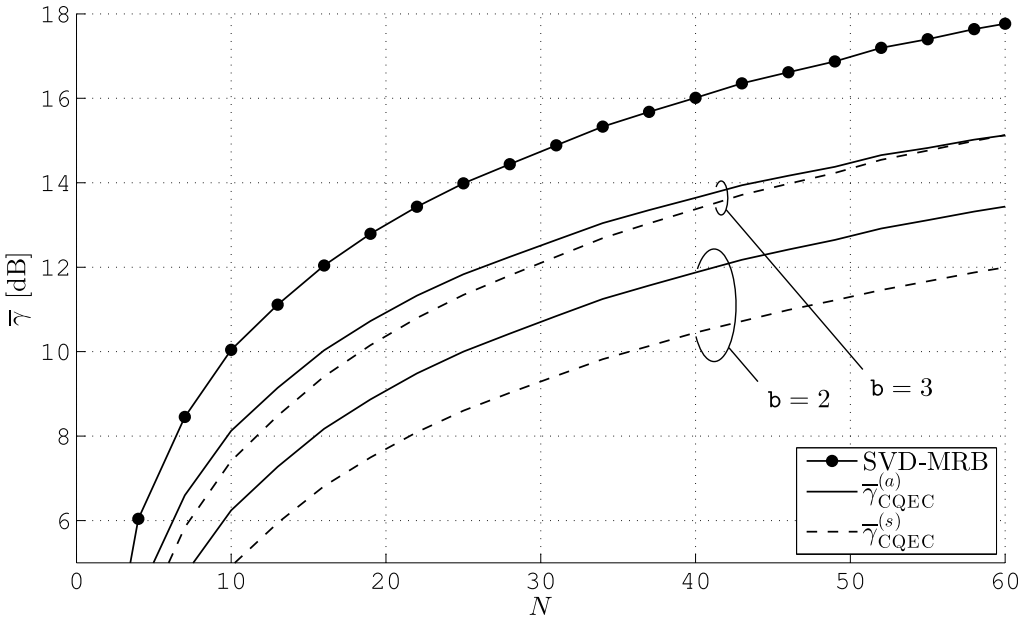

Figure 3.10: Analytical and simulative CQ-EC average γ curves vs. the number of antennas N. The values are averaged over 1000 noise realizations and 5000 channel realizations, $\Gamma_{\mathrm{AWGN}} = 5$ dB, $K = 3$.

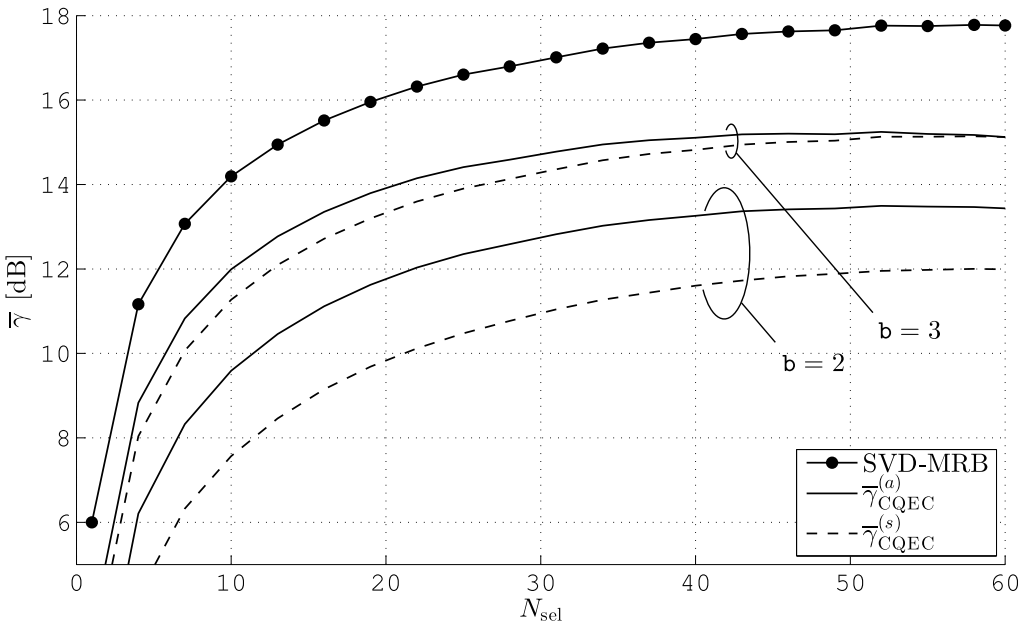

Figure 3.11: Analytical and simulative CQ-EC average γ curves vs. the number of selected antennas N_{sel} over $N = 60$ Rx antennas. The values are averaged over 1000 noise realizations and 5000 channel realizations, $\Gamma_{\mathrm{AWGN}} = 5$ dB, $K = 3$.

Chapter 4

Non-coherent D-PSK

In Chapter 2 we have considered full CSI at both Tx and Rx, in Chapter 3 we have relaxed the strong assumption of channel knowledge at Tx and investigated a low-complexity quantization MRB with known and estimated CSI at Rx. Now we go to the case where no CSI, is known also at Rx.
In this chapter we seek to explore the receiver multi-antenna array gain in non-coherent[1] differential phase shift keying (D-PSK) SIMO configuration. As in Chapter 3 antenna selection is investigated with the aim to have a simpler receiver with few RF chains which do not consider the worst branches.

4.1 The system description

An extension to the SIMO case of the implementation for the classical D-PSK is considered. It is assumed that the receiver recovers the signal carrier, except for a phase offset, in other terms it is as if the constellation at the receiver is rotated by that offset. By the *differential non-coherent method*, a receiver detects the data computing the difference between the phase of signals at successive time instants.
In Figure 4.1 is considered a SIMO system with one transmit antenna and N receive antennas. At instant k, the transmitter sends a D-PSK symbol s_k, which is obtained

[1]In our framework we say that a system is coherent if it is able to recover the phase as well as the carrier frequency of the received signal, otherwise, a non-coherent receiver oscillates only at the carrier frequency and no informations about the phase are recovered.

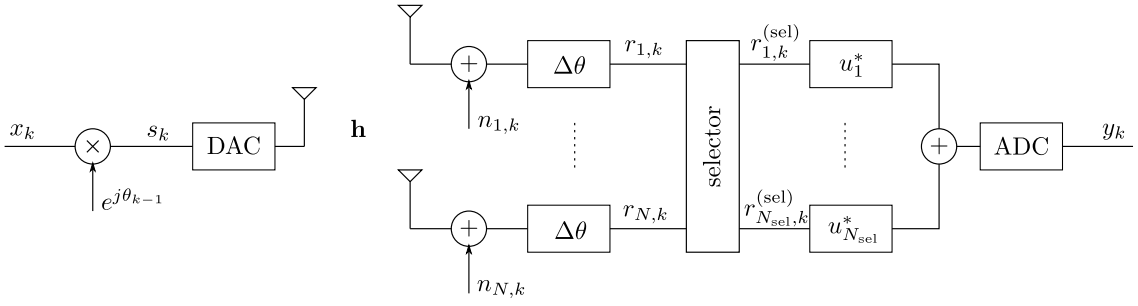

Figure 4.1: SIMO DPSK system.

from x_k by adding the phase $\theta_{k-1} = \angle(s_{k-1})$ of the previous transmitted sample. Each receiver processes the received signal by an operation in the analog domain (denoted as $\Delta\theta$ in Figure 4.2) that yields the phase difference between s_k and s_{k-1} in order to suppress the channel phase offset. Next, $N_{\text{sel}} \leq N$ entries of the received vector

$$\mathbf{r}_k = \begin{bmatrix} r_{1,k} & \cdots & r_{p,k} & \cdots & r_{N,k} \end{bmatrix}^{\mathsf{T}} \in \mathbb{C}^{N\times 1} \tag{4.1}$$

are chosen by a *selector* in a proper way to form the vector

$$\mathbf{r}_k^{(\text{sel})} = \begin{bmatrix} r_{1,k}^{(\text{sel})} & \cdots & r_{p,k}^{(\text{sel})} & \cdots & r_{N_{\text{sel}},k}^{(\text{sel})} \end{bmatrix}^{\mathsf{T}} \in \mathbb{C}^{N_{\text{sel}}\times 1}. \tag{4.2}$$

Finally, the N_{sel} components of $\mathbf{r}_k^{(\text{sel})}$ are joined by the combiner

$$\mathbf{u} = \begin{bmatrix} u_1 & \cdots & u_p & \cdots & u_{N_{\text{sel}}} \end{bmatrix}^{\mathsf{T}} \in \mathbb{C}^{N_{\text{sel}}\times 1} \tag{4.3}$$

and the output y_k is obtained as

$$y_k = \mathbf{u}^{\mathsf{H}}\mathbf{r}_k^{(\text{sel})}. \tag{4.4}$$

If the channel is denoted by the vector

$$\mathbf{h} = \begin{bmatrix} h_1 & \cdots & h_p & \cdots & h_N \end{bmatrix}^{\mathsf{T}} \in \mathbb{C}^{N\times 1}, \tag{4.5}$$

after the *selector*, the channel vector,

$$\mathbf{h}^{(\text{sel})} = \begin{bmatrix} h_1^{(\text{sel})} & \cdots & h_p^{(\text{sel})} & \cdots & h_{N_{\text{sel}}}^{(\text{sel})} \end{bmatrix}^{\mathsf{T}} \in \mathbb{C}^{N_{\text{sel}}\times 1}, \tag{4.6}$$

to be gathers the N_{sel} channel samples chosen in a way that fulfil the selector policy described in Section 4.1.2.
The vector noise is

$$\mathbf{n}_k = \begin{bmatrix} n_{1,k} & \cdots & n_{p,k} & \cdots & n_{N,k} \end{bmatrix}^{\mathsf{T}} \in \mathbb{C}^{N\times 1} \tag{4.7}$$

as defined in (2.8).

4.1.1 Input-output relationship

Let x_k denotes the the phase shift keying (PSK) symbol to be transmitted at instant k, if $\mathcal{M}$ represents the constellation size, x_k assumes the values

$$x_k = e^{j\psi_k}, \qquad \psi_k \in \left\{ \frac{\pi}{\mathcal{M}}(2m-1) \;\middle|\; m = 1, \ldots, \mathcal{M} \right\}. \tag{4.8}$$

The transmitted symbol s_k is equal to

$$s_k = e^{j\theta_k} = e^{j(\psi_k+\theta_{k-1})}, \tag{4.9}$$

where $\theta_{k-1} = \angle(s_{k-1})$ is the phase of the transmitted symbol at the previous instant. The signal at the generic p^{th} ($p = 1, \ldots, N$) receive antenna is processed by a $\Delta\theta$

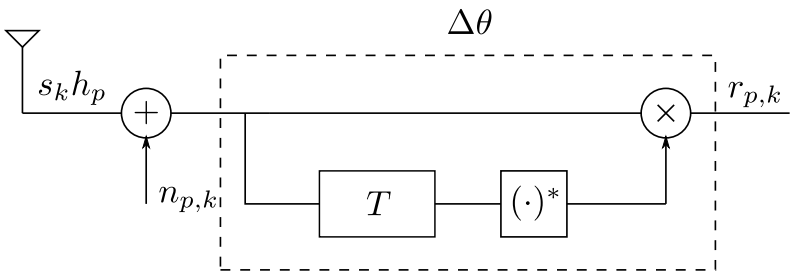

Figure 4.2: Baseband equivalent representation of $\Delta\theta$ block for the p^{th} receive antenna.

block, represented in Figure 4.2, to yield $r_{p,k}$. Referring to Figure 4.2, where T denotes a delay and $(\cdot)^*$ the complex conjugation, the output signal is equal to

$$\begin{aligned} r_{p,k} &= (s_k h_p + n_{p,k}) (s_{k-1} h_p + n_{p,k-1})^* \\ &= |h_p|^2 x_k + s_k h_p n_{p,k-1}^* + s_{k-1}^* h_p^* n_{p,k} + n_{p,k} n_{p,k-1}^*. \end{aligned} \tag{4.10}$$

In the presence of a selector, the received signal becomes

$$r_{p,k}^{(\text{sel})} = \left|h_p^{(\text{sel})}\right|^2 x_k + s_k h_p^{(\text{sel})} n_{p,k-1}^* + s_{k-1}^* h_p^{(\text{sel})*} n_{p,k} + n_{p,k} n_{p,k-1}^* \tag{4.11}$$

which is combined by u_p, to obtain y_k as given by (4.4).

4.1.2 The selector policy

In Figure 4.1 the *selector* chooses N_{sel} antennas from the total set of N receive antennas. After the differential block $\Delta\theta$, the signal to noise ratio for each branch will be denoted by Θ_p, $p = 1, \ldots, N$, and considering (4.10), it is

$$\Theta_p = \frac{\mathbb{E}_x \left[\left| |h_p|^2 x_k \right|^2 \right]}{\mathbb{E}_n \left[\left| s_k h_p n_{p,k-1}^* + s_{k-1}^* h_p^* n_{p,k} + n_{p,k} n_{p,k-1}^* \right|^2 \right]} = \frac{|h_p|^4}{\sigma_n^2 \left(2 |h_p|^2 + \sigma_n^2 \right)}, \tag{4.12}$$

because noise samples are assumed statistically independent in time and across the different branches. The *selector* chooses the N_{sel} branches with the largest Θ_p.
We also consider a random selection policy, in this case, the *selector* chooses $N_{\text{sel}} \leq N$ branches randomly. This is not a selection policy at all, but can represent an interesting performance comparison.

4.2 SNR characterization

The output sample y_k, expanding (4.4) and considering (4.11) is equal to

$$y_k = \sum_{p=1}^{N_{\text{sel}}} u_p^* \left(\left|h_p^{(\text{sel})}\right|^2 x_k + s_k h_p^{(\text{sel})} n_{p,k-1}^* + s_{k-1}^* h_p^{(\text{sel})*} n_{p,k} + n_{p,k} n_{p,k-1}^* \right). \tag{4.13}$$

The statistical power of the useful term of equation (4.13) is equal to

$$\begin{aligned}\mathbb{E}_x\left[\left|\sum_{p=1}^{N_{\text{sel}}} u_p^* \left|h_p^{(\text{sel})}\right|^2 x_k\right|^2\right] &= \left|\sum_{p=1}^{N_{\text{sel}}} u_p^* \left|h_p^{(\text{sel})}\right|^2\right|^2 \mathbb{E}_x\left[|x_k|^2\right] \\ &= \left|\sum_{p=1}^{N_{\text{sel}}} u_p^* \left|h_p^{(\text{sel})}\right|^2\right|^2\end{aligned} \tag{4.14}$$

while the statistical power of the noise is

$$\begin{aligned}&\mathbb{E}_{n,s}\left[\left|\sum_{p=1}^{N_{\text{sel}}} u_p^*\left(s_k h_p^{(\text{sel})} n_{p,k-1}^* + s_{k-1}^* h_p^{(\text{sel})*} n_{p,k} + n_{p,k} n_{p,k-1}^*\right)\right|^2\right] \\ \overset{(1)}{=}&\sum_{p=1}^{N_{\text{sel}}}\left(\mathbb{E}_{n,s}\left[\left|u_p^* s_k h_p^{(\text{sel})} n_{p,k-1}^*\right|^2\right] + \mathbb{E}_{n,s}\left[\left|u_p^* s_{k-1} h_p^{(\text{sel})*} n_{p,k}\right|^2\right] + \mathbb{E}_{n,s}\left[\left|u_p^* n_{p,k} n_{p,k-1}^*\right|^2\right]\right) \\ =&\sigma_n^2 \sum_{p=1}^{N_{\text{sel}}} \left|u_p^*\right|^2 \left(2\left|h_p^{(\text{sel})}\right|^2 + \sigma_n^2\right),\end{aligned} \tag{4.15}$$

where the equality (1) comes from the uncorrelation of noise samples in time and across the different antennas.
Then the SNR Γ, is equal to

$$\Gamma = \frac{\left|\sum_{p=1}^{N_{\text{sel}}} u_p^* \left|h_p^{(\text{sel})}\right|^2\right|^2}{\sigma_n^2 \sum_{p=1}^{N_{\text{sel}}} \left|u_p^*\right|^2 \left(2\left|h_p^{(\text{sel})}\right|^2 + \sigma_n^2\right)}. \tag{4.16}$$

4.2.1 Two combiners

In order to handle D-PSK diversity we try two combining solutions.

1. The first combiner weights all branches with same coefficients

$$u_p = \frac{1}{\sqrt{N_{\text{sel}}}}, \quad \text{for} \quad p = 1, \ldots, N_{\text{sel}}, \tag{4.17}$$

this is the simplest approach and is equivalent to sum together all the branches. In this case the SNR improvement respect to single antenna configuration is equal to

$$\gamma_{\text{DPSK}}^{(1)} = \frac{\left|\sum_{p=1}^{N_{\text{sel}}} \left|h_p^{(\text{sel})}\right|^2\right|^2}{\sum_{p=1}^{N_{\text{sel}}} \left(2\left|h_p^{(\text{sel})}\right|^2 + \sigma_n^2\right)}. \tag{4.18}$$

2. The second combiner tries to increase the SNR by weighting each contribution with the square root of the SNR of the branch. The weights u_p are equal to

$$u_p = \sqrt{\Theta_p}, \quad \text{for} \quad p = 1, \ldots, N_{\text{sel}}, \tag{4.19}$$

where Θ_p is given by (4.12). In this second approach the expression of γ becomes

$$\gamma^{(2)}_{\text{DPSK}} = \frac{\left| \sum_{p=1}^{N_{\text{sel}}} \frac{\left|h_p^{(\text{sel})}\right|^4}{\sqrt{2\left|h_p^{(\text{sel})}\right|^2 + \sigma_n^2}} \right|^2}{\sum_{p=1}^{N_{\text{sel}}} \left|h_p^{(\text{sel})}\right|^4}. \tag{4.20}$$

We note that the second combiner is more complex than the first one, moreover to set the combiner weights we need to know the channel gains.

4.3 Performance analysis

The performance are evaluated, as usual, in terms of the average γ. We consider different size N of the receiver array of antenna elements and two different thermal noise powers. For the description of the channel model and the propagation environment we refer to Section 2.2.2.
Figures 4.3 and 4.4 show plots of (4.18), for $\Gamma_{\text{AWGN}} = 0$ dB and $\Gamma_{\text{AWGN}} = 5$ dB respectively, whereas in Figures 4.5 and 4.6 are showed values of (4.20), in the same conditions. The horizontal axis of each plot represent a double scale, one is for the number of selected antennas N_{sel} and one for the total number of receiver antennas. More precisely, for the SVD-MRB bound (solid line) we have to read the numbers of horizontal axis as the size N of the array, without selection. The same interpretation is valid also for the random selection (dashed line) because choosing antennas *randomly*, on average, does not lead to better performance if the array size increases. For the curves with different marker shapes, the horizontal axis represent the number of selected antennas N_{sel} over the total array size N indicated in the legend.

4.3.1 Remarks on performance

From a comparison between the four figures we note that the two combining strategies (4.17) and (4.19) yield very similar performance, hence it is preferable to use (4.17) due to its simplicity with no need of CSI. Antenna selections enables great γ improvement with few antennas (the best ones), while when N_{sel} get closer to N the curves becomes more flat.
The SNR improvement γ, in contrast to the MRB with coarse quantization of Chapter 3, increases with the decreasing of the thermal noise power.
It is interesting to underline that the non-coherent SIMO D-PSK with optimal selection, in spite of its simplicity, achieves good performance. In order to underline this

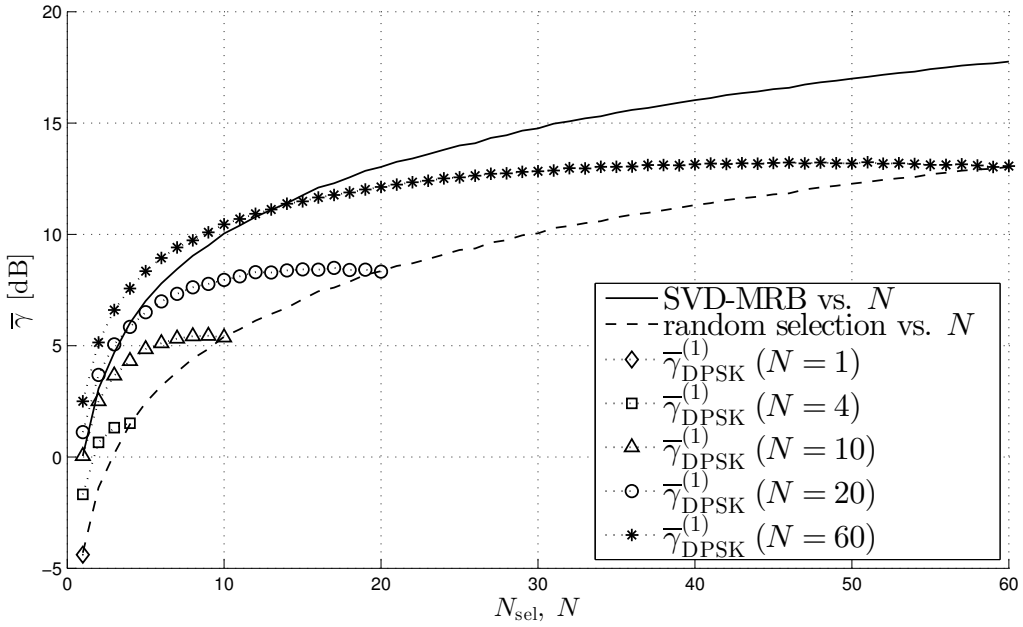

Figure 4.3: Average values of γ as given by (4.18) for different Rx arrays sizes versus the number of selected antennas over 5000 channel realizations, $\Gamma_{\text{AWGN}} = 0$ dB.

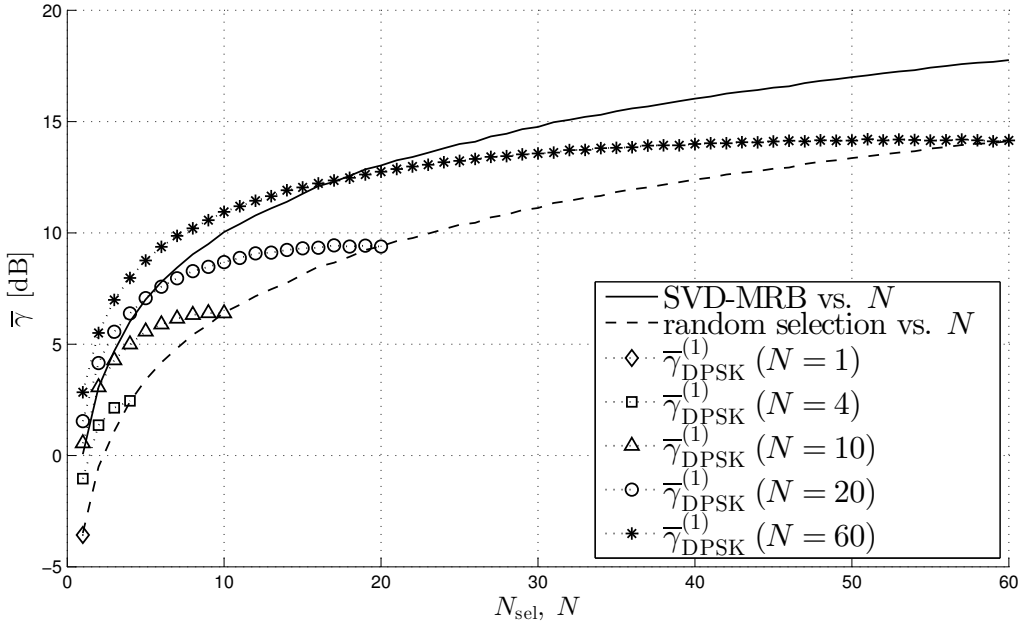

Figure 4.4: Average values of γ as given by (4.18) for different Rx arrays sizes versus the number of selected antennas over 5000 channel realizations, $\Gamma_{\text{AWGN}} = 5$ dB.

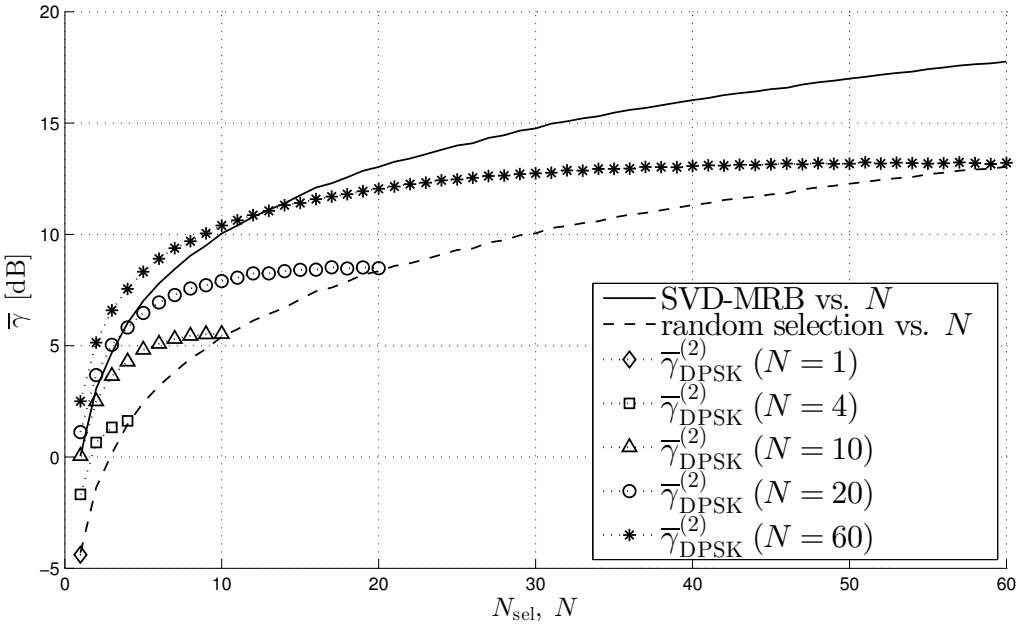

Figure 4.5: Average values of γ as given by (4.20) for different Rx arrays sizes versus the number of selected antennas over 5000 channel realizations, $\Gamma_{\mathrm{AWGN}} = 0$ dB.

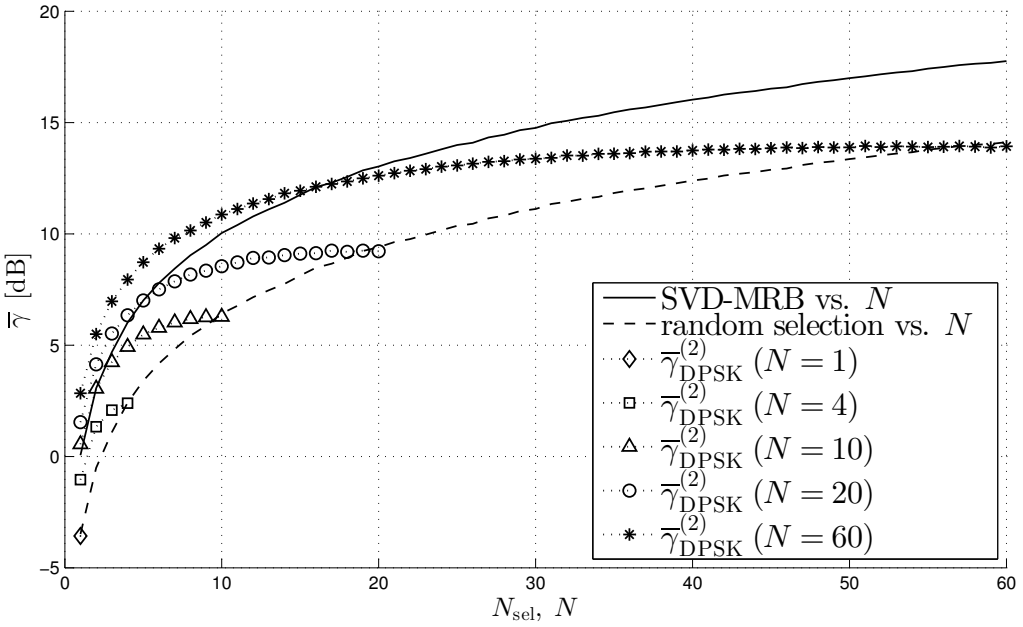

Figure 4.6: Average values of γ as given by (4.20) for different Rx arrays sizes versus the number of selected antennas over 5000 channel realizations, $\Gamma_{\mathrm{AWGN}} = 5$ dB.

Table 4.1: Sample performance comparison between SVD-MRB and SIMO DPSK.

	N	N_{sel}	Γ_{AWGN} [dB]	$\overline{\gamma}$ [dB]	σ_γ [dB]
SVD-MRB ($M = 1$)	30	30	whatever	14.78	10.47
SIMO DPSK (optimal selection)	60	30	5	13.57	8.77
SIMO DPSK (random selection)	60	30	5	11.12	7.26

fact, in Table 4.1 we give an example comparison between the optimum SVD-MRB in a SIMO configuration ($M = 1$) and the D-PSK.

Appendix A

A different coarse ADC approach

In this appendix we propose the same system of Chapter 3, characterized by a one antenna at the transmitter and by multiple-antennas at the receiver which implements a digital MRB with ADCs with few bits. In this system, however, we do not use MMSE ADCs, but we design the saturation thresholds $\tau^{(\mathrm{sat})}$ based on the useful signal, ignoring the presence of thermal noise. In this perspective, in the case of high thermal noise, the ADC works mainly in saturation and this may degrade performance, however, in the case of low noise this approach could be more convenient. The structure of the appendix traces Chapter 3, the new ADC model is briefly described and all the expressions of γ in Chapter 3 are reprised with the reference of the new quantization model. Finally, performance evaluations are provided.

A.1 A new ADC model

The system reference structure is described at the beginning of Chapter 3 and its graphical representation is reported in Figure 3.1, the signals and the selector policy are the same, but we introduce a different ADC model.
The in-phase and quadrature components of the p-th, $p = 1, \ldots, N$, received signal r_p are digital converted by two identical ADCs. Both converters, as in Chapter 3, are characterized by an uniform quantization with symmetrical saturation levels $\tau_p^{(\mathrm{sat})}$ and $2^{\mathtt{b}}$ thresholds, where $\mathtt{b}$ denotes the number of bits.
If $\alpha \geq 1$ is a real number and $|x|_{\mathrm{M}} = \max_x |x|$ represents the maximum value over the Tx constellation symbols amplitude, it holds that the in-phase and quadrature parts of the p-th useful signal xh_p are smaller than $\alpha\,|h_p|\,|x|_{\mathrm{M}}$:

$$|\Re\{xh_p\}|\,,\ |\Im\{xh_p\}| \leq \alpha\,|h_p|\,|x|_{\mathrm{M}}\,, \tag{A.1}$$

where $\Re\{\cdot\}$ and $\Im\{\cdot\}$ represent the real and imaginary parts respectively. Therefore, ignoring the noisy part of the received signal r_p, $\tau_p^{(\mathrm{sat})}$ can be set equal to (A.1)

$$\tau_p^{(\mathrm{sat})} = \alpha\left|h_p^{(\mathrm{sel})}\right|\,|x|_{\mathrm{M}}\,, \tag{A.2}$$

where α is intentionally not fixed in order to keep a scale factor degree of freedom.

A.2 Analytical performance evaluation

In this section we provide the analytical expression of γ for the known channel CQ-KC and its estimate CQ-EC.
The p-th double ADC can be render with a simple equivalent model that is characterized by the introduction of the complex quantization noise w_p in addition to the noise n_p on the useful signal. In absence of saturation and if $\mathtt{b}$ is large enough, the in-phase and quadrature components of the quantization noise w_p can be modelled as uniform random variable

$$\Re\{w_p\},\ \Im\{w_p\} \sim \mathcal{U}\left[-\frac{\Delta_p}{2};\ \frac{\Delta_p}{2}\right], \tag{A.3}$$

where $\Delta_p = 2\tau_p^{(\mathrm{sat})} \Big/ 2^{\mathtt{b}}$ represents the quantizer step size. In this case, the statistical power of the complex random variable w_p is equal to

$$\begin{aligned}
\mathtt{M}_{w_p} &= \mathbb{E}\left[|w_p|^2\right] \\
&= \mathbb{E}\left[(\Re\{w_p\})^2 + (\Im\{w_p\})^2\right] \\
&= \frac{\Delta_p^2}{6} \\
&= \frac{2}{3}\frac{\alpha^2 \left|h_p^{(\mathrm{sel})}\right|^2 |x|_{\mathrm{M}}^2}{2^{2\mathtt{b}}}.
\end{aligned} \tag{A.4}$$

The assumptions that lead to (A.3) and (A.4) may be in contrast with the requirements of low-complexity ADCs characterized by few bits.

A.2.1 Analytical CQ-KC

As in Chapter 3 we start from evaluating the analytical performance of beamforming with channel known at Rx side.
The received signal at the decision point is given by (3.14), if the entries of $\mathbf{n}$ and $\mathbf{w}$ are supposed uncorrelated and $\mathbf{u}$ is equal to (3.13), the overall noise power component of y yields

$$\begin{aligned}
\mathbb{E}_{\mathbf{n},\mathbf{w}}\left[\left|\mathbf{u}^{\mathsf{H}}(\mathbf{n}+\mathbf{w})\right|^2\right] &= \sum_{p=1}^{N_{\mathrm{sel}}} \mathbb{E}_{\mathbf{n},\mathbf{w}}\left[\left|u_p^*\right|^2 |n_p + w_p|^2\right] \\
&= \frac{1}{\|\mathbf{h}^{(\mathrm{sel})}\|^2} \sum_{p=1}^{N_{\mathrm{sel}}} \left|h_p^{(\mathrm{sel})}\right|^2 \left(\sigma_n^2 + \mathtt{M}_{w_p}\right) \\
&= \sigma_n^2 + \frac{1}{\|\mathbf{h}^{(\mathrm{sel})}\|^2}\frac{2}{3}\frac{\alpha^2 |x|_{\mathrm{M}}^2}{2^{2\mathtt{b}}} \sum_{p=1}^{N_{\mathrm{sel}}} \left|h_p^{(\mathrm{sel})}\right|^4.
\end{aligned} \tag{A.5}$$

Under the same conditions the power of the useful component of y is

$$\mathbb{E}_x\left[\left|\mathbf{u}^{\mathsf{H}} x \mathbf{h}^{(\mathrm{sel})}\right|^2\right] = \frac{1}{\|\mathbf{h}^{(\mathrm{sel})}\|^2}\left|\sum_{p=1}^{N_{\mathrm{sel}}} \left|h_p^{(\mathrm{sel})}\right|^2\right|^2 \mathbb{E}_x\left[|x|^2\right] = \left\|\mathbf{h}^{(\mathrm{sel})}\right\|^2. \tag{A.6}$$

Therefore, the signal to noise ratio Γ becomes

$$\begin{aligned}\Gamma &= \frac{\left\|\mathbf{h}^{(\mathrm{sel})}\right\|^2 / N_{\mathrm{sel}}}{\frac{1}{N_{\mathrm{sel}}}\left(\sigma_n^2 + \frac{N_{\mathrm{sel}}}{\left\|\mathbf{h}^{(\mathrm{sel})}\right\|^2}\frac{2}{3}\frac{\alpha^2|x|_{\mathrm{M}}^2}{2^{2\mathtt{b}}}\frac{1}{N_{\mathrm{sel}}}\sum_{p=1}^{N_{\mathrm{sel}}}\left|h_p^{(\mathrm{sel})}\right|^4\right)} \\ &= \frac{\widetilde{\mathtt{M}}_h}{\frac{1}{N_{\mathrm{sel}}}\left(\sigma_n^2 + \frac{2}{3}\frac{\alpha^2|x|_{\mathrm{M}}^2}{2^{2\mathtt{b}}}\frac{\widetilde{\mathtt{Q}}_h}{\widetilde{\mathtt{M}}_h}\right)}\end{aligned} \tag{A.7}$$

and, the SNR improvement

$$\gamma_{\mathrm{CQKC}}^{(a)} = \frac{\widetilde{\mathtt{M}}_h}{\frac{1}{N_{\mathrm{sel}}}\left(1 + \frac{2}{3}\frac{\alpha^2|x|_{\mathrm{M}}^2}{2^{2\mathtt{b}}}\frac{\widetilde{\mathtt{Q}}_h}{\sigma_n^2\widetilde{\mathtt{M}}_h}\right)}, \tag{A.8}$$

where $\widetilde{\mathtt{M}}_h$ and $\widetilde{\mathtt{Q}}_h$ are defined in (3.10) and (3.11) respectively.

A.2.2 Analytical CQ-EC

Now we provide the γ expression of analytical performance in the case of channel estimation. In the same way as in Chapter 3 the channel $\mathbf{h}^{(\mathrm{sel})}$ is estimated by a correlation method that uses a training sequence a_k of length K. The estimate $\widehat{h}_p^{(\mathrm{sel})} = h_p^{(\mathrm{sel})} + z_p$ of the p-th channel gain is provided by equation (3.24) and the estimation error z_p is assumed that is distributed as a Gaussian random variable described in (3.25). Under these assumptions we can provide the CQ-EC analytical performance

$$\gamma_{\mathrm{CQEC}}^{(a)} = \frac{\widetilde{\mathtt{M}}_h}{\frac{1}{K}\left\{\frac{1}{N_{\mathrm{sel}}} + \frac{\sigma_n^2}{\|\mathbf{h}^{(\mathrm{sel})}\|^2} + \frac{1}{\|\mathbf{h}^{(\mathrm{sel})}\|^2}\frac{2}{3}\frac{\alpha^2|x|_{\mathrm{M}}^2}{2^{2\mathtt{b}}}\left[\frac{\widetilde{\mathtt{Q}}_h}{\sigma_n^2}\left(1 + \frac{2}{3}\frac{\alpha^2|x|_{\mathrm{M}}^2}{2^{2\mathtt{b}}}\right) + 2\widetilde{\mathtt{M}}_h\right]\right\} + \frac{1}{N_{\mathrm{sel}}}\left(1 + \frac{2}{3}\frac{\alpha^2|x|_{\mathrm{M}}^2}{2^{2\mathtt{b}}}\frac{\widetilde{\mathtt{Q}}_h}{\sigma_n^2\widetilde{\mathtt{M}}_h}\right)}. \tag{A.9}$$

A.3 Simulative evaluation

In this section we focus on the simulative performance for the known channel in CQ-KC approach and for the channel estimate in CQ-EC approach. As in Chapter 3, in the simulative approach we consider the overall noise vector $\mathbf{v}$, which contains the degradation of both thermal and quantization noises, by the difference between the signal after quantization and the useful received signal part.
We note that the expressions of γ are equal to the equation in Chapter 3, in particular the CQ-KC simulative performance expression is equal to (3.30) and CQ-EC is equal to (3.34). For simplicity we rewrite them

$$\gamma_{\mathrm{CQKC}}^{(s)} = \frac{\widetilde{\mathtt{M}}}{\frac{1}{\sigma_n^2 N_{\mathrm{sel}}\left\|\mathbf{h}^{(\mathrm{sel})}\right\|^2}\mathbb{E}_{\mathbf{v}}\left[\left|\mathbf{h}^{(\mathrm{sel})\mathsf{H}}\mathbf{v}\right|^2\right]} \tag{A.10}$$

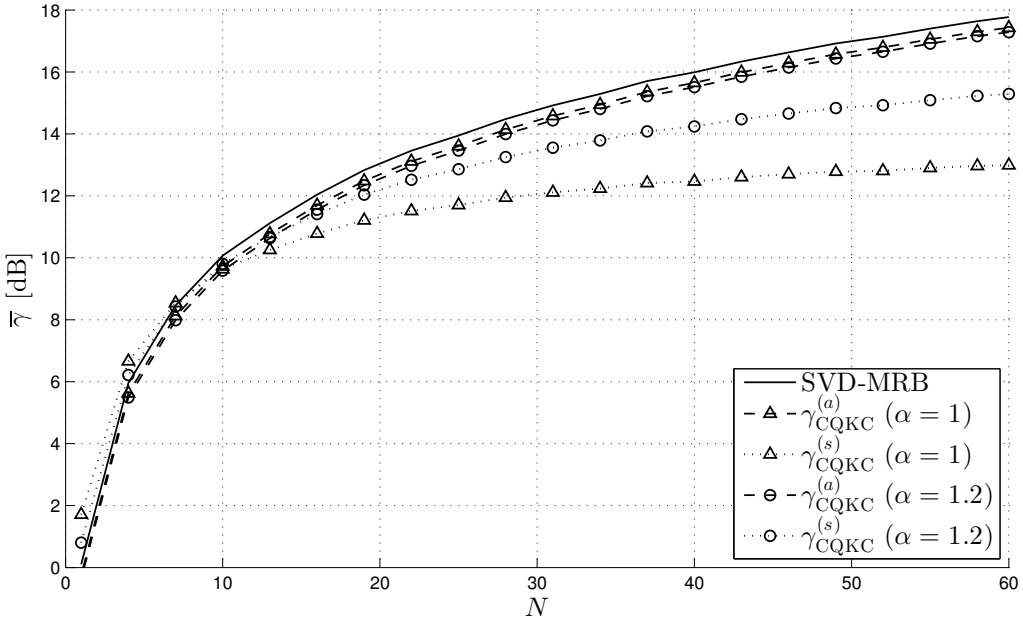

Figure A.1: Analytical and simulated CQ-KC average γ curves vs. the number of antennas N. The values are averaged over 1000 noise realizations and 5000 channel realizations. $|x|_{\mathrm{M}} = 1$, $\mathtt{b} = 2$ and $\Gamma_{\mathrm{AWGN}} = 0$ dB.

and

$$\gamma^{(s)}_{\mathrm{CQEC}} = \frac{\widetilde{\mathtt{M}}_h}{\frac{1}{\sigma_n^2 N_{\mathrm{sel}} \left\| \mathbf{h}^{(\mathrm{sel})} \right\|^2} \mathbb{E}_{\mathbf{v},\mathbf{z}} \left[\left| x\mathbf{z}^{\mathsf{H}}\mathbf{h}^{(\mathrm{sel})} + \mathbf{h}^{(\mathrm{sel})\mathsf{H}}\mathbf{v} + \mathbf{z}^{\mathsf{H}}\mathbf{v} \right|^2 \right]}. \tag{A.11}$$

We note that although expressions of γ are the same as those of Chapter 3, the ADCs use different setting that lead to different system performance.

A.4 Performance evaluations

With the same channel settings and propagation characteristics of Section 2.2.2, we give some average performance results for CQ-KC and CQ-EC for different values of the saturation threshold scaling factor α.

A.4.1 CQ-KC performance

Figures A.1 and A.3 show the average γ versus the number of receiver antennas N, with two different thermal noise powers, while Figures A.2 and A.4 represent the performance with antenna selection. The solid curve is the SVD-MRB bound in presence of perfect digital conversions, or equivalently for $\mathbf{w} = \mathbf{0}$. The dashed curves denote analytical performance, while the dotted ones simulated performance as from (A.8) and (A.10), respectively. Moreover triangles and circles indicate, correspondingly, two different values of the saturation scaling factor α.

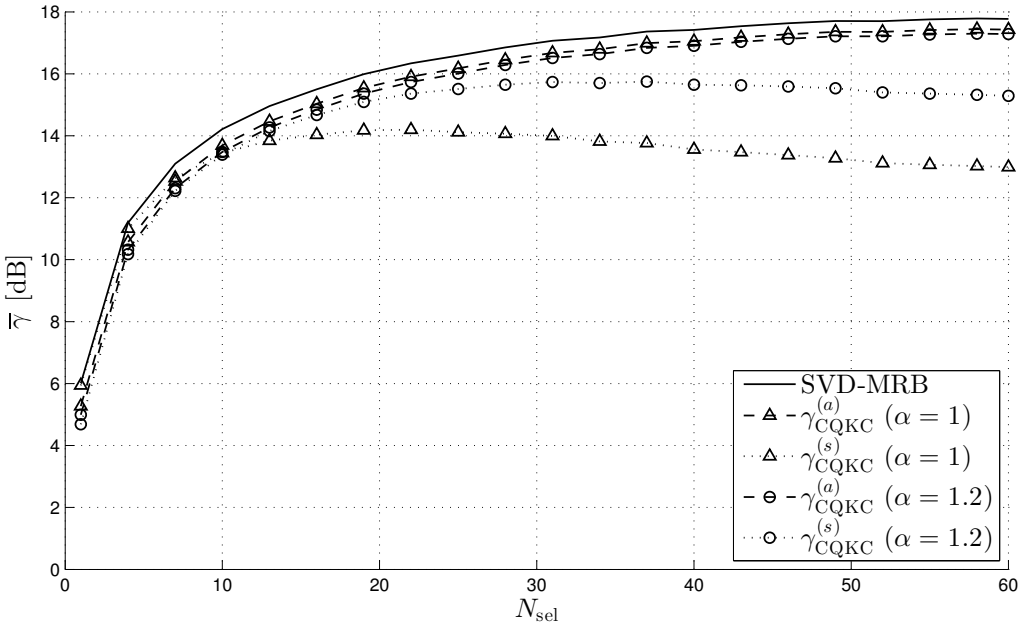

Figure A.2: Analytical and simulated CQ-KC average γ curves vs. the number of selected antennas N_{sel} over $N = 60$ Rx antennas. The values are averaged over 1000 noise realizations and 5000 channel realizations. $|x|_{\text{M}} = 1$, $\mathtt{b} = 2$ and $\Gamma_{\text{AWGN}} = 0$ dB.

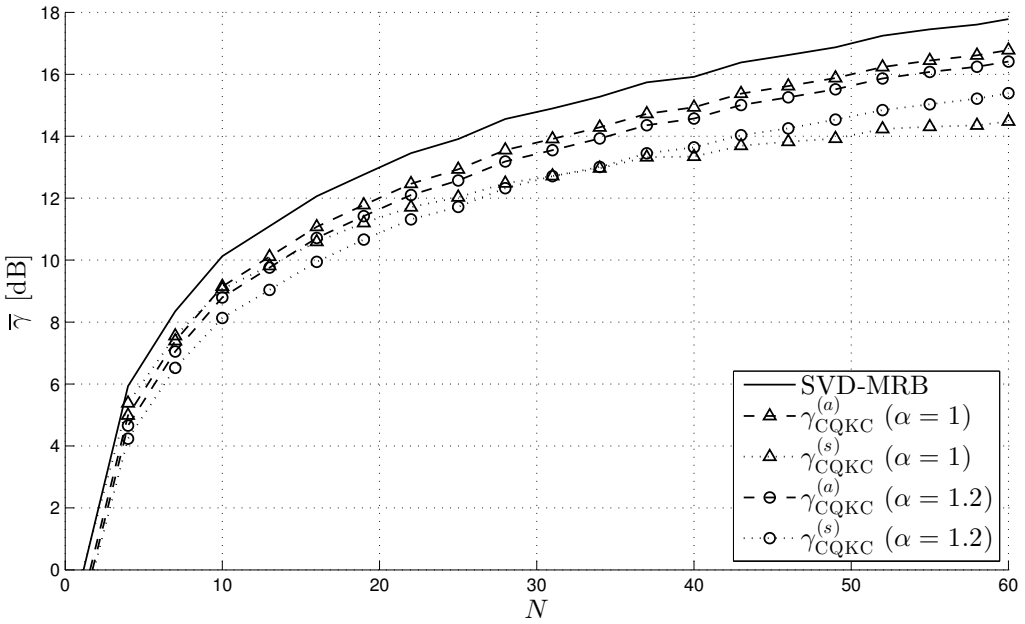

Figure A.3: Analytical and simulated CQ-KC average γ curves vs. the number of antennas N. The values are averaged over 100 noise realizations and 1000 channel realizations. $|x|_{\text{M}} = 1$, $\mathtt{b} = 2$ and $\Gamma_{\text{AWGN}} = 5$ dB.

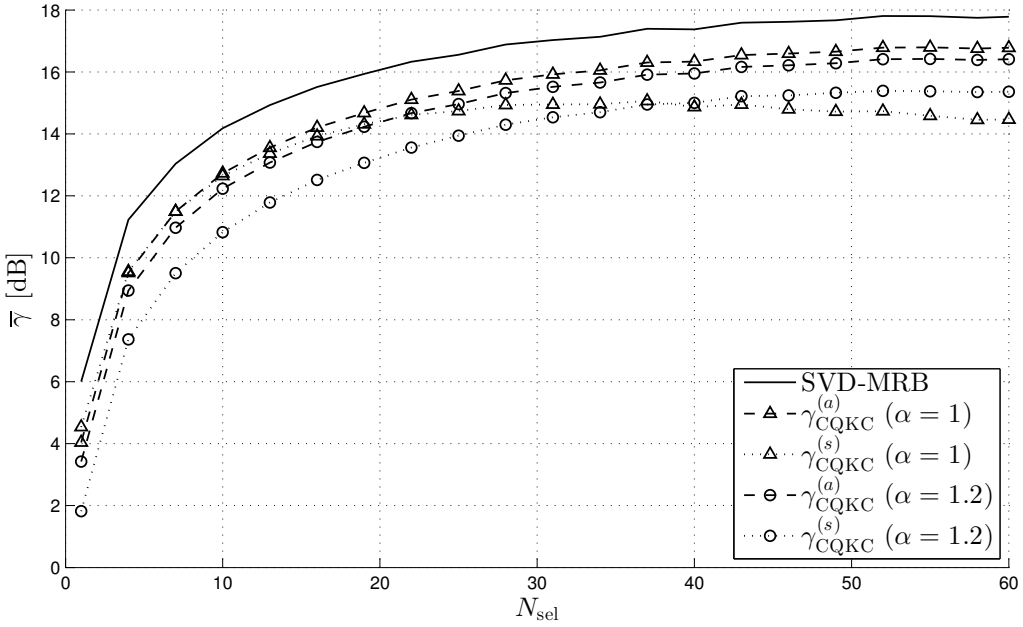

Figure A.4: Analytical and simulated CQ-KC average γ curves vs. the number of selected antennas N_{sel} over $N = 60$ Rx antennas. The values are averaged over 100 noise realizations and 1000 channel realizations. $|x|_{\text{M}} = 1$, $\mathtt{b} = 2$ and $\Gamma_{\text{AWGN}} = 5$ dB.

Remarks on performance

The simulated performance is closer to analytical performance in the low thermal noise ($\Gamma_{\text{AWGN}} = 5$) configuration.
We note that the simulated curves in Figures A.1 and A.2 are affected by a saturation phenomenon which limits the performance with an high number of antennas. In the case of antenna selection, the saturation is grater and can turn in an inversion of the increasing trend. This behaviour is more important when in the received signal the Gaussian noise dominates and is due to ADC model that clips signals to the saturation threshold, phenomenon represented schematically in Figure A.5. This problem is more remarkable in antenna selection because the channel gain are chosen with decreasing power, while the noise power is the same. If the few bits ADCs work in saturation, it implies that a great number of $\widehat{\mathbf{r}}$ entries can be equal and $\mathbf{v}$, from (3.28), may inherit the correlation that affects $\mathbf{h}$, as expressed in (1.35). Moreover, also if entries of $\mathbf{h}$ are optimistically uncorrelated, we expect no improvement due to the MRB weighing at the denominator of γ. We can limit the problem of a coloured noise $\mathbf{v}$ by enlarging the dynamic of the ADC by selecting $\alpha > 1$, the drawback will be in terms of quantization accuracy when few antennas are used.
About Figures A.3 and A.4, when the noise is low ($\Gamma_{\text{AWGN}} = 5$), it can be said that the drawback on performance due to the saturation of the quantizer is less notable. Therefore, the alteration of the saturation threshold by the setting of $\alpha > 1$ could leads to worse performance. From a general point of view, in the case of low noise, the quantization error $\mathbf{w}$ dominates over $\mathbf{n}$ and only with a higher number of bits

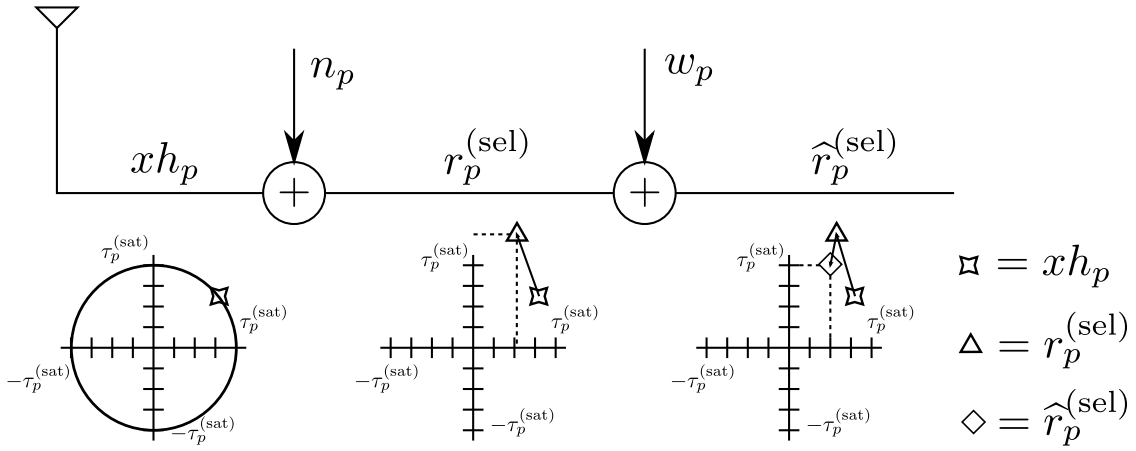

Figure A.5: A representation of the generic ADC model working in saturation.

($\mathtt{b} > 2$) we can reduce the gap to the MRB bound.

A.4.2 CQ-EC performance

Figures A.6 and A.8 show the average γ versus the number of receiver antennas N in the case of channel estimation, Figures A.7 and A.9 represent the performance with antenna selection.

Remarks on performance

The CQ-KC performance remarks are valid also in the case of channel estimation. In addition, in CQ-EC we note a greater gap between the analytical and simulated curves due to the channel estimation error.

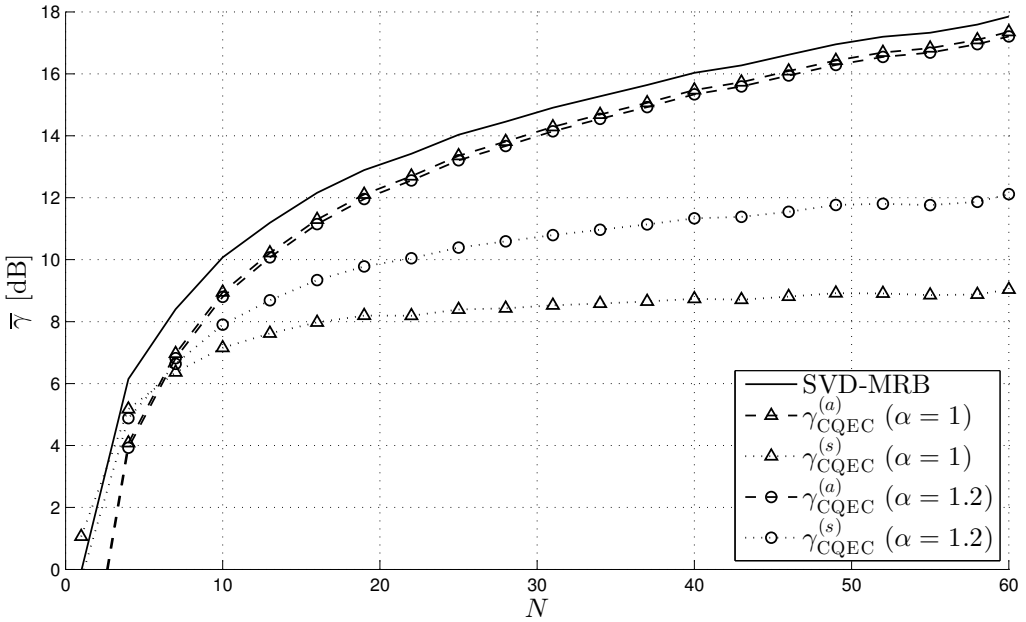

Figure A.6: Analytical and simulated CQ-EC average γ curves vs. the number of antennas N. The values are averaged over 100 noise realizations and 1000 channel realizations. $|x|_{\mathrm{M}} = 1$, $\mathtt{b} = 2$, $K = 3$ and $\Gamma_{\mathrm{AWGN}} = 0$ dB.

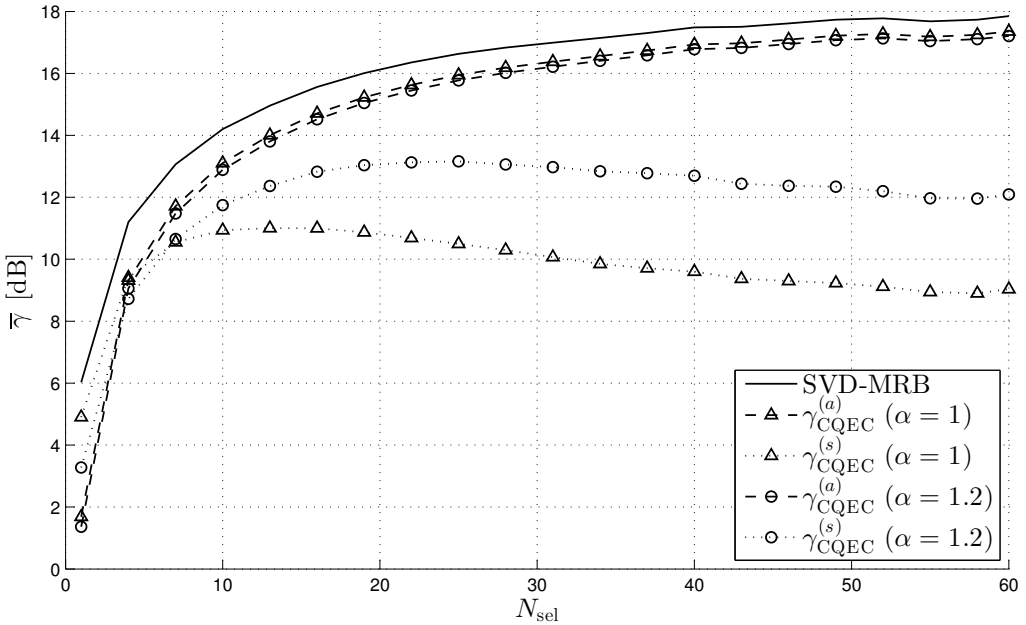

Figure A.7: Analytical and simulated CQ-EC average γ curves vs. the number of selected antennas N_{sel} over $N = 60$ Rx antennas. The values are averaged over 100 noise realizations and 1000 channel realizations. $|x|_{\mathrm{M}} = 1$, $\mathtt{b} = 2$, $K = 3$ and $\Gamma_{\mathrm{AWGN}} = 0$ dB.

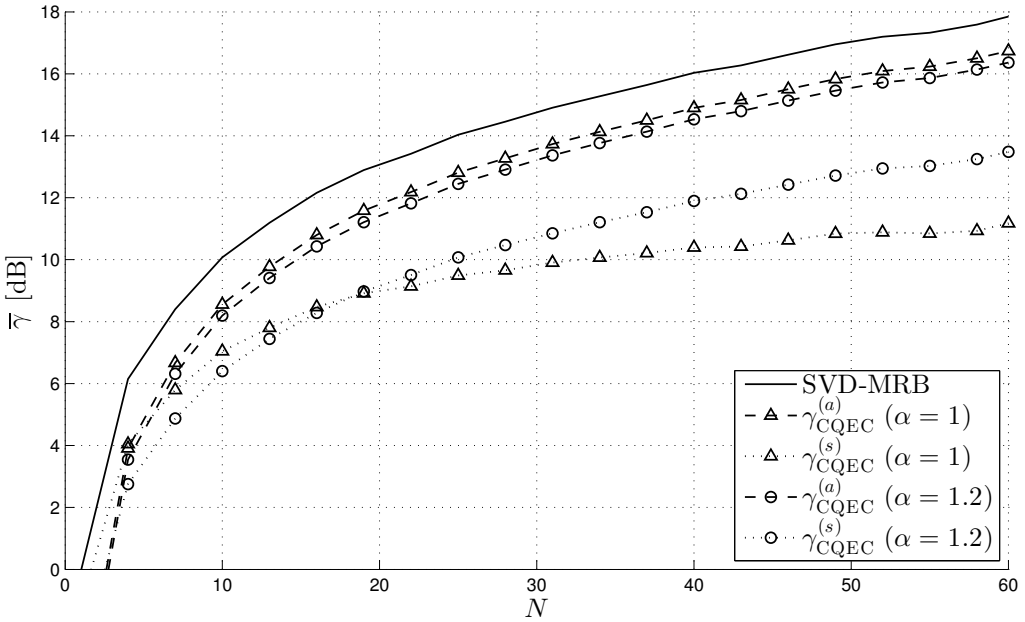

Figure A.8: Analytical and simulated CQ-EC average γ curves vs. the number of antennas N. The values are averaged over 100 noise realizations and 1000 channel realizations. $|x|_{\mathrm{M}} = 1$, $\mathtt{b} = 2$, $K = 3$ and $\Gamma_{\mathrm{AWGN}} = 5$ dB.

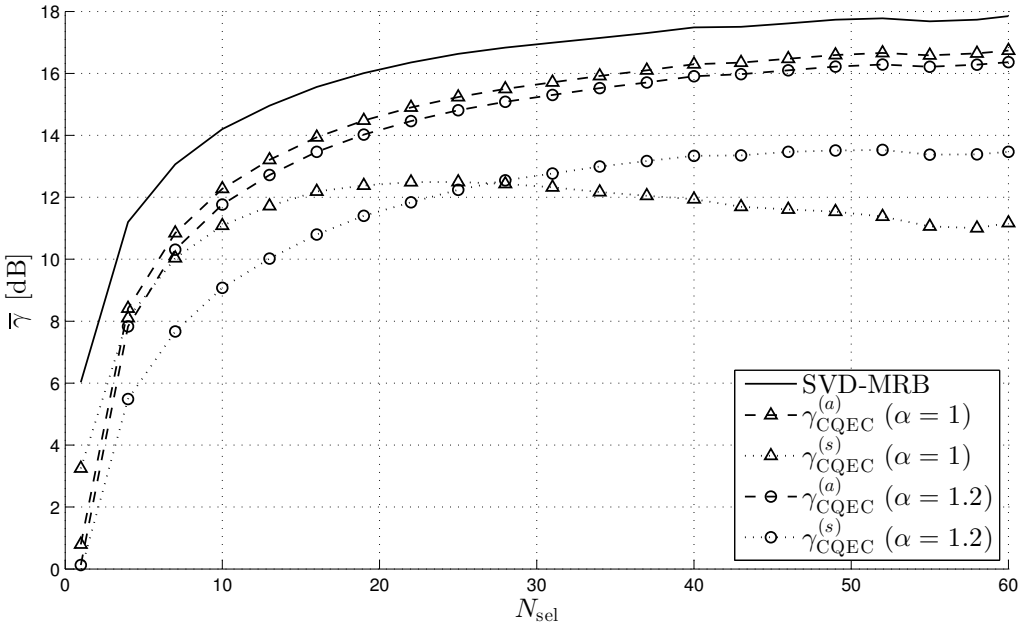

Figure A.9: Analytical and simulated CQ-EC average γ curves vs. the number of selected antennas N_{sel} over $N = 60$ Rx antennas. The values are averaged over 100 noise realizations and 1000 channel realizations. $|x|_{\mathrm{M}} = 1$, $\mathtt{b} = 2$, $K = 3$ and $\Gamma_{\mathrm{AWGN}} = 5$ dB.

Bibliography

[1] Z. Pi and F. Khan, "An introduction to millimeter-wave mobile broadband systems", *IEEE Communications Magazine*, vol. 49, no. 6, pp. 101–107, 2011. DOI: 10.1109/MCOM.2011.5783993.

[2] Y. Kishiyama, A. Benjebbour, T. Nakamura, and H. Ishii, "Future steps of LTE-A: evolution toward integration of local area and wide area systems", *IEEE Wireless Communications*, vol. 20, no. 1, pp. 12–18, 2013. DOI: 10.1109/MWC.2013.6472194.

[3] H. Xu, T. Rappaport, R. Boyle, and J. Schaffner, "Measurements and models for 38-ghz point-to-multipoint radiowave propagation", *IEEE Journal on Selected Areas in Communications*, vol. 18, no. 3, pp. 310–321, 2000. DOI: 10.1109/49.840191.

[4] O. Ayach, R. Heath, S. Abu-Surra, S. Rajagopal, and Z. Pi, "Low complexity precoding for large millimeter wave mimo systems", pp. 3724–3729, 2012. DOI: 10.1109/ICC.2012.6363634.

[5] F. Gholam, J. Via, and I. Santamaria, "Beamforming design for simplified analog antenna combining architectures", *IEEE Transactions on Vehicular Technology*, vol. 60, no. 5, pp. 2373–2378, 2011. DOI: 10.1109/TVT.2011.2142205.

[6] S. Rajagopal, S. Abu-Surra, Z. Pi, and F. Khan, "Antenna array design for multi-gbps mm-wave mobile broadband communication", pp. 1–6, 2011. DOI: 10.1109/GLOCOM.2011.6133699.

[7] C. Doan, S. Emami, D. Sobel, A. Niknejad, and R. Brodersen, "Design considerations for 60 ghz cmos radios", *IEEE Communications Magazine*, vol. 42, no. 12, pp. 132–140, 2004. DOI: 10.1109/MCOM.2004.1367565.

[8] T. Rappaport, *Wireless Communications-principles and practice, 2nd edition*. Prentice Hall, 2002.

[9] P. Smulders and L. Correia, "Characterisation of propagation in 60 ghz radio channels", *Electronics Communication Engineering Journal*, vol. 9, no. 2, pp. 73–80, 1997. DOI: 10.1049/ecej:19970204.

[10] F. Khan and Z Pi, "Mm-wave mobile broadband (mmb): unleashing the 3-300ghz spectrum", pp. 1–6, 2011. DOI: 10.1109/SARNOF.2011.5876482.

[11] S. Yong, "Tg3c channel modeling sub-committee final report", *IEEE 802.15-07-0584-00-003c*, 2007.

[12] P. Smulders, "Statistical characterization of 60-ghz indoor radio channels", *IEEE Transactions on Antennas and Propagation*, vol. 57, no. 10, pp. 2820–2829, 2009. DOI: 10.1109/TAP.2009.2030524.

[13] A. Goldsmith, *Wireless communications*. Cambridge University Press, 2005.

[14] A. Van Zelst, "A compact representation of spatial correlation in mimo radio channels", *submitted to International Conference on Communications (ICC)*, 2004.

[15] K. Yu, "Modeling of multiple-input multiple-output radio propagation channels", PhD thesis, 2002.

[16] H. Zhang, S. Venkateswaran, and U. Madhow, "Channel modeling and mimo capacity for outdoor millimeter wave links", pp. 1–6, 2010. DOI: 10.1109/WCNC.2010.5506714.

[17] A. Paulraj, R. Nabar, and D. Gore, *Introduction to Space-Time Wireless Communications*. Cambridge University Press, 2003.

[18] X. Zheng, Y. Xie, J. Li, and P. Stoica, "Mimo transmit beamforming under uniform elemental power constraint", *IEEE Transactions on Signal Processing*, vol. 55, no. 11, pp. 5395–5406, 2007. DOI: 10.1109/TSP.2007.896058.

[19] T. Lo, "Maximum ratio transmission", *IEEE Transactions on Communications*, vol. 47, no. 10, pp. 1458–1461, 1999. DOI: 10.1109/26.795811.

[20] N. Benvenuto and G. Cherubini, *Algorithms for Communications Systems and their Applications*. Wiley, 2002.

Acknowledgements (ringraziamenti)

My first care goes to my parents Pina and Fabiano, thank you to allow me to be the protagonist of my life, thank you for your physical and moral support and for your constant and, in the same time, discreet presence. An affectionate thought is for my grandmother Anna, who repeatedly encourage me throughout my study experience and, with a great miss, to Marino and Ida, I will forever remember happy moments spent together.
I am very grateful to my supervisor Nevio Benvenuto, for his fundamental and constant guidance in the developing of this project and for letting me grow from an academic point of view and as a person. I have felt privileged for have had available the experience and the support of Federico Boccardi from Bell Laboratories Alcatel-Lucent; I extend my gratitude to his colleagues Paolo Baracca and Hardy Halbauer for the further reviews on the thesis.
My acknowledgement is also for all my friends and partners in adventures of Rovereto, in particular Federico, Michele, Paolo and Diego, we have shared important moments and thanks to all of you I preserve images and memories of the carefree years.
Thanks to all my flatmates during the period of university studies: Veronica, Marco, Suela, Matteo, Giacomo, Christian, Daniele, Desireé, Gisella and Ludovico, everyone has taught me something and made my life in Padova much more interesting!
Last but not least a special thanks to the people which daily, for a year and half, increase my experience from a human and professional point of view, I refer to all my apprentice workmates in Telecom Italia, especially to Claudio and Enrico that have faced with me two challenging homeworks; it is also for your merit that I am graduate now.

Il primo pensiero è rivolto ai miei genitori Pina e Fabiano, grazie per avermi dato la possibilità di essere stato il protagonista della mia vita, grazie per avermi sostenuto materialmente e moralmente e per essere stati sempre presenti e allo stesso tempo discreti. Un affettuoso riconoscimento alla mia nonna Anna, che ripetutamente mi ha incoraggiato durante gli studi e, con non poca nostalgia, a Marino e Ida di cui conserverò per sempre i bei momenti trascorsi assieme.
Sono particolarmente grato al mio relatore Nevio Benvenuto per la sua fondamentale e costante guida nello sviluppo di questo progetto e per avermi fatto crescere a livello personale ed accademico. Mi sento privilegiato nell'aver avuto a disposizione l'esperienza e il supporto di Federico Boccardi dai Bell Laboratories Alcatel-Lucent; la mia gratitudine si estende ai suoi colleghi Paolo Baracca e Hardy Halbauer, per le ulteriori revisioni alla tesi.
La mia riconoscenza inoltre a tutti gli amici e compagni di avventure di Rovereto, in particolare Federico, Michele, Paolo e Diego, abbiamo condiviso tanti momenti importanti e grazie a tutti voi conservo immagini e ricordi degli anni spensierati.
Grazie a tutti i miei compagni di appartamento nel corso degli studi universitari: Veronica, Marco, Suela, Matteo, Giacomo, Christian, Daniele, Desireé, Gisella e Ludovico, ognuno di voi mi ha insegnato qualcosa e ha reso la vita a Padova molto più interessante!
Infine un ringraziamento speciale alle persone che da un anno e mezzo, quotidinamente, arrichiscono umanamente e professionalmente il mio bagaglio, mi riferisco a tutti colleghi di apprendistato in Telecom Italia, in particolare a Claudio ed Enrico assieme ai quali ho avuto modo di affrontare due progetti di esame impegnativi; se oggi sono dottore è anche per merito vostro.